ISSN 1512-0325

JOURNAL OF THE GEORGIAN CERAMISTS' ASSOCIATION

CERAMICS

AND ADVANCED TECHNOLOGIES

Scientific, technical and industrial illustrated, registered, referral magazine

Vol. 24. 2(48).2022

CONTENTS

UDC 543.42

DETERMINATION OF BIOLOGICALLY ACTIVE SUBSTANCES BY CHROMATOGRAPHIC METHOD

N. Amashukeli, G. Kenkebashvili

Chemical and Biological Technology Department, Georgian Technical University, Georgia, 0175, Tbilisi, Kostava str, 69

E-mail: natamashukeli@gmail.com, Giorgikenkebashvili5@gmail.com

Resume: ***Purpose.*** The aim of the work was chromatographic analysis of biologically active substances. Determine the possibility of quantitative analysis of water-soluble and fat-soluble vitamins without preliminary separation of components.

Solution of specific tasks was planned:

- Predictability of high-performance liquid chromatography, determination of desired accuracy in multicomponent mixtures.

- Selection of a convenient chromatographic method for the study of a mixture of multicomponent vitamins.

- Selection of the best environment (PH) and solvents for this method.

- Selection of wavelengths for spectral analysis.

Method. High-efficiency liquid chromatography may be used to analyze a mixture of vitamins of highly complex composition. Analysis is possible without prior separation, provided the appropriate chromatographic column and mobile phase are selected.

Results. In the course of studies, it has been theoretically proven and based on experiments that using high-performance liquid chromatography it is possible to simultaneously determine not only water-soluble organic compounds but also fat-soluble and water-soluble compounds without prior separation.

The type of reverse-phase chromatography was selected. Chromolith was selected as the real phase. The pH of the moving phase was increased to 6. At the same time it was found that the moving phase can be used only in gradient or variable mode.

It was found that the peak areas in the selected range and their corresponding concentrations are in a linear relationship, which allows us to determine the concentration with high accuracy.

High-performance liquid chromatography allows to determine the purity, authenticity of the substance, and to conduct quantitative analysis. The advantage of this method is the possibility of simultaneous analysis of thermally unstable compounds.

Conclusion; High-efficiency liquid chromatography can be used to determine the concentration of vitamins with different properties, without prior separation, either through the normal phase as well as the reverse-phase real phase and the gradient moving phase.

Conclusion. High-performance liquid chromatography allows to determine the authenticity and

purity of multicomponent mixtures. Simultaneous quantitative analysis for fat-soluble and water-soluble vitamins should also be performed.

Chromatographic column turned out to be optimal, chromolite 18 C. Reagent input PH = 3 later PH=6. The solvent, acetonitrile and isopropyl alcohol in the 4: 1 irrational state, ensures the smooth operation of the chromatography.

Research has shown that by increasing the pH of the mobile phase to 6, with the correct selection of an organic solvent, it is possible to simultaneously determine fat-soluble and water-soluble vitamins with an error of up to 1-3%. The chromatographic peak areas of the study substances and the corresponding concentrations are linearly correlated.

Key words: Water-soluble and fat-soluble vitamins; Concentration; Without separation; High efficiency liquid chromatography.

1. INTRODUCTION

Methods of Chromatographic analysis are widely used in practice. This method is known for its high accuracy and sensitivity. High efficiency liquid chromatography methods hold an important spot in multicomponent mixture analysis.

The downside of the above mentioned method is that it takes a long time to determine water-soluble and fat-soluble vitamins and is inconvenient for serial analysis.

Chromatographic columns become contaminated during the analysis of water-soluble and fat-soluble vitamins, which stay in immobile phase. This requires multiple washes of chromatographic columns. In the literature there are mentioned different methods to solve this problem. To separate vitamins they use solid phase extraction for which they use C18 Sorbent.

C18(Si-C18H17) is classically an opposite phase sorbent which is known for holding up well in nonpolar solvents. It also works well in nonionic chromatography and is used to separate vitamins. Diameter of the slides is 300A. When searching liquid and methanol is applied to C18, fat-soluble vitamins get transferred on sorbent and water is left in the liquid. After that, fat-soluble vitamins are transferred in the liquid using acetonitrile-tetrahydrofuran (1:1). After carrying out this procedure, the mixture is analyzed.

This method is also pretty lengthy and requires hard work. Because of that there is high scientific and practical interest to come up with a method where complex mixture quantities in fat-soluble and water-soluble vitamins are determined simultaneously.

This method is used in analysis of pharmaceutical drugs, because it is more effective during analysis of the high quantities of the same type of samples. Factory laboratories and quality control facilities are interested in analysis of multiple samples simultaneously using the express method because the quantities of imported products are growing and it is very common that the declared and factual content of these products do not match.

2. MAIN PART

Pharmacopeias that exist in the Georgian market oftentimes have methods that are used for analysis which have low accuracy and sensitivity, they are lengthy and require hard labor. These

methods when used during the mixture analysis require separation of certain components in advance and determination of their content one by one using chemical reactions. Because of this it is important to have methods which will allow us to conduct analysis without prior separation of the mixture components. Complex vitamin mixture analysis is possible using high efficiency liquid chromatography.

During the data analysis of the experiments the least square method was chosen.

Chromatograph water alliance 2695 was used in the experiments with diode matrix detector waters 2996. Four component gradient low pressure mixer was used. Separation of components is done on polymer chromatographic columns with sizes 100/4. 5mm using the monolithic sorbent chromolith performance RP-18C.

To prepare mobile phases we used distilled water, acetonitrile, isopropyl alcohol, sodium hexanesulfonate and sodium octanesulfonate, which are meant for liquid chromatography.

Experimental solution contained vitamins;

1. **A** (Retinyl palmitate)
2. **B1** (Thiamine chloride)
3. **B2** (Riboflavin-5-phosphate)
4. **B3** (Calcium D pantothenate)
5. **B6** (Pyridoxine hydrochloride)
6. **C** (Ascorbic acid)
7. **E** (a-tocopherol)
8. **PP** (Nicotinamide)

Conservants used: Nipagine, Nipasol, Sodium benzoate.

Optimal-phase chromatography has hydrophilic immobile phase. Water-soluble or hydrophilic vitamins elute from the chromatographic column by increasing the polarity of mobile phase.

Hydrophobic molecules, in our case fat-soluble vitamins do not stay in normal phase columns and are eluted in the first place. Because of this, the reverse immobile phase is used. In this case immobile phase has covalent bonds with the alkyl chain. Due to it this is a hydrophobic phase.

The usage of hydrophobic solid phase is also considered in the opposite of normal phase chromatography. Polar mobile phase was used in reverse-phase analysis. As a result, fat-soluble vitamins are adsorbed in the hydrophobic solid phase.

Hydrophilic ones eluted in the first place and hydrophobic ones eluted during reduction of polarity in the mobile phase. To do this, water is mixed with nonpolar solvents which weakens hydrophobic interactions. More hydrophobic the molecule is, the stronger it is adsorbed to immobile phase and more organic solvent is required in the mobile phase.

For eluting in an opposite-phase columns was used: water, acetonitrile, isopropyl alcohol and sodium hexanesulfonate.

Water-soluble vitamins are retained not very strongly in immobile phase and may be separated using eluents of reversal phase which can be prepared by adding organic modifiers.

Fat-soluble vitamins are hydrophobic. This group is similar to the surface of immobile phase. Because of it, to determine fat-soluble vitamins, normal-phase and reverse-phase can be used. To elute experimental substances in the reverse-phase chromatographic column, gradient is used. Which

in itself means changing of mobile phase solvent (water-soluble solvent) during the process, usually by decreasing polarity. During this process **PH** is crucial. Selectivity and order of the eluted substances depend on the **PH.**

Table 1

Gradient Elution Options

Option	Sorbent	Change in mobile phase composition
1	chromolith	CN3CN:0,005m KClO4 PH=6(0:1)1:1(K 4mn) CH3CN:isopropyl alcohol4:1(8mn)
2	performance RP_8c Reversed phase	CH3CN:0,5M KClO4 PH=3+2,5% sodium hexanesulfonate(0:1)(K6mn)CH3CN
3	chromolith	CH3CN:0,5M KClO4 PH=3+2,5%sodium hexanesulfonate(4:1)(k8mn)CH3CN
4	Reversed phase Performans 18C	CH3CN:0,5M KClO4 PH=3+2,5%sodium hexanesulfonate(4:1)(K8mn)CH3CN PH=6

Option 4 turned out to be the best in eluting the water-soluble and fat-soluble vitamins.

For eluting the water and fat soluble vitamins, during the last stage of the gradient, was used prior processing of the mobile phase using airionic reagent **PH=3.**

Problems also occurred during the process which were due to air bubble formation and mobile phase stream weakening because of switching from water-organic solvent 100% to acetonitrile.

Uninterrupted work was done by adding isopropyl alcohol (4:1).

Research mixture components differ not only by chromatographic but also spectral properties.

More accurate results are obtained on a wavelength where absorption is maximal.

Diode-matrix detector helped obtain results which provided four wavelengths. The absorption of Calcium pantothenate is maximal on 210nm. Retinol palmitate absorption is 328nm, Thiamine chloride absorption happens at 246nm and Riboflavin 267nm. This allows us to conduct selective definitions of each component.

Table 2. Shows the experimental results of three samples and their meteorological features.

Table 2

Three Samples of Vitamin Mixture Analysis Results

Components	Norm mg/mL	Content mg/mL	S Peak area	L Peak height	K proportionality coefficient
Ascorbic Acid	10,8-20,2	21,57	0,532	0,177	0,41
		21,369	0,661	0,22	0,509
		20,785	0,52	0,24	0,554
Nicotinamide	2,2-4,4	3,669	0,122	0,041	0,094
		3,594	0,19	0,063	0,146
		3,577	0,148	0,049	0,114
Thiamine chloride	0,22-0,4	0.347	0,011	0,004	0,008
		0,334	0,014	0,005	0,011
		0,338	0,017	0,006	0,013
Riboflavin-5 phosphate	0,22-0,4	0,353	0,022	0,007	0,017
		0,349	0,026	0,008	0,02
		0,352	0,014	0,009	0,011
Calcium D pantothenate	1,08-2,02	2,16	0,01	0,037	0,085
		1,977	0,094	0,031	0,072
		1,995	0,086	0,029	0,066
Pyridoxine hydrochloride	0,27-0,51	0,472	0,021	0,007	0,016
		0,447	0,032	0,011	0,025
		0,452	0,024	0,008	0,018

Components	Norm mg/mL	Content mg/mL	S Peak area	L Peak height	K proportionality coefficient
Retinol-palmitate	0,108-0,2025	0,223	0,0120	0,004	0,009
		0,193	0,013	0,004	0,01
		0,174	0,011	0,004	0,008
Tocopheryl acetate	1,08-2,025	2,148	0,123	0,041	0,095
		1,982	0,121	0,04	0,093
		1,8	0,114	0,038	0,088
Nipagin	0,68-0,82	0,771	0,032	0,011	0,025
		0,692	0,044	0,015	0,034
		0,702	0,041	0,014	0,032
Nipazol	0,22-0,28	0,286	0,018	0,006	0,014
		0,24	0,016	0,005	0,012
		0,24	0,013	0,004	0,01
Sodium benzoate	0,9-1,1	1,002	0,026	0,009	0,02
		0,918	0,029	0,01	0,022
		0,917	0,028	0,009	0,022

To ensure the accuracy of the research, test-solutions were prepared, which contained every substance that needed to be determined and their helping substances.

Concentration range in experimental solutions consisted of the plus minus 20% of the nominal value. results were processed using the least square method.

3. CONCLUSION

High efficiency liquid chromatography allows us to determine purity and content of multicomponent mixtures. Also it allows us to conduct simultaneous quantitative analysis of fat-soluble and water-soluble vitamins.

Chromolite 18C was found to be optimal. In mobile phase reagent application PH=3 and

increase during process PH=6. acetonitrile and isopropyl alcohol 4:1 in nonionic condition allows uninterrupted work of Chromatography.

Experiment confirmed that in a given range, chromatographic peak areas of the researched substances and their concentrations have linear correlation which allows the detection of the concentration in the researched substances.

Four wavelengths were selected for spectral analysis: 210nm, 246nm, 267nm and 328nm. This allows the conduction of selective determination of the components.

REFERENCES

1. Ghudushauri Tsiala. Physico-chemical methods of analisis – Georgia Technical university. 2008.261p-305p
2. Aivazov B.V. introduction to chromatoghraphy. Moscow. High school. 1983.
3. V.N. Alekseev Quantitative Analysis. Moscow. Mir. 1972.
4. Chaimbault, Patrick. Recent Advances in Redox Active Plant and Microbial . — 2007. — P. 151-194
5. Rudakov O.B Vostrov I.A Mompanion of the chromatograoher. Voronezh: Aquarius, 2004. - 528 p. - ISBN 5-88563-049-6
6. Yashin I.I. Iashin I.E. Iashin A.Y. gas chromatography. Moscow, 2009p— 528 p. — ISBN 978-5-94976-825-9
7. Dolgonosovc A.M. Column methods of analytical chromatography. Guidelines for students of chemical specialties. Dubna. 2009.
8. Dettmer-Wilde, Katja, Engewald, Werner Practical Gas Chromatography A Comprehensive Reference. - 2014 - ISBN 978-3-642-54640-2
9. Greibrokk, T., & Andersen, T. (2003). High-temperature liquid chromatography. Journal of Chromatography A, 1000(1-2), 743-755.
10. Dugo, P., Cacciola, F., Kumm, T., Dugo, G., & Mondello, L. (2008). Comprehensive multidimensional liquid chromatography: theory and applications. Journal of Chromatography A, 1184(1-2), 353-368
11. Vissers, J. P., Claessens, H. A., & Cramers, C. A. (1997). Microcolumn liquid chromatography: instrumentation, detection and applications. Journal of Chromatography A, 779(1-2), 1-28
12. Nawrocki, J. (1997). The silanol group and its role in liquid chromatography. Journal of Chromatography A, 779(1-2), 29-71
13. Sawardeker, J. S., Sloneker, J. H., & Jeanes, A. (1965). Quantitative determination of monosaccharides as their alditol acetates by gas liquid chromatography. Analytical Chemistry, 37(12), 1602-1604
14. Sloneker, J. H. (1972). Gas–liquid chromatography of alditol acetates. In General Carbohydrate Method (pp. 20-24). Academic Press
15. Moreno, P., & Salvado, V. (2000). Determination of eight water-and fat-soluble vitamins in multi-vitamin pharmaceutical formulations by high-performance liquid chromatography. Journal of chromatography A, 870(1-2), 207-215
16. Taguchi, K., Fukusaki, E., & Bamba, T. (2014). Simultaneous analysis for water-and fat-

soluble vitamins by a novel single chromatography technique unifying supercritical fluid chromatography and liquid chromatography. Journal of Chromatography A, 1362, 270-277

17. El-Khoury, J. M., Reineks, E. Z., & Wang, S. (2011). Progress of liquid chromatography-mass spectrometry in measurement of vitamin D metabolites and analogues. Clinical biochemistry, 44(1), 66-76
18. Kamao M., Tsugawa N. et All. T. (2007). Quantification of fat-soluble vitamins in human breast milk by liquid chromatography–tandem mass spectrometry. Journal of Chromatography B, 859(2), 192-200
19. Heudi, O., Kilinç, T., & Fontannaz, P. (2005). Separation of water-soluble vitamins by reversed-phase high performance liquid chromatography with ultra-violet detection: application to polyvitaminated premixes. Journal of Chromatography A, 1070(1-2), 49-56
20. Leporati, A., Catellani, D., Suman, M., Andreoli, R., Manini, P., & Niessen, W.M. (2005). Application of a liquid chromatography tandem mass spectrometry method to the analysis of water-soluble vitamins in Italian pasta. Analytica chimica acta, 531(1), 87-95
21. Hirauchi, K., Sakano, T., Notsumoto, S., Morimoto, A., Fujimoto, K., Masuda, S., & Suzuki, Y. (1989). Measurement of K vitamins in animal tissues by high-performance liquid chromatography with fluorimetric detection. Journal of Chromatography B: Biomedical Sciences and Applications, 497, 131-137,

UDC 669.01

INFLUENCE OF STRUCTURAL FACTORS ON THE FRICTIONAL CHARACTERISTICS OF BAINITIC CAST IRONS

S. Gvazava[1], N. Khidasheli[2], T. Badzoshvili[1], M. Chikhradze[2], G. Zakharov[1]

[1] LEPLF. Tavadze Metallurgy and Materials Science Institute

[2] Georgian Technical University, Institute of Bionanoceramics and Nanocomposite Teqnology. Georgia, 0175, Tbilisi, Kostava Str. 69

E-mail: s.gvazava@bk.ru; salomegvazava@gmail.com

Resume: ***Goal.*** In the presented work, the tribotechnical characteristics of boron microalloyed bainitic cast irons under different conditions of frictional loading are studied. The interaction of frictional surfaces of the material was studied, both with sliding under dry friction conditions and with periodic wetting with rainwater of the contact surfaces.

The experimental cast irons differed from each other in the ratios of structural components, namely, the amount of residual austenite (10-40%) and the type of bainite (lower and upper). The formation and management of the above-mentioned structural components in the metal-base of the material was carried out by optimizing the thermal treatment modes.

It is determined that the temperature of the surface layers in the friction zone depends on the magnitude of the contact load and it can reach 500-550^{0}C. It has been shown that wetting the working surfaces with rain water leads to a slight decrease in the coefficient of friction.Optimizing the amount of residual austenite in the metal base of bainitic cast irons ensures stabilization of frictional characteristics and improves tribotechnical parameters. Microalloying of liquid metal with boron reduces the corrosion rate of the material, which is due to the formation of finely dispersed boron chemical compounds (carbides, borides, nitrides and carbo-nitrides) in the metal base.

Method. The study of structural constituents of the material was carried out by means of microscope Neophot-32. In the process of frictional interaction of the research alloy, their tribotechnical characteristics were determined on tribometer СМЦ-2. By the use of Scanning electron microscopy (SEM) were determined the stability and density of oxide layers in the contact zone on the wear surface of bainitic cast irons.

Results. The results of the conducted investigations indicate the high resistance of bainitic cast irons to corrosion damage in the mode of periodic rainwater wetting.

The amount of residual austenite up to 10% in the structure of the research material ensures improvement of tribological characteristics. At the expense of microalloying with 0.03% boron, there is the formation of dispersed phases in the metal base of the material, for example carbides, nitrides and borides, which has a positive effect on the dispersion of the structure of bainitic cast irons,

the quality of distribution and tribo corrosion characteristics.

Conclusions. According to the results obtained from the present work, the following conclusions can be made:

- Ductile irons containing up to 10-12% residual austenite in the metal are characterized by a more stable friction coefficient in the process of cyclic frictional loading
- Ductile irons microalloyed with boron with residual austenite content up to 10–12% in the lower bainite metal matrix have the highest corrosion resistance during periodic wetting.
- Microadditives of boron (0.03%) can slow down the corrosion destruction of ductile iron in contact with rainwater.
- It has been established that the supply of water to rubbing surfaces causes a slight decrease in the coefficient of friction.

Goal of the research: Studying the functional characteristics of boron microalloyed bainitic cast irons with different structures in sliding dry friction conditions and improving their tribocorrosive properties.

1. INTRODUCTION

When developing and designing modern materials for brake systems, it must be taken into account that for operation in extreme conditions, they must have high mechanical strength, corrosion, temperature and wear resistance, as well as an optimal coefficient of friction.

To ensure the reliability of braking, the dependence of the listed characteristics on the parameters of various frictional loading conditions (different in magnitude and nature of the load, temperature in the friction contact zone, environmental influences, etc.) should be studied. This is due to the fact that, depending on the features of the structure, efforts and duration of braking, the temperature conditions, the wear resistance of the materials of the braking systems and the braking efficiency may change significantly.

The required set of properties of bainitic cast irons, as is known [1–3], can be achieved by developing new chemical compositions of alloys, controlling the kinetics of structure formation, optimizing the structure, distribution, and quantitative ratio of phase components [4].

In this regard, high-strength cast irons microalloyed with boron, deserves attention. It is known [8,9] that the modification of bainitic cast iron with boron, improves its tribological characteristics and increases the value and stability of the friction coefficient due to the formation of carbon borides and borides in the structure [10]. Castings made from cast iron microalloyed with boron (0.005-0.01%) have higher tightness, impact and fatigue lifetime, thermal cycling strength and low sparking during braking.

It has been established [3] that under the influence of boron micro additives, the corrosion resistance of Fe-C alloys increases under the conditions of cyclic oxidation. This is due to the fact that the oxidation of iron borides is slower [5-7]. The use of boron micro additives is also more expedient from an economic point of view.

Accordingly, micro-alloying of a melt (liquid metal) with boron introduces features into the formation of the structure and complex of proper-

ties of high-strength cast iron [12]. At the same time, the dependence of the tribotechnical characteristics of these materials on frictional loading conditions remains less studied [11].

In the presented work, the regularities of the influence of friction loading conditions on the kinetics of changes in the friction coefficient, wear intensity and corrosion rate of bainitic cast irons with micro additives of 0.03% B are studied.

2. Experimental Investigations

Cast iron was smelted in an МГП-102 induction furnace with a main crucible lining with a capacity of 50 kg. Cast iron (C- 4.20%; 1.8% Si; 0.25% Mn; 0.03% S; 0.04% P) and steel scrap were used as starting raw materials. To spheroidize graphite inclusions, magnesium metal was introduced into the cast iron melt at a temperature of 1320–1330°C. After completion of spheroidization, the molten metal was superheated to 14500C, boron micro-additives were added, and poured into a Y-shaped sand mold. Once the spheroidization treatment has been completed the molten metal was cast into Y-hapsed sand mold.

Table 1 represents the chemical composition of high-strength cast iron, which was studied in the present work.

TABLE 1

CHEMICAL COMPOSITION OF EXPERIMENTAL DUCTILE IRON

Ductile iron	Chemical composition of high strength cast iron, mass. %							
	C	Si	Mn	S	P	B	Mg	Fe
Basic	3.420	2.120	0.310	0.005	0.005	-	0.040	94.105
By Boron alloyed	3.450	2.200	0.250	0.003	0.060	0.030	0.045	93.935

The experimental samples were subjected to heat treatment according to the following regime: austenitization at 900°C temperature for 60 and 120 minutes → isothermal hardening at temperatures: 280°C or 400°C with 10 minutes holding time. Then the microstructures for different heat treated specimens were observed by metallographic microscope Neophot 32. Phase analysis of the structure was studied with a magnetometer and was studied by diffractometer DRON-4.

Dry sliding wear tests were carried out using a conventional tribometer: model СМЦ-2–„pin-on-disk“, capable of maintaining a constant unidirectional, sliding velocity between the pin and disk. Wear tests were performed at 20N and 50N normal loads, with 2,3 m/s sliding speed and 6280 m sliding distance in dry running conditions. The quenched carbon steel (0.9% carbon content) disk with 62 HRC hardness was used as a counter-body. During each test, the echange of the friction coefficient was recorded electronically.

Corrosion testing of high-strengt cast irons under conditions of periodic wetting with rain-water was carried out on polished samples with a diameter of 60 mm and a thickness of 4 mm. Experimental samples were wetted with 6 hours

intervals. The duration of the tests was 2160 hours. The corrosion rate was estimated from the change in the mass of the samples in every 168 hours.

3. Results and Discussion

The main object of investigation was basic and 0.03% B microalloyed ductile irons with various types of bainitic matrix, in which 10 or 40% of residual austenite was formed by heat treatment. Fig.1 shows the microstructure of cast irons with different content of residual austenite.

In order to achieve this goal, two groups of samples were subject to austenitization at 900°C for 60 and 120 minutes, after they were isothermally hardened at 280°C and 400°C. The obtained samples were tested for wear in unidirectional continuous dry sliding at a constant speed and load for 10 minutes.

During the experiments, the kinetics of the increase in the temperature of the surface layers of the samples as a result of the conversion of mechanical energy into thermal energy was determined. According to the obtained data, the temperature values in the friction zone of friction pairs with identical structural characteristics of ductile iron largely depend on the magnitude of the contact load. Fig. 2.

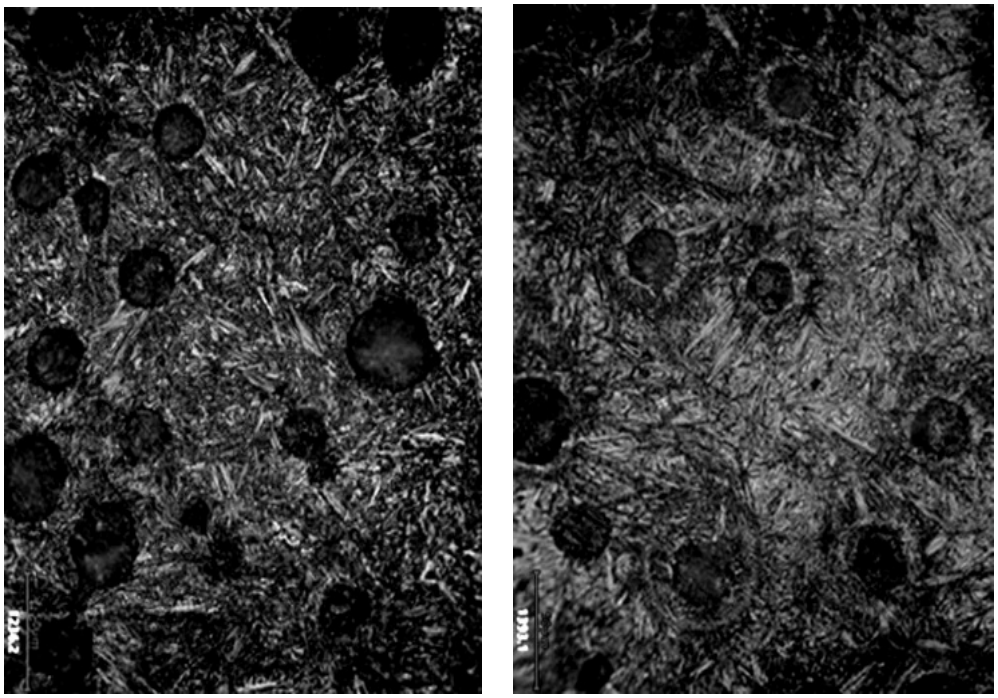

a) X400 b) X400

Fig. 1. Typical microstructure of boron microalloyed a - with 12% Aret., b - with 40% Aret.

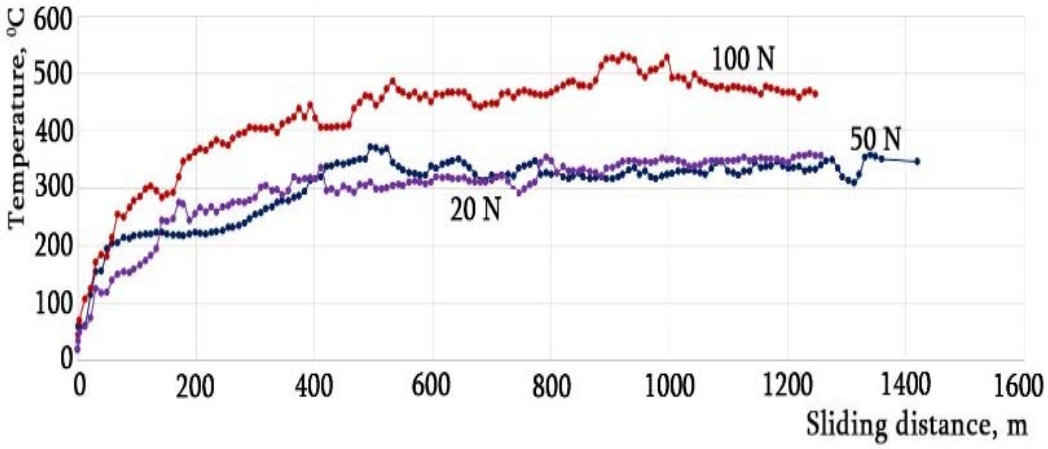

Fig. 2. Influence of the contact load on the kinetics of change temperature in the friction zone during dry sliding wear

It has been established that high-strength cast irons micro-alloyed with boron during the first 30-40 seconds continuous dry sliding under experimental conditions are characterized by a comparable increased rate of the temperature of surface layers, regardless of the magnitude of the contact load. With steady frictional interaction in the dry friction mode, the average temperatures in the friction zone during contact loads of 20 and 50 N differ from each other by 25–30 °C.

With an increase in the contact load to 100 N, the temperature of the friction surface of the experimental samples increases by 75–90°C for cast irons with a lower bainite structure and 10% Aret. reaches 470-520°C. This contributes to the intensification of oxidation processes and the formation of a thin layer of iron oxides, predominantly hematite, on the surface of cast irons.

Scanning Electron microscopic (SEM) studies show that the formed oxide film has a low density (figure 3) and mechanical stability, which limits its protective properties and does not effectively influence the corrosion and wear properties.

Subsequent frictional loading destroys and removes the oxidized layers in the form of wear products, and the abovedescribed processes is repeated.

Depending on the load and the structure of the metal matrix, the friction coefficient of boron-micro-alloyed ductile irons in dry sliding friction ranges from 0.2 to 0.61.

Cast irons with a content of metal up to 10% of residual austenite in the process of cyclic frictional loading are characterized by more stable values of this parameter (Fig.4). An increase in the amount of residual austenite up to 40% causes an increase in temperature in the contact zone, which is reflected in the kinetics of the change in the friction coefficient (Fig.5-1). The processes of plastic deformation of the surface layers of experimental cast irons are intensified, which causes a cyclic decrease in the friction coefficient.

More clearly it is noticed with an increase in the contact load, which is confirmed by an increase in the amplitude of oscillations of the friction coefficient values under repeated frictional loading (Fig. 5-2).

Periodic wetting of heated rubbing pairs with rainwater causes the formation of water vapor and a decrease in the temperature of the contacting surfaces. At the same time, there is a decrease in the values and stabilization of the level of the coefficient of friction (Fig 5-1).

According to the topographical analysis of the frictional surfaces of the test samples, it was established that the cyclic temperature change did not cause the formation of microcracks on the surface of boron microalloyed bainitic cast irons Fig. 6.

Topographic analysis of friction surfaces shows that under conditions of cyclic temperature fluctuations, microcracks do not form on the surface of boron-micro-alloyed high-strength bainitic cast irons.

Corrosion testing of experimental cast irons under conditions of periodic wetting with rainwater showed that the microstructure of high-strength cast irons has a significant effect on the rate of corrosion failure.

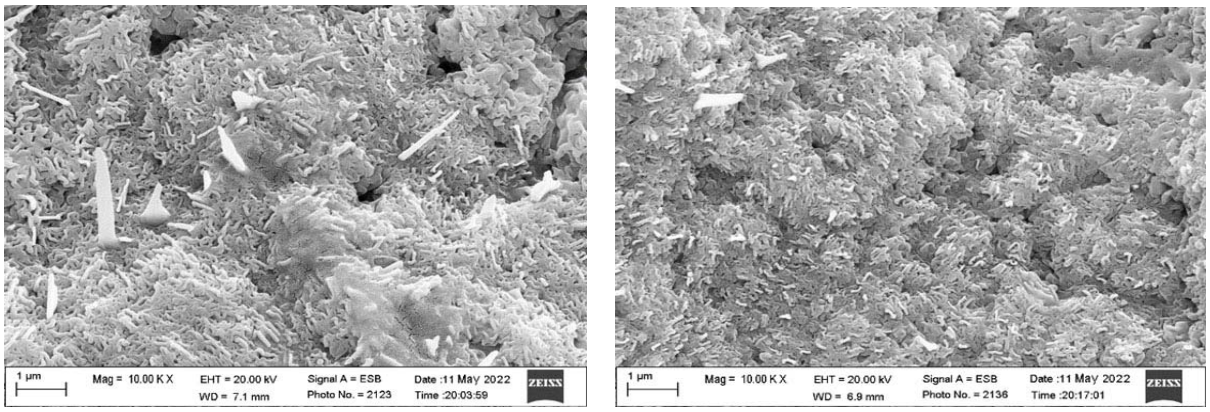

a ***b***

Fig. 3. Oxide film isothermally hardened at 280^{0}C With bainitic cast iron with different content in the structure of residual austenite; a - from 10%, b- from 40%

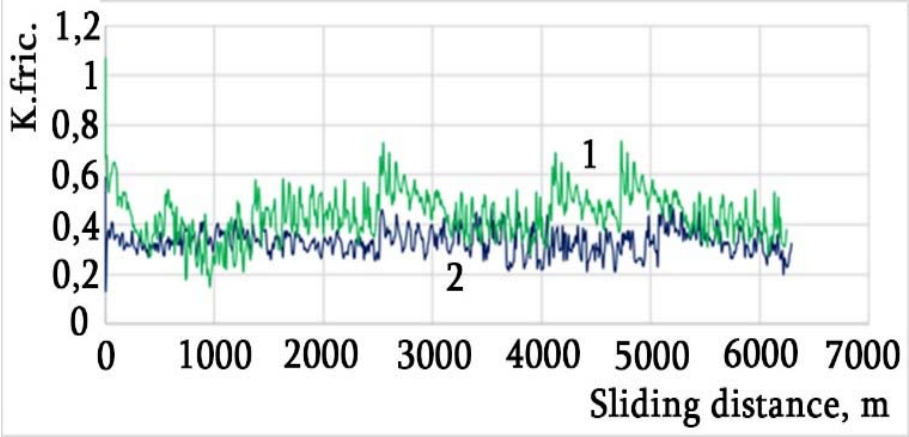

Fig. 4. The friction coefficient evolution of isothermal quenched
at 280°CADI with 10 % Aret.under sliding distance
1-with dry friction; 2-with repeated wetting

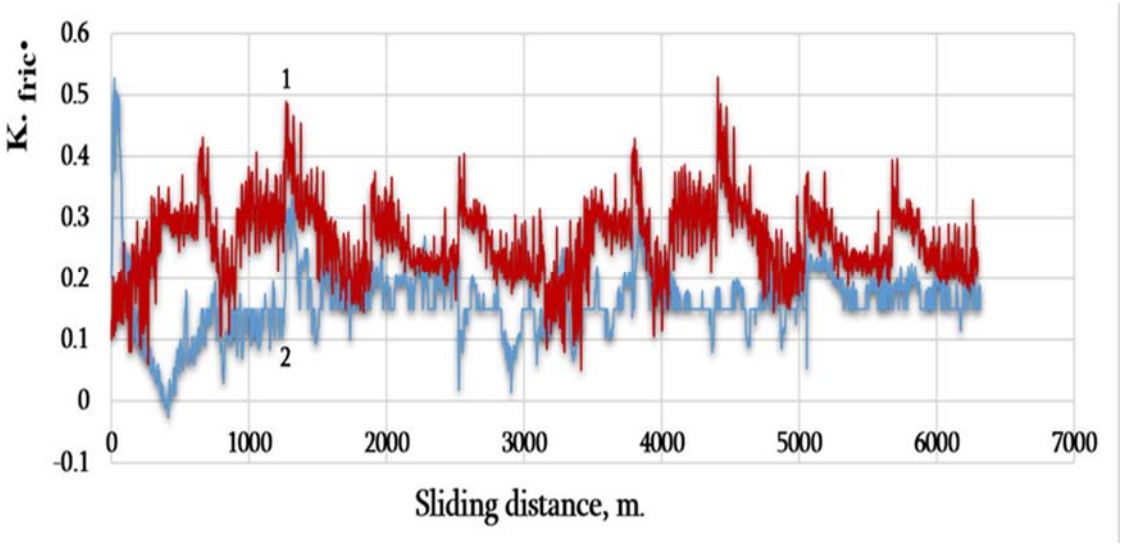

Fig. 5. The friction coefficient of ductile iron
isothermal quenched at 280°C (40% retained austenite)
depending under different contact load:
1- 25N; 2-50N;

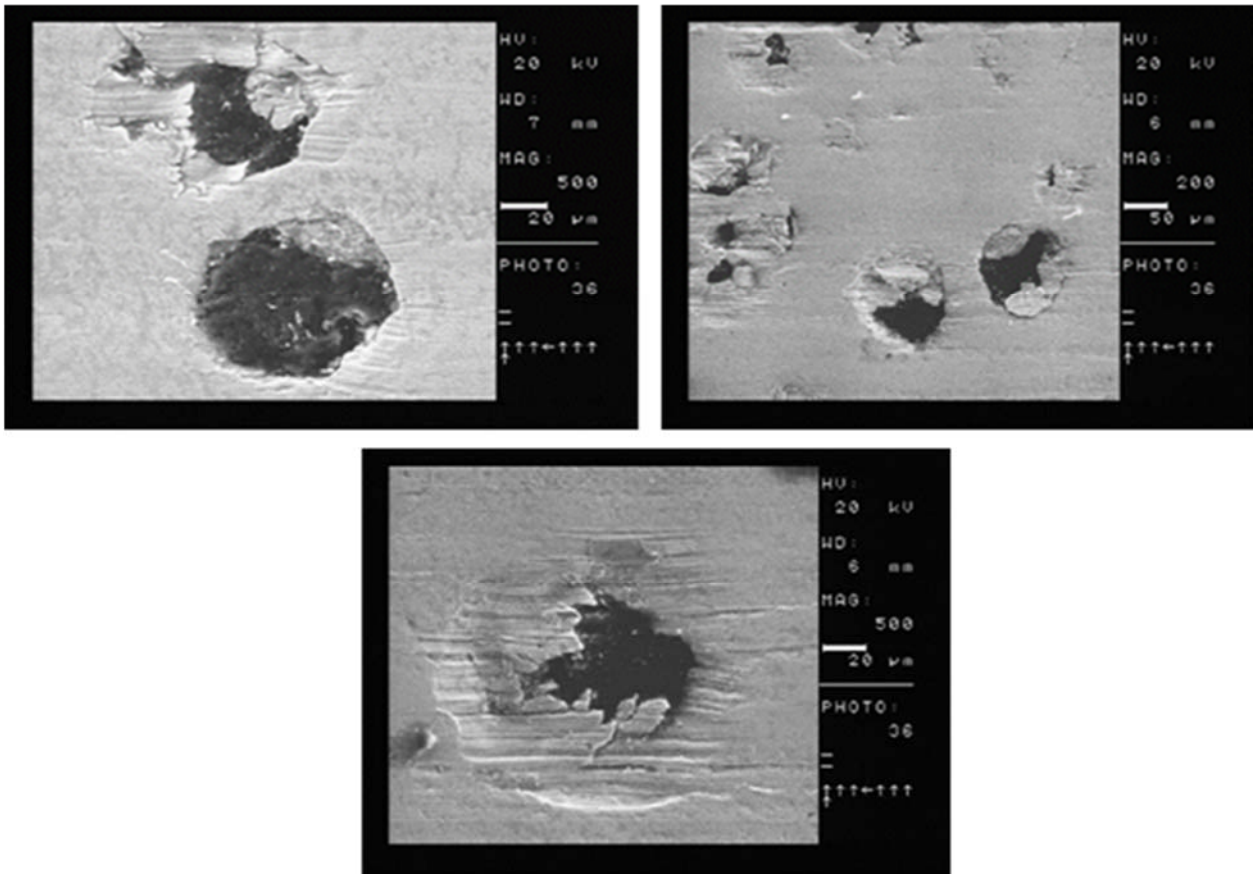

Fig. 6. Results of topographic analysis of frictional surfaces

TABLE 2

CORROSION RATE OF DUCTILE IRONS WITH DIFFERENT METAL MATRIX STRUCTURE

Ductile iron	Aret. %	Corrosion rate, mm/y.
Unalloyed	-	0.08
Boron added and isothermal quenched at 280°C	10	0.015
Boron added and isothermal quenched at 280°C	38	0.019
Boron added and isothermal quenched at 400°C	12	0.024
Boron added and isothermalquenched at 400°C	42	0.028

As shown from the obtained experimental data (Tab.2), the highest corrosion rate was recorded in unalloyed high-strength cast irons.

Bainitic cast irons microalloyed with boron are characterized with significantly lower rate of corrosion processes. At the same time, bainitic cast irons with the structure of lower bainite better resist oxidation processes during periodic wetting with rainwater, which can be explained by a higher density and a favorable state of interphase boundaries.

The highest corrosion resistance is exhibited by isothermally hardened at 280^0C high-strength cast irons with a structure content of about 10-12% of residual austenite. An increase in the amount and not unified distribution of residual austenite is accompanied by an intensification of the corrosion destruction of bainitic cast irons, which, in our opinion, is associated with the formation of galvanic microcouples between the structural components.The same effect is mentioned in investigations carried out independently by two groups of scientists [13, 14], which is in correlation with the data obtained within the prsented experimental works.

4. CONCLUSION

According to the results obtained from the present work, the following conclusions can be made:

- Ductile irons containing up to 10-12% residual austenite in the metal are characterized by a more stable friction coefficient in the process of cyclic frictional loading
- Ductile irons microalloyed with boron with residual austenite content up to 10–12% in the lower bainite metal matrix have the highest corrosion resistance during periodic wetting.
- Microadditives of boron (0.03%) can slow down the corrosion destruction of ductile iron in contact with rainwater.
- It has been established that the supply of water to rubbing surfaces causes a slight decrease in the coefficient of friction.

REFERENCES

1. Bakhshinezhad, H.; Honarbakhshraouf, A.; Abdollah- Pour, H. (2019). A Study of effect of vanadium on microstructure and mechanical properties of as-cast and austempered ductile iron. Physics of Metals and Metallography, 120(5), 441–446.
2. Victor H. Gutiérrez Pérez, A. C. Ramírez, Seydy L. OlveraVázquez and etc (2022). Study of the effects of vanadium and molybdenum on the microstructure of ductile iron (DI) and austempered ductile iron (ADI) and their corrosion resistance, 32, 1–20.
3. Dokumaci, E.; Özkan, I.; Önay, B. (2013). Effect of boronizing on the cyclic oxidation of stainless steel. Surface and Coatings Technology, 232(), 22–25.
4. Górny, M., Tyrała, E., & Sikora, G. (2018). Transformation Kinetics and Mechanical Properties of Copper-Alloyed and Copper-Nickel Alloyed ADI.Materials Science Forum, 925, 181–187.

5. Sellamuthu, P., Samuel, D., Dinakaran, D., Premkumar, V., Li, Z., &Seetharaman, S. (2018). AustemperedDuctile Iron (ADI): Influence of AustemperingTemperature on Microstructure, Mechanical and Wear Properties and Energy Consumption. Metals, 8(1), 53.
6. Batra, U., Ray, S., &Prabhakar, S. R. (2004). The Influence of Nickel and Copper on the Austempering of Ductile Iron. Journal of Materials Engineering and Performance, 13(1), 64–68.
7. Khidasheli N., Gordeziani G., Gvazava S., Tavadze G., Tabidze R., BatakoADL. Influence of Structural Parameters on the Wear Resistance of ADI During Dry Sliding Friction (2022). Global Congress on Manufacturing and Management. pp. 109-116. Springer, Cham.
8. V. Jain, G. Sundararajan, Surf. Coat. Technol. 149 (2002) 21.
9. I. Özbek, C. Bindal, Surf. Coat. Technol. 154 (2002). 14.
10. Бабич В.Е. и др. Актуальные проблемы прочности монография. В 2-х т. Т. 2. / под ред. В. В. Рубаника.– Витебск :УО «ВГТУ», 2018. – 512 с.
11. Zakharov G., Khidasheli N., Gvazava S., Wear behaviour of austempered, ductile iron microalloyed with boron under different contact load by dry sliding wear conditions. (2021). IOP Conference Series: Materials Science and Engineering, 1190, pp. 012004.
12. Guerra L, F.V., Bedolla-Jacuinde, A., Mejía, I., Zuno, J., & Maldonado, C. (2015). Effects of boron addition and austempering time on microstructure, hardness and tensile properties of ductile irons. Materials Science and Engineering: A, 648, 193–201.
13. Li, Xiangrong; Liu, Junbo; Xiong, Ji; Yang, Lu; Gou, Qingshan; Song, Xiangyu; Guo, Zhixing; Hua, Tao; Liang, Mengxia (2020). Wear and corrosion resistant Mn-doped austenitic cast iron prepared by powder metallurgy method. Journal of Materials Research and Technology, 9(3), 6376– 6385.
14. Gutiérrez Pérez, V. H., Cruz Ramírez, A., Olvera Vázquez, S. L., Colin García, E., Sánchez Alvarado, R. G., Rivera Salinas, J. E. Efecto del vanadio y molibdeno en la microestructura del hierrodúctil (DI) y el hierrodúctilaustemperizado (ADI) y suresistencia a la corrosión. (2022). ActaUniversitaria, 32, 1–20.

UDC 621.9.02

THE FORMULA OF DEPENDENCE OF MECHANICAL CHARACTERISTICS OF MATERIALS ON CRYSTALLINE PHASE COMPOSITION IN THE MATRIX

Z. Kovziridze

Georgian Technical University, Institute of Bionanoceramics and Nanocomposites Technology. Georgia, 0175, Tbilisi, Kostava str. 69

E-mail: kowsiri@gtu.ge

Goal. For materials science and generally, for long-term operation of work-pieces in industry the significant role is attributed to dependence of macro-mechanical properties of consolidated body on crystalline phase composition, its dimensions, form, distribution in matrix and the form factor. While working in responsible fields of technology of ceramics and ceramic composites the above referred properties are attributed extremely great role with the view of durability and endurance at the terms of heavy mechanical loads. For description of the resistance of any concrete type work-piece, the crystalline phase plays the greatest role in mechanical strength or deformation of any material. It plays the important role in correlative explanation of materials mechanics and matrix properties. In our case, in the process of destruction of ceramic materials and composites, which will give us exhaustive response to the role of macro- and micro-mechanical properties of materials, the role of a macro- and micro-structural component, that is, of crystalline phase in the process of transition of stable state of materials into meta-stable state is extremely big. Our study aims to develop a formula of dependence of macro-mechanical properties of ceramic and ceramic composites on crystalline phase, the most powerful component of their structure, which will enable theorists and practitioners to select and develop technologies and technological processes correctly.

Method. On the basis of the study of micro- and macro-mechanical properties of ceramics and ceramic composites and the morphology of crystalline phase and the analysis of the study we determined and created parameters of the formula.

Results. The formula covers macro-mechanical properties, that is when the work-piece is thoroughly destructed: mechanic at bending at three and four-point load, mechanic at contraction; among morphological characteristics: composition of crystalline phase and their spreading in matrix, their sizes, form factor; correlative dependence of the above listed properties. Absolutely new definition of a factor of spreading of crystalline phase in matrix is offered.

Conclusion. The created formula is of consolidated nature and it can be used in technology of any ceramic material and ceramic composites. The formula will help practitioners to plan correctly and fulfill accurately all positions of technology of production of work-pieces, to carry out the most responsible thermal treatment process of technology of manufacture of work-pieces; to determine

correlation between mechanical and matrix properties of materials.

Keywords: crystalline phase; macro-mechanical properties; mechanic at bending; mechanic at compaction; factor of spreading of crystalline phase in matrix.

1. INTRODUCTION

Decomposition of crystals takes place in two stages: the first stage is formation of a crack, the second is its growth before the sample is completely decomposed. The speed of this process as a whole can be controlled by the speed of the flow of any stage. The process of decomposition is rather complicated. The influence of those basic factors participating in the decomposition process isextremely important. It is observed that fragile isotropic materials are decomposed when a critical stretching tension is achieved in any direction, as well as critical stress strains are an unavoidable feature for plastic deformations. In a number of cases decomposition is not connected with a crystallographic factor and the crack in the sample develops randomly. If an isotropic solid body extends, stretches under mechanical loadings, then the distance between the atoms will be increased. For this reason we need to put such a load on the sample that will be equal to the dependence of the interatomic binding on the existing distances and the extension of the sample will be consistent with the certain energy required to achieve the elastic deformation of the sample and which must be expended during the decomposition process to increase the surface energy of the system to produce new surfaces in it.

If the specific surface energy is equal to y, then the energy expended by splitting the fractions on the surfaces of the sample, which is equal to one, will be equal to 2y.

A significant proportion of the energy required at the time of decomposition must be accumulated between atoms (or between molecules) that are close directly to the decomposition surface. So, if $6_{av.}$ is the average strain at which the decomposition begins, then $6^2_{av.}/2E$ is the density of the elastic deformation or the hook law is maintained and the value of the elastic modulus is also normal.$6^2_{av.}/2EE$ energy on two planes of atoms spaced from each other at a distance of “a” should be equal in magnitude to the surface energy y. Accordingly we can find the magnitude of the decomposing stress from the equation [1]

$$\sigma_{av.} \approx \sqrt{\frac{2yE}{a}} \approx \frac{E}{10}. \qquad [1]$$

For crystalline substances the magnitude of the elastic modulus of which is at the interval of (1-5) 105 MPa, the theoretical strength is approximately (1-5) 104 MPa.Stretch strains of this magnitude can withstand a varietyof crystal material (Brenner, 1958). Such difference between practical and theoretical data was first explained by Griffith A.A [2.,3]. According to the theory of Griffith-Orowan the difference between the theoretical and real strength in solid materials is a result of the narrowest invisible cracks existed in them, with which there is a strong concentration of tension. So, the stress at which the disintegration occurs is equal to the theoretical strength, although it occurs in some small areas of the sample while the average magnitude of the stress on the sample is not yet large. In calculating the stress concentrations at the

edge of the crack, Griffith used the theory developed by Inglis C.E. [4] for the case of the distribution of stress around a very thin elliptical-shaped cavity.If there is a normal stretching stress $\sigma_{av.}$ in the direction of the 2c main axis of the crack, then the greatest tensile stress at the end of the crackwill be:

$$\sigma_{max} = 2\,\sigma_{av.}\sqrt{\frac{c}{\rho}}, \qquad [2]$$

Where ρis a curvature radius of the crack edge.

The formula shows that if ρ tends to zero, then the maximum stress tends to infinity even if the average stress level is too small.A surface crack on a crystal at a depth of c will create approximately the same concentration of stresses as an internal crack with a magnitude of 2c. Accordingly, Griffith's results are acceptable as for surface cracks, as well as for cracks inside the sample. Orowan later [5] argued that due to physical condition, the radius of curvature could not be equal to zero. At the edge of the crack it should be approximately equal to the distances "a" between atoms. If we put the magnitude of "a" instead of 2ρ and equate the resulting image of the right side of the equation to 1, we get the average magnitude of the direct strain, during which the microscopic tensions at the edge of the crack, with the curvature about the distances between the atoms, reach the theoretical tension.

$$\sigma_{st.} = \sqrt{\frac{yE}{2C}} \qquad [3]$$

According to this theory decomposition of solid materials in which there are cracks and which are acting as concentrators of tension, will take place in the conditionьs of those tensions, which are really observed. These cracks must have the length of 1mkm and the curvature at the crack edge must be about the value of distances between the atoms. According to Charles [6], the fact that the process leads to relatively fast solubility of the substance at the edge of the crack compared to its solubility (which is necessary for gradual increase in crack and increase in stress concentration) is due to the increase in stretching tension at the edge of the crack which leads the process to the relatively strong expansion of the crystal lattice at its edges.At the expense of this, the rate of corrosion increases in this area of the lattice.

2. MAIN PART

Static Fatigue

In addition to the fragile decomposition characteristic of crystalline ceramics, their strength also depends on the load time or the speed at which the applied load is increasing, i.e the load velocity. (Picture 1) [7].

Most ceramic materials have a glassy phase that contains oxidized elements of alkaline elements, and there are rare cases where decomposition occurs slowly.At this time, the dependence of the load on the speed is frequent (Table 1).

Slowly decomposing or static fatigue should generally be considered as a general occurrence with respect to crystalline materials that do not contain a glassy phase.

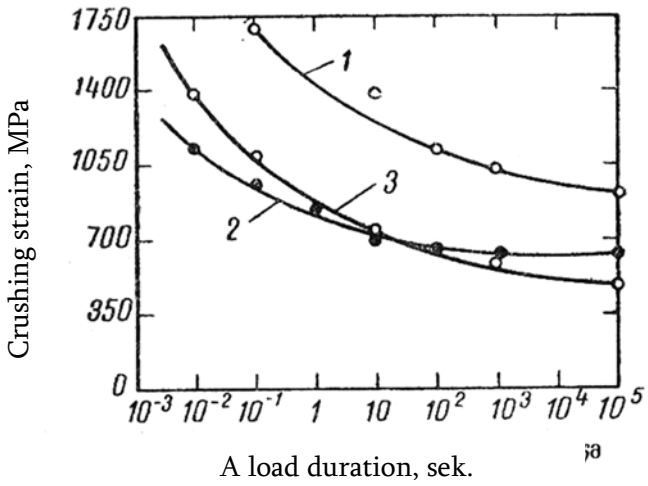

Picture 1. Dependence of the magnitude of the tensile stress on the duration of the load action 1. quartz glass(damp); 2. Porcelain (dry); 3. Sodium-calcium silicateglass (damp)

Table 1

Strength of ceramic crystalline materials on compression or bending -MPa load velocity 0.13 mm / min. In different gaseous environments and at different temperatures

Material	Trial conditions			
	Liquid nitrogen, -195^{0}C	Dry nitrogen 240^{0}C	Water-saturated steam	
			240^{0}C	25^{0}C
Quartz glass (compression)	4 600	4 530	2 570	3 910
Granite (compression)	2 620	1 380	420	1 640
Spodumen (Compression)	6 680	4 020	3 200	2 710
Quartz (compression)	5 720	4 480	2 510	3 670
MgO-Crystal (bending)	2 140	1 870	560	1 000
Al_2O_3-Crystal (bending)	10 700	8 200	4 800	7 730

Influence of microstructure

For most ceramic materials, the role of the microstructure will be mainly influenced by the porous phase. Existing pores reduce the cross-sectional area of the material on which the load is applied and act as tension concentrators. In isolated spherical pores the tension increases twice. Experiments show that the hardness of porous ceramics is reduced and by increasing porosity it changes approximately exponentially [8].[1] We have already proposed the dependence of the macromechanical characteristics on the porous phase [9]. Very significant in it are the dimensions, shape, and defects of Winkelmann and Shotck crystals, such as various types of dislocations and others. In materials such as aluminum and beryllium oxides decomposition can be observed along grain boundaries (Pictures 2 and 3).

Experiments have shown that fine-grained specimens are more durable than large-grained specimens [10,11,12,13], since the length of Griffiths microcracks is determined by the size of the grains (Picture 4). Presumably this phenomenon is related to the formation of tensions at the grain boundaries as a result of anisotropic thermal expansion.1900 degree As a result of burning of aluminum oxide ceramics at 1900^0 C temperature grains of several millimeters in sizecan be produced. Under these conditions, quite large tensions are revealed at the grain boundaries, which can lead to such a large self-cracking of the ceramics that individual grains can be ejected with the tip of a knife.If we assume that half the length of the most dangerous crack for the material will be equal to the grain diameter, then, as it follows from the equation [2], the magnitude of the decomposing stress must be inversely proportional to the square root from the grain size. In multi-layered systems different factors can play a key role in relation to the decomposition types.

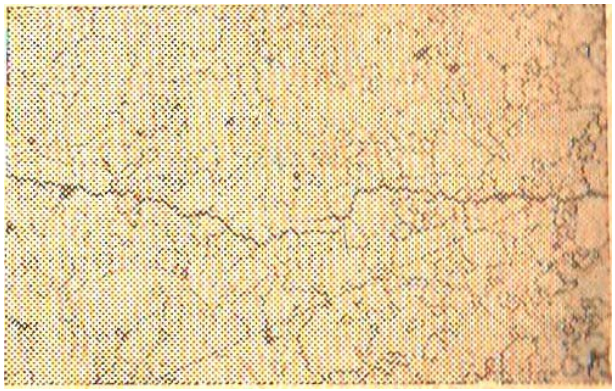

Picture 2. Crack propagation under the influence of thermal shock of aluminum oxide polycrystalline ceramics x150 according to Coble R. L.

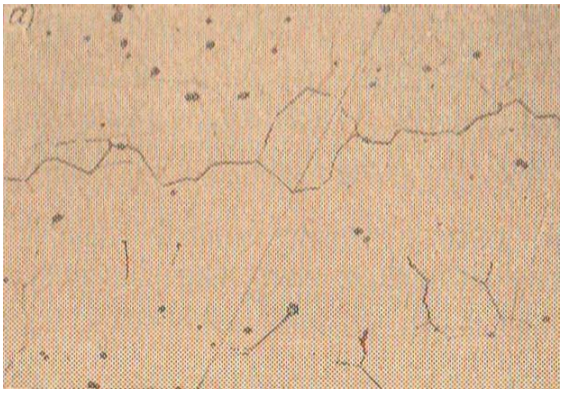

Picture 3. Disintegration of grains along the grain, in large-grained dense aluminum oxide ceramics - anshlif x150

---

[1]exponent - from Latin: exponentis, which means show. Exponential function is the same as representative function y=expx.

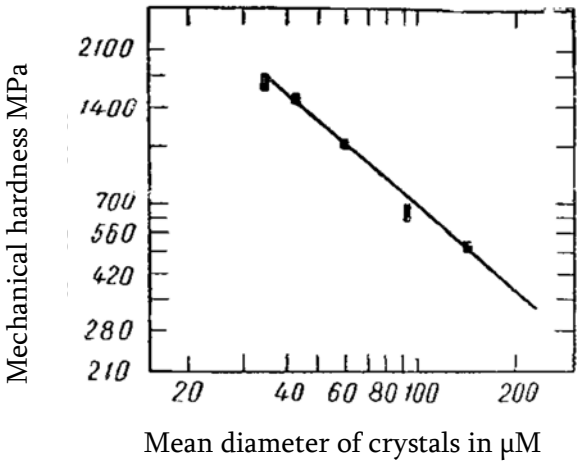

Picture 4. Polycrystalline baked ceramics
Dependence of beryllium oxide strength on grain size

In general, the dependenceofstrength on the formation of stresses on the boundaries of phases is relatively characteristic, which is due to their different thermal expansion coefficients, which can cause formation of internal cracks, which are common in the presence of quartz grains in porcelain [14] (Pictures 5, 6, 7, 8).

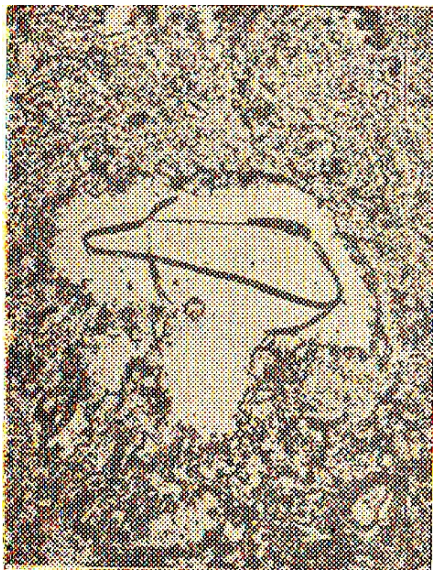

Picture 5. Partially soluted quartz grains in electrical insulation porcelain (poisoning 10sec, at 0⁰C 40% HF-Si. aluminum replica, x2750 according to Landin)

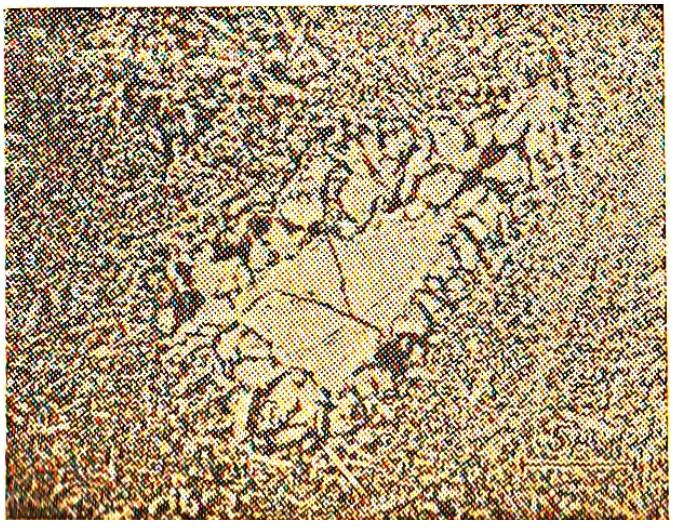

Picture 6. Quartz grain created on the surface with Christobalite inserts (poisoning 20 min., at 100⁰C in 50%-NaOH. Quartzreplica, x3650), according to Landin

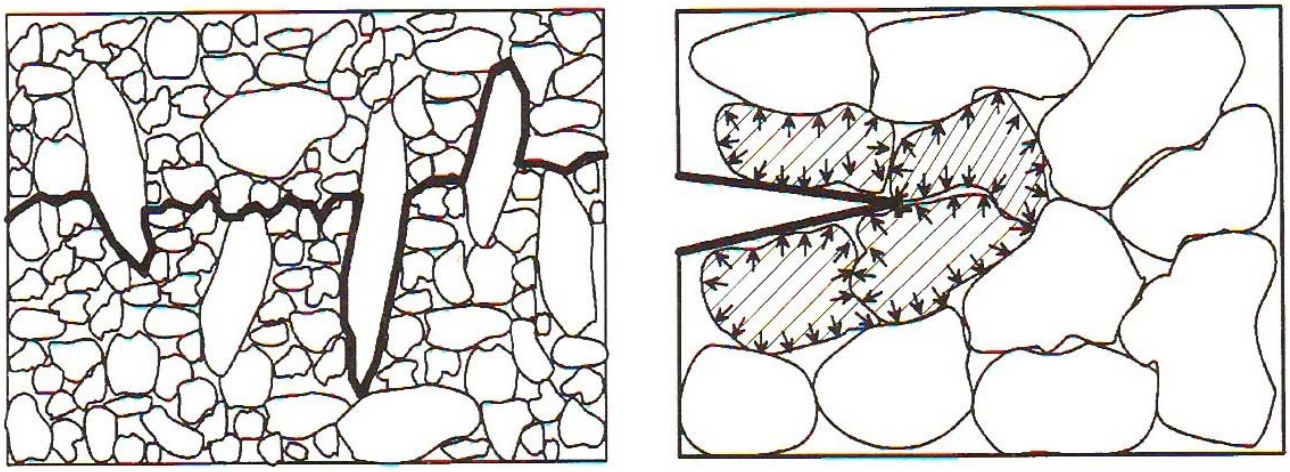

Picture 7. Mechanisms of crack resistance in ceramics.
a - crack bridge in Si_3N_4 in ceramics. b - transforming reinforcement in ZrO_2 ceramics.

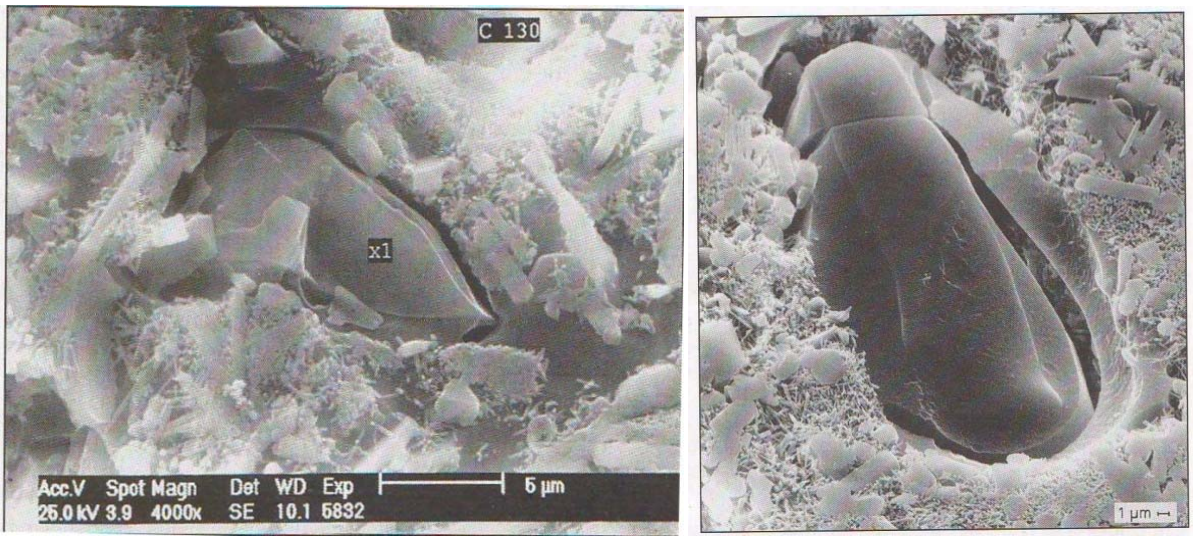

Picture 8. Cracked quartz grains with tension crack
in porcelain containing aluminum oxide

We must promptly consider the second plastic phase as a means of stopping the growth of cracks that have arisen in the fragile phase. This applies, for example, to cermets such as tungsten carbide-cobalt and titanium carbide-nickel.They have high strength and durability, but their disintegration is fragile. Observations have shown that cracks are formed in thecarbide crystals but stop at the phase boundary. This has been confirmed in our studies (Picture 9).

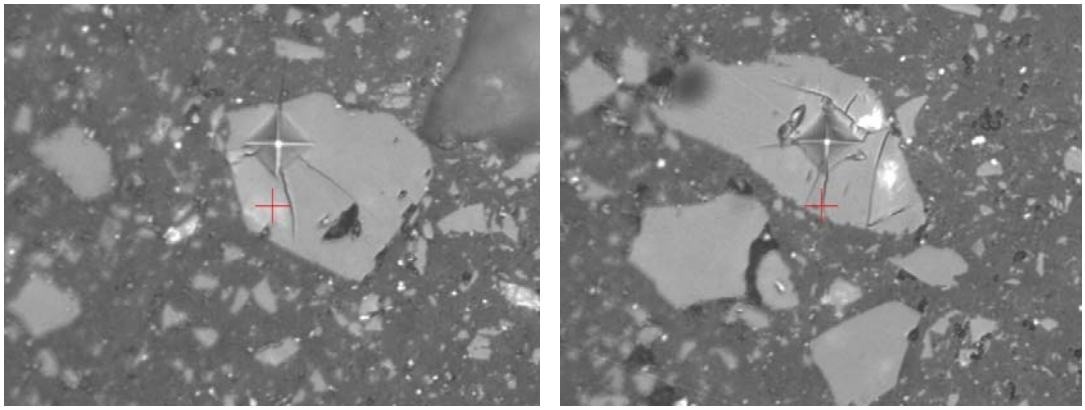

a **b**

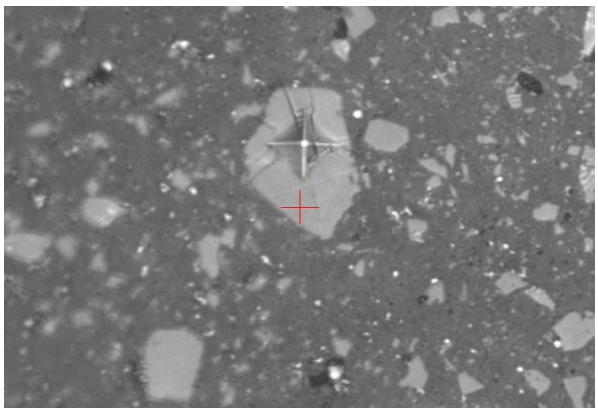

c

Picture 9. a, b, c imprints are taken on a silicon carbide grain

Thermal stability

If the ceramic material undergoes sharp temperature changes - thermal shocks, then they develop significant stresses, which damage not only the matrix, but also the main reinforcing component - the crystalline phase. The higher the strength limit, the higher the thermal resistance is, the lower the elastic modulus and the thermal expansion coefficient. It should be noted here that such a ratio is acceptable when the surface cools down so rapidly that its temperature reaches its final value before the average temperature of the sample changes.This condition is quite goodif the bio criterion $\beta = r_m h / k$ is 20 or more than 20. Herer$_m$-half the thickness of the work piece; h-heat transfer coefficient; k-thermal conductivity.

In general, if we use the second coefficient of thermal stability $R1 = k\sigma_{hardness} (1-\mu) Ea$, where $\sigma_{hardness}$- mechanical strength on bending; μ - Poisson's ratio; E -elasticity modulus; a - thermal expansion coefficient.

$$\Delta T_{fail..} = R^1S\ 1/0.31\ r_{mh} \qquad 4$$

R[1] which is determined by the properties of the material, also takes into account its thermal conductivity, and the maximum temperature change that a sample can withstand without disintegration is inversely proportional to its size.Thus, the situation here is very difficult and requires a more accurate analysis of the conditions under which the material is tested or a detailed study of the operational properties of this finished product.As shown above, the operational properties of any ceramic material and composites are significantly determined by the properties of the main component, the crystalline phase, in it.

It should also be notedthat other phases in the material, such as glass and porous phases, to some extent determine the operational properties of the product. The dimensions of the crystalline compound, their lattice structure, shape, distribution factor in the matrix, the defects in it significantly determine the operational properties of the product. Based on the above, we considered it necessary to offer a formula for the correlation[1] dependence of the influence of the crystallinephase 1 [15] on the mechanical properties of materials:

$$\text{Б}_d = \frac{P.F_{kd}}{.Km\ Kv\ F_{kf}},$$

where: P -is loading MPa; Km–mean size of the crystalsμM; Kv - volumetric share of crystals in the matrix %; F_{kd}–factor of distribution of crystals in the matrixis defined by a researcher. In case of equal distribution = 1, in case of unequal distribution = 0.9. F_{kf}–shape factor of the crystals is taken as the ratio of the largest characteristic size of the crystal to the smallest, which allows us to characterize the shape of a given combination of crystals. Table 2 shows the data of the crystalline phase of the sialone composite obtained by us by metallothermic and nitrogenation processes and then synthesized by hot pressing at 1620^0C, [16], according to which we can calculate the correlation of the mechanical characteristic with the characteristics of the crystalline phase with the formula proposed by us.

$$\text{Б}_d = \frac{470 \times 1}{5 \times 90.6 \times 5} = \frac{470}{2265} = 0.21,$$

where 470 MPa is mechanic of SiAlON composite on bending. In case of compression:

$$\text{Б}_d = \frac{1910 \times 1}{5 \times 90.6 \times 5} = \frac{1910}{2265} = 0.84\ ,$$

Where 1910 MPa is mechanic of the material on compression.

---

[1] (From late Latin - correlation-ratio, relations that do not have a sharply defined regularity of change, since it is impossible to accurately consider the influence of several simultaneously changing factors. It is used to determine statistical and probabilistic regularities in physics, chemistry, technology, it is also used in probability theory, cybernetics, etc.

Table 2

SiC, Al_2O_3 and SiAlON grain sizes and contents in the matrix

Print Picture №	Phase name	Sight area S, μM²	Number of grains counted, n	The greatest Grain Dmax.. μM	The smallest Grain Dmin. μM	Grains Dmid. μM	Phase content %
17	SiC	1740	85	33.3	2,70	4,80	26,8
13	SiC	3225	300	23,0	2,75	4,90	27,6
Average						4,85	27,2
5	SIALON	35500	250	19,6	5,50	8,60	53,0
32	SIALON	8200	200	24,3	5,80	7,50	59,8
26	SIALON	1400	220	21,7	5,30	8,50	59,3
Average						8,20	57,4
5	Al_2O_3	35500	60	2.6	1.27	1.93	6.0
The overall average size of the grains						5.00	

3. CONCLUSION

The formula envisages volume and surface defects of crystals, micro and macrostructural volume and surface morphology of the crystalline phase, their composition in the matrix, their distribution in the matrix and the existing transformations in the process of consolidation of materials as a result of chemical and physico-chemical processes. These properties are determined experimentally. It is important that our formula is applicable to any ceramic materials and ceramic composites such as: metal-ceramic, biceramic, glass-metal-ceramic and others.

Our formula, which shows the dependence of macromechanical or characteristics of the complete decomposition of the materials on the size, shape, distribution, and content of crystals in a matrix, the shape factor of the crystal, takes into account the influence of the most powerful phase of the structural components of the consolidated material on the combination of properties that significantly determine the use and durability of products in industry. In the process of thermal processing extremely important is dynamics of the formation of crystals, their redistribution in the matrix, the formation of the shape, which is shown in our study, takinginto account the physico-chemical processes that take place during thermal aggression.Our formula provides a complete answer to the correlation between the morphology of the crystalline phase of ceramic products and the macromechanical properties and can be used for all types of ceramic and ceramic composites used in advanced technologies, in many fields of technology, household conditions and etc.

REFERENCES

1. Kingery U. D. Кингери У.Д. Introduction in Ceramic. Izdatelstvo literaturi po stroitelstvu. Moskow. 1967 pp. 390-391.

2. Griffith A.A. Phil. Trans.Roy. Soc. London. A221. 163.1920. First International Congress for Applied Mechanics (Delft). 1924. ed. J. Waltman Delft 1925.
3. Griffith A.A. Phil.Trans. Roy. Soc. London. A221. 163. 1920.
4. Inglis C.E. Trans. Inst. Nav. Archit. 55. 1. 219. 1913.
5. Orowan E.Z. Krist. A89. 327. 1934.
6. Charles R.J. Journ. Appl. Phys. 29. 1549. 1958.
7. Baker T.C. Preston F.W. Journ. Appl. Phys. 17. 170. 1946.
8. Z. Kovziridze. The formula for the dependence of macromechanical characteristics on the porous phase. Sakpatenti. Certificate 7276. 2018.03.07.
9. I.I. Artobolevski, Polytechnic Dictionary. "Soviet encyclopedia". Moscow. 1977. p. 572
10. Zviad Kovziridze. Jimsher Aneli. Natela Nijaradze. Gulnazi Tabatadze. Ceramic and Polymer Composites. Monograph. Lambert Academic Publishing. ISSN:978-620-2-06984-7 International Book Market Service LTD, Member of Omni Scriptum Publishing Group. 2017. Germany.
11. Z. Kovziridze. N. Nizharadze. G.Tabatadze. J. Aneli. Ceramic and polymer composites. Monograph. Georgian Technical University. Tbilisi. Georgia. 2016. ISSN 978-9941-20-685-6 http://www.gtu.ge.
12. Z. Kovziridze. N. Nizharadze. G.Tabatadze. N. Darakhvelidze. Sialon and low tungsten composites. Monograph, Georgia Technical University. Tbilisi, Georgia. 2017. ISSN 978-9941-20-808-9 http://www.gtu.ge.
13. Z. Kovziridze. N. Nizharadze. G.Tabatadze. High-strength heteromodular composites. Monograph. Georgian Technical University. Tbilisi, Georgia. 2014. ISSN 978-9941-20-479-1 http://www.gtu.ge.
14. W. Kollenberg. Technische Keramik. Vulkan-Verlag ESSEN. 2004. S. 52. Germany.
15. E.L. Shvedkov et al., Explanatory dictionary of New Ceramics. "Naukova Dumka". Kiev. 1991. page 91
16. Zviad Kovziridze et All. Obtaining of SiAlON Composite via Metal-Thermal and Nitrogen Processes in the SiC-Si-Al-Geopolymer System. Journal of Electronics Cooling and Thermal Control. 2017. 7. 103-122. http://www.scirp.org/journal/jectc USA. Delaware.

UDC 621.9.02

FAILURE STRESS ENERGY FORMULA

Z. Kovziridze

Institute of Bionanoceramics and Nanocomposites Technology, Georgian Technical University, Georgia, 0175, Tbilisi, Kostava Str. 69

E-mail: kowsiri@gtu.ge

Resume: ***Goal***: In the process of exploitation of ceramic composites often we encounter not only high mechanical stresses but also thermal loads and air-thermal shocks. These loads are transformed into failure/rupture stress energy, when strength of work-pieces is less than loads, which develops pluck from the crack top, resulting in destruction of objects. Considering such extreme operation conditions computation of energies which contribute to materials catastrophe seems rather interesting.

Method: The formula parameters were selected on the basis of study and generalization of micro- and macro-mechanical characteristics of ceramic materials.

Results: The formula covers the process of creation of energies as a result of mechanical and thermal loads affecting the work-piece and analyses of mechanisms of impact of these energies on the cracks existing in the material; results of energies affecting the existing cracks as a result of such loads and results of starting of mechanisms of spreading of energies developed inside the work piece, which lead material to the catastrophe.

Conclusion: On the basis of crack development mechanisms the universal relationship of total energy of the work-piece and its mass was established considering crack developing speed under critical stress conditions. Failure stress energy formula has been offered.

Keywords: Crack Development Speed; Failure/Destruction Stress; Mechanical and Thermal Loads; Mass.

1. INTRODUCTION

Material strength implies maximum resistance to external and inner tensions. Distances between atoms in the crystalline lattice and interaction forces between atoms determine theoretical strength of materials. Strength of aluminum oxide destruction at bending, according to the power of bonds between atoms, approximately equals to 50,000 MPa, while majority of technical versions of strength shows 300 -350 MPa and materials characterized by extremely high hardness show 1000 MPa [1].

Such great discrepancy between theoretical and practical strengths is conditioned by the fact that ceramic materials reveal extreme sensitivity to non-homogeneities and structure defects, such

as: inclusions, pores, macro-and micro-cracks. It should be stated that even in case of high technologies it is a very hard problem to avoid such structural flaws. At the morphological study of materials a significant role is attributed to crystalline phase, which is the component that intensifies most the structure. Rearrangement of crystalline phase in the lattice and its sizes exert significant impact on mechanical properties. Fine dispersion dimensions below 5 mcm and their homogeneous spreading increase mechanics of any type ceramic, while their big sizes such as 20 - 40 mcm and higher and unequal spreading in the material mass, decrease not only mechanical but also exploitation properties such as resistance to thermal and air-thermal shocks, electro-and magnetic properties, durability and exploitation at heavy stress conditions, e.g. on power transmission lines, reduction of stress threshold values and others [2] [3] [4]. Vitreous phase compared to the crystalline phase is the weak component of a lattice, but if crystals and pores are homogeneously arranged in it, it acts as connecting and compacting component for these phases. Of course in this case small content of vitreous phase will play a relatively positive role, e.g. at the sintering of solid phases, when volumetric share of vitreous phase is less than 12%.

Similarly, porous phase exerts complex impact on various properties of ceramics. Great significance is attributed to dimension of pores, their volumetric share, form, closed and round form, through or semi-through form.

The more fine-dispersion are pores which are homogeneously spread in the lattice, the stronger is the material; material is durable and resistant to thermal, air-thermal shock, mechanical stress and shocks. Pores markedly affect complex properties of work-pieces. Their rounded forms, small size pores, less than 5 mcm and their equal arrangement increase resistance of ceramics to external loads. When open porosity according to water absorption equals to zero, volumetric share of closed pores in the lattice varies within 0.5 -9 vol. %. As to the invisible micro cracks, according to Griffiths they exist in any thermally treated material [5] [6]. At the terms of mechanical load, thus for example, in water turbines or air-turbines and in flying apparatuses in the process of starting, stress intensities are maximal. At this moment, stress intensities are evident at the crack top and in the critical case the cracks, and especially big size cracks are developed via detachment. At this moment, cracks can be developed by 2000 m/sec speed [7] and it can result immediate catastrophe. In this case critical coefficient of stress intensity—Kic plays the significant rope, which is connected with critical intensity of release of elastic energy, or with decomposition viscosity Gic. At the volumetric stress condition $K^2ic=E\ Gic(1-\mu^2)$, μ , where - μ, is a Poisson coefficient. Stress intensity coefficient (SIC) is a value, which determines normal stress at the $\sigma_y$point, which is located in short distance from r—crack top and expresses local stresses near the crack.

Under the load a body with a crack reaches marginal state of equilibrium, when the crack starts movement or it can move from the place at the slight increase of the given load. In this case stress intensity coefficient will be limiting, critical for this material at the given load conditions. In the elastic body with a crack, if axis is per-

pendicular to the fault direction, SIC in asymptotic approximation will be expressed by $K = \lim \sqrt{2\pi r \sigma y}$ where Kic is a value, that characterizes viscous decomposition of material [7]. Material properties, especially at mechanical loads are determined mainly according to the forms of atom bonds and their inter-distribution in solid body [8].

2. MAIN PART

At the impact of forces of interaction between atoms the crystalline structures are created with strictly ordered distances between atoms. In equilibrium state sum of repulsion and attraction between two neighbor atoms equals to zero (Figure 1).

Displacement of atoms from balanced state becomes possible only at the impact of external forces. Figure 1 shows schematically the sum of F forces acting between two atoms, as the function of a distance "a" from each other. In equilibrium condition atoms will acquire a0 inter-space characteristic for such atoms. In case of displacement by Δa distance, effect of counteraction/resistance is formed that corresponds to the forces for attraction—repulsion. If displacement is small, ratio of the resistance forces and distance between atoms is linear. After removal of load the balanced state is restored, deformation is reversible that is recoverable, relaxed. Thus, most types of materials are linearly elastic till definite limits [9].

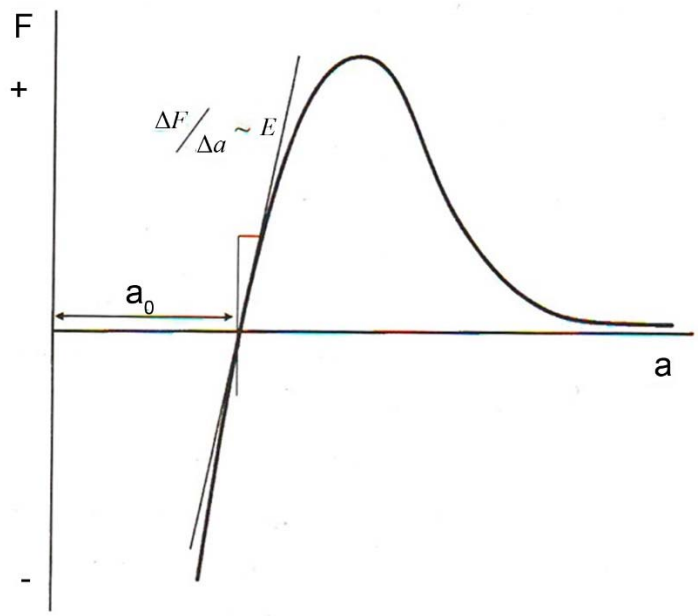

Figure 1. F - force (attraction +, repulsion –; balanced space a_0) that resulted between two neighbor atoms in solid body, at a distance a

For consideration of excess stress and stress displacement around the pore the elliptic form of the pore in the plate (Figure 2) serves as the vivid phenomenon. Elliptic dimensions are defined by

the main axes b and a. Radius of curvature at the external S elliptic point reaches ρ = b^2/a. At this spot stress σs in the direction of the loaded force σ are aches maximum:

$$\sigma S/\sigma a = 1 + 2(a/\rho)^{1/2} \quad (1)$$

According to the above given equation, in case of circular pore at the excess of stress we receive factor 3. Stresses will be higher when curvature radius at elliptic edge is sharp. In case of marginal stress in the ellipsis a crack with the curvature radius ρ = 0 will be created. Stresses in this case will be infinitely large. In reality, such mathematical case can't be encountered since minimal curvature radius equals to the distance between the atoms. In reality immediately at the crack top extremely high stresses are formed, which are close to the theoretical hardness [10].

2.1. Stress Intensity Factor

Crack curvature radius ρ at the crack top is very small and because of it $(a/\rho)^{1/2}$ will be rather high. Thus in the Equation (1) the summand 1 may become insignificant. Excess of pressure at the crack top is approximately proportional of external pressure σa (distant field of compression) on the crack-containing material as well as of a root from crack length a. This law leads us to determination of the stress intensity coefficient Ki, as tension measure at the crack top section.

$$Ki = \sigma\sqrt{aY} \quad (2)$$

Geometrical factor ϒ considers geometrical dimensions of crack-containing work-pieces and stress distribution in it. This factor is computed by means of numerical method according to various type loads and it is given in standard tables. Stress intensity factor index shows crack load regime, where the most risky section for material decomposition is loading state that is expressed by modus 1. In distinct from it, load at the crack sides is given by modus II, while load as a result of twisting - is given by modus III. II and III modi in special cases are of technical significance (e.g. composite materials or coatings). In case of monolith materials practically only modus I is used [11].

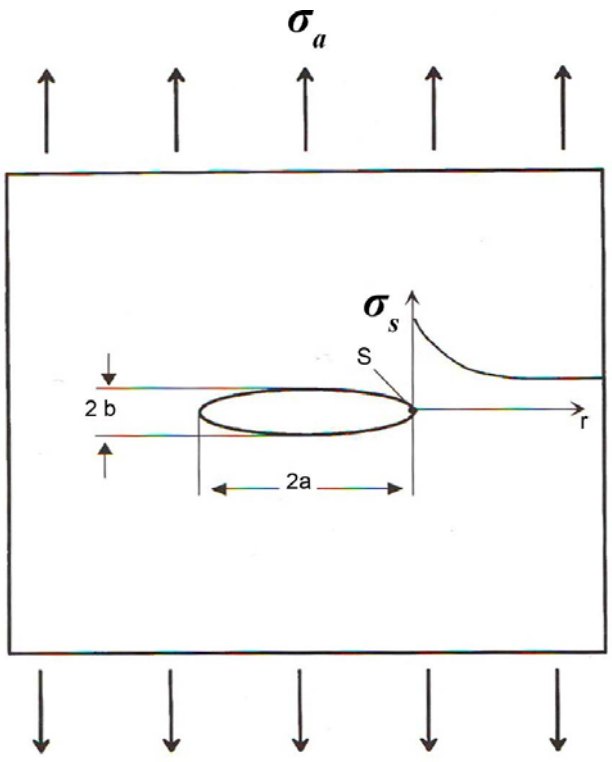

Figure 2. Excess stress σ_s around elliptic pore, in model plate.

Stress spreading near the crack top is given by polar coordinates (Figure 3), where r-is distance from the crack top, and φ is the angle.

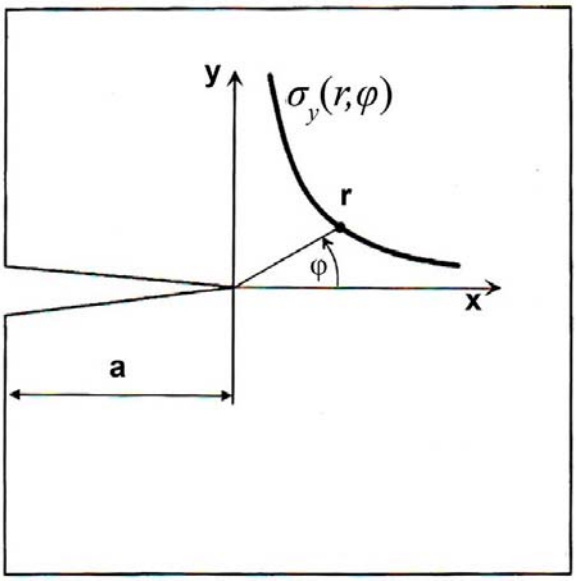

Figure 3. Stress distribution at the crack top section

2.2. Crack Propagation at the Terms of Critical Loading

Cracks start to grow slowly when stress intensity factor acquires critical value, that is, when the crack tolerance in the process of loading and resistance energy are minimal and when even minimal increase of any load will turn into decomposition energy. Such process of loading results in increase of crack sizes. This phenomenon is called preceding critical period of crack increase [11]. To describe this process we consider crack increase speed, as Ki function of stress intensity factor. Many materials act so, as we see on the typical v-Ki curve (Figure 4). Crack increase at the Ki_{th} threshold value is not registered. At the increase of loading, initially we observe slow acceleration of crack increase (mostly at 10^{-12}m/sec), which alongside with the increase of the stress intensity factor in the first section it is increased within the frames of ratio regularities [10].

$$V = AKIn = A^* \left(\frac{K_i}{K_{ic}} \right) \qquad 3$$

Where K_{IC} is coefficient of stress intensity factor. Parameters A (respectively A*) and n depend on the material, temperature and environment. Correspondingly, for crack propagation speed at the 1 section, we consider environment diffusion at the crack top and the available stress. For most ceramics the exponent n > 15. For some materials section II is acceptable, when crack spreading speed stops growing. Crack speed is so high, that increase of the stress intensity factor does no more affect crack speeding, and the diffusion, as the process that determines acceleration (that runs very slowly) slows down.

When stress intensity factor overcomes crack resistance (section III), the stress disintegration energy develops and rapid growth of the crack occurs by its detachment and the process practically reaches the top speed. It is namely in this moment that crack spreading speed develops that equals to approximately 2000 m/sec (Figure 4, section III). When we deal with the stress permanently (thus e.g. on power transmission lines, on electro-technical devices or at the operation processes) and the crack slowly increases, the stress intensity factor will always grow. In this case crack increase in material life period is always permanent. When at the late stage the section II is achieved the life-duration somewhat decreases, and technically it loses significance for relevant evaluation of life duration.

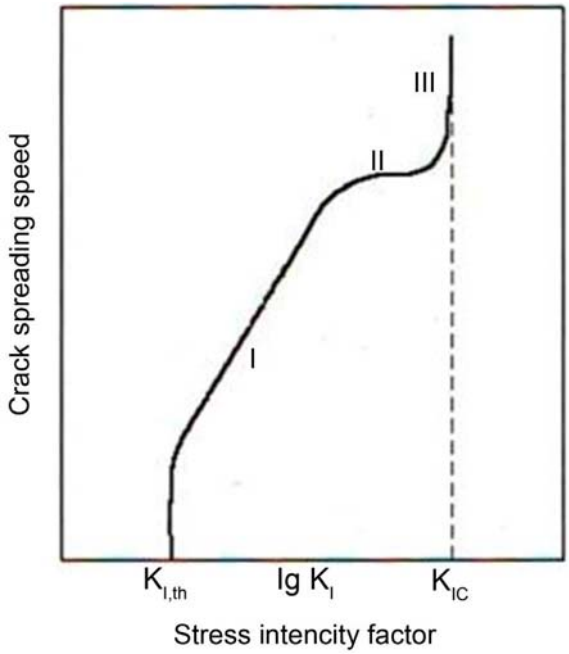

Figure 4. Typical graph of crack spreading speed according to stress intensity factor, when pre-critical state of crack increase (v-K-curve) develops. On the horizontal – stress intensity factor; on the vertical—crack increase speed.

2.3. Criteria Evaluation of Resistance to Thermal and Air-Thermal Shocks in the Process of Stress Distribution in Materials

Materials, which operate in transitional/critical temperature fields and under high mechanical loads, are characterized by thermal stresses and deformations in the conditions, when their mechanical and chemical properties don't suffer significant changes. The problem is complicated since as a rule, alongside with thermal stresses mechanical stresses are acting from external loads, which contribute to development of high energies in materials. In this case developed energies exert marked impact on cracks and where there is a weak section in the lattice and there are cracks there, their development occurs via detachment plucking. In such cases catastrophic destruction of material is inevitable [12]. Thermal stresses can be formed mostly: at the restricted thermal expansion of a body, at equal spreading of temperature in polycrystalline body with anisotropic crystals, or in isotropic body which up to loading was fixed by limiting forces, at temperature gradients in the body, by cyclic changes of body temperature, when it is mechanically well fixed, by single non-standard thermal heating [13] [14] [15] [16]. At long-term operation conditions almost complete relaxation of thermal stresses takes place; therefore at gradual changes of temperature danger of destruction is caused mainly by mechanical loads. Thermal cyclic stresses (thermal fatigue and drastic changes in temperature—thermal shock) are the main causes or factors for material destruction. Thus, testing in strict conditions provides relatively wide sphere of exploitation of workpieces. It is necessary to take into consideration

inner stresses, according to their locality [17].

1) Zero order stress is formed in the system of reciprocally connected bodies, due to unequal thermal impact on those bodies or because of different linear temperature expansion coefficients.

2) First order (microscopic) stresses, which are balanced in the spheres of body sizes, are conditioned by non-homogeneity of temperature fields or by body properties.

3) Second order (microscopic) stresses can be formed in case of absence of the first order stresses and they have independent values.

4) Third order defects (sub-microscopic) can't be called stresses, since stresses are measured in the least zones spheres and they are insignificant. Such defects are revealed in the distances between atoms and their study is difficult.

Identification of faults in separate grains or at their borders and then complete destruction of the material is conditioned by accumulation of defects, which are formed at the effect of thermo-structural stresses as a result of multiple cycles of high temperature impacts or during high mechanical stresses (Figure 5).

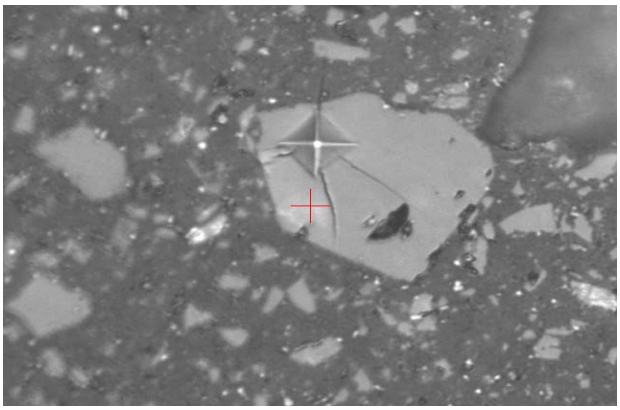

(a)

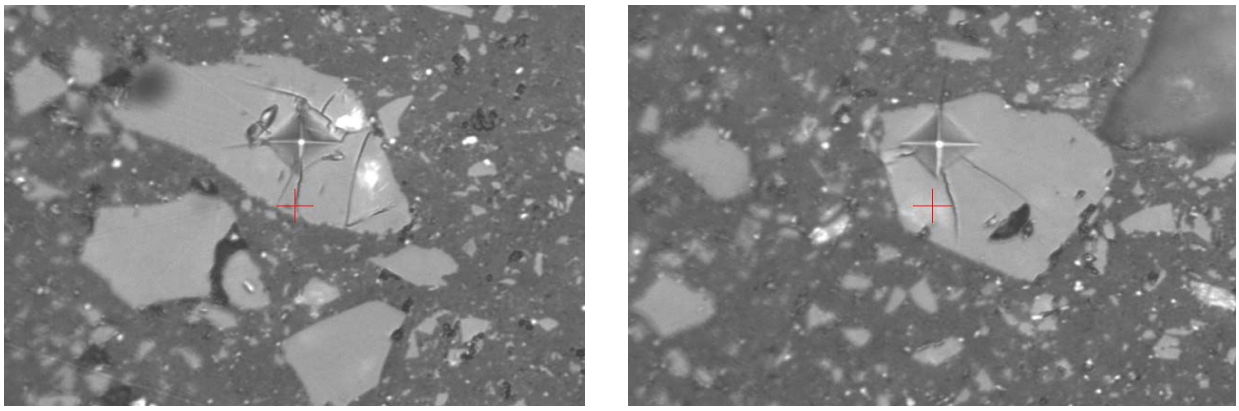

(b)(c)

Figure 5. Morphological pattern of hot-compressed (1620˚C) Si-Al-O-N composite. Micromechanical indent is made in silicon carbide grain

Dynamic micro-hardness and elasticity module of the obtained Si-Al-O-N material were determined on the modern dynamic micro-hardness tester "rome DUH-211S" according to the demands of ISO-14577 International standards, used for determination of mechanical characteristics of solid body surfaces (micro-hardness, elasticity module). Results are offered in Table 1 [18] [19].

Phase composition (%) of Si-Al-O-N composite according to the morphological pattern is: Si-Al-O-N –62.6; silicon carbide –28.0; aluminum oxide –6.2; porous phase –3.2. Composite was obtained at the first stage by metal-thermal and nitriding processes at 1450˚C. Then the composite was dispensed in Teflon mill and was hot-compressed at 1620˚C.

Table 1 offers results of tests of SiAlON composite specimens, hot compressed at 1620˚C. Indent was obtained in SiC grain, they were taken several times and results are given in Table 1, where average hardness is HV: 19.70 GPa. Dynamic hardness DH—8.9 GPa, elasticity module E—145 MPa. Table 1 offers results of tests of SiC grains of the composite microstructure. Indentation was performed in Sic grains at 2 N loading.

Borders of indents taken from silicon carbide grains are sharp (Figures 5(a)-(c)). Crack that is formed as a result of indenter load on the grain doesn't spread beyond the grain limits. Matrix, due to its high mechanical properties and energy dissipation, subdues crack spreading and composite hardness retains its value. Such large grains are few and speaking about mechanical properties of the material according to such grains should not be relevant, since increase of their dispersion rate is not a problem, while it gives interesting picture for the purposes of investigation. Especially interesting is Figure 5(b). In this case a crack on the right side of the indent develops so intensely and by such high energy, that the crack spreads up to the matrix, attacks energetically the matrix, returns back, transects diagonally the grain and collides again with the matrix from the other side of the grain, but fails to destruct it. It should be stated that the crack retains high energy and develops diagonally on the other side of SiC grain, and losing energy it fails to reach matrix. The crack that is developed from the lower edge reaches matrix, but energy dissipation in the grain and critical coefficient of matrix stress intensity—Kic are so high that the crack disappears at the matrix. Figure 5(a) and Figure 5(b) shows vividly directions of crack propagation. As is known, in this case too Kic has great significance for material crack-resistance, since after detachment, the flaw develops approximatively by 2000 m/sec speed and at this moment, material resistance is defined not only by the speed of shock on the crack matrix but also by Kic value of the material.

Table 1

Technical characteristics of Si-Al-O-N composite. (a) "Testcondition-SiAlon-200"; (b) "Test result". (a) Test mode Load-unload

Test mode	Load-unload		
Sample name	SiAlon-zv	Sample No.	#1
Test force	200.000 [gf]	Minimum force	0.200 [gf]
Loading speed	1.0 (7.1448 [gf/sec])	Hold time at load	5 [sec]
Hold time at unload	3 [sec]	Test count	21
Parameter name	Temp	Parameter	20
Comment	21.06.17-SiAlon-zv-200; DHV5-3		
Poisson's ratio	0.190		
Cf-Ap, As Correction	ON	Indenter type	Vickers
Read times	2	Objective lens	50
Indenter elastic	1.140e+006 [N/mm2]	Indenter poisson's ratio	0.070

(b)

SEQ	Fmax	hmax	hp	hr	DHV-1	DHV-2	Eit	Length	HV	Data name
	[gf]	[um]	[um]	[um]			[N/mm2]	[um]		
1	200.710	4.7107	1.9264	3.1017	442.157	2643.803	7.211e+004	15.792	1492.537	SiAlon-200(2)
2	200.786	4.2612	1.6795	2.7414	540.546	3479.868	8.707e+004	14.621	1741.886	SiAlon-200(4)
3	200.800	4.9636	1.7638	3.3296	398.419	3155.263	6.588e+004	16.959	1294.659	SiAlon-200(5)
4	200.674	4.5307	1.7788	3.0421	477.884	3100.234	8.083e+004	15.644	1520.484	SiAlon-200(6)
5	200.675	4.3294	2.1587	2.9575	523.381	2105.199	9.024e+004	15.498	1549.415	SiAlon-200(7)
6	200.662	3.5295	1.5855	2.1773	787.444	3902.198	1.254e+005	16.595	1351.275	SiAlon-200(8)
7	200.661	3.6147	1.8441	2.4494	750.723	2884.448	1.349e+005	17.179	1260.907	SiAlon-200(9)
8	200.738	3.0333	1.1085	1.7530	1066.516	7985.353	1.660e+005	12.866	2248.651	SiAlon-200(10)
9	200.959	2.8595	1.0929	1.5884	1201.396	8224.728	1.857e+005	12.134	2531.125	SiAlon-200(11)
10	200.866	3.0653	1.3375	2.0446	1045.024	5488.768	1.924e+005	-	-	SiAlon-200(12)
11	200.737	3.1154	1.3372	2.0317	1011.028	5488.160	1.790e+005	-	-	SiAlon-200(13)
12	200.960	2.5787	1.1425	1.5447	1477.302	7525.888	2.536e+005	12.135	2530.738	SiAlon-200(14)
13	200.923	2.7215	1.1113	1.5055	1326.134	7952.513	2.077e+005	11.989	2592.358	SiAlon-200(16)
14	200.501	2.8549	1.0966	1.5509	1202.544	8150.998	1.824e+005	12.135	2524.953	SiAlon-200(17)
15	200.497	3.4966	1.3136	2.2145	801.640	5679.626	1.320e+005	-	-	SiAlon-200(18)
16	200.702	2.9626	1.1801	1.6771	1117.798	7044.719	1.729e+005	12.428	2409.746	SiAlon-200(19)
17	200.589	3.4541	1.4444	2.0858	821.888	4700.234	1.288e+005	14.474	1775.634	SiAlon-200(20)
18	201.195	3.0666	1.0307	1.5932	1045.886	9257.288	1.515e+005	11.698	2726.384	SiAlon-200(21)
Average	200.757	3.5082	1.4407	2.1882	890.984	5487.183	1.449e+005	14.143	1970.050	
Std.Dev.	0.174	0.738	0.346	0.611	324.195	2330.548	52250.109	2.028	548.126	
CV	0.087	21.043	23.994	27.907	36.386	42.473	36.057	14.341	27.823	

Dynamic hardness (DH) is determined according to the indenter load value and the depth of its indentation in the material in the process of testing and its value is computed by the formula $DH = a \times F/h^2$; where a - is a constant value and depends on indenter form; for Vicker's indenter a=3.8584. Advantage of the method compared to measuring of common static, that is, linear dimensions of indents (diagonal) is that it covers plastic, as well as elastic components. Results of measuring don't depend on indent sizes, loads and non-homogeneity of elastic recovery.

Dynamic hardness was determined in load-unload regime before elastic relaxation took place. For each concrete load seven readings were taken, two marginal values were discarded and remaining five values were averaged. Relevant micro-hardness values were determined automatically. Hold-time at maximum loading equaled to 5 sec, at the end of unloading - 3 sec. (Figure 5).

Indentation was performed in sample matrix, which consisted of B-SiAlON. As a result of testing its average dynamic hardness equaled to, DHV=8.9 GPa this is a rather high value.

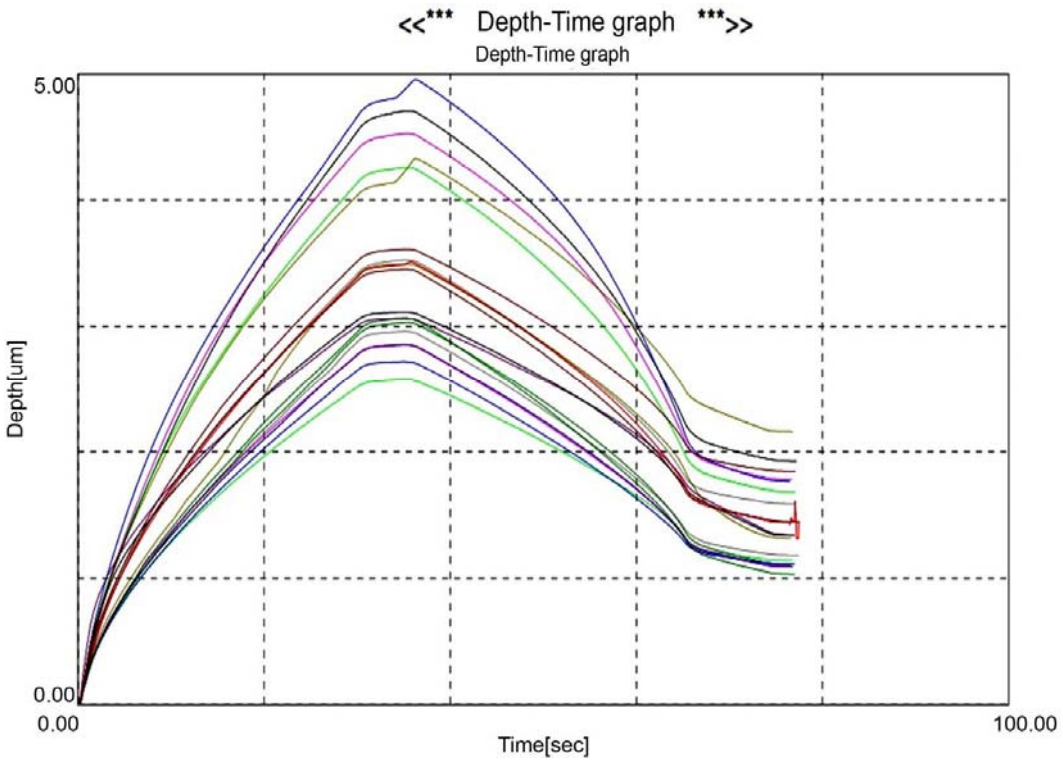

(a)

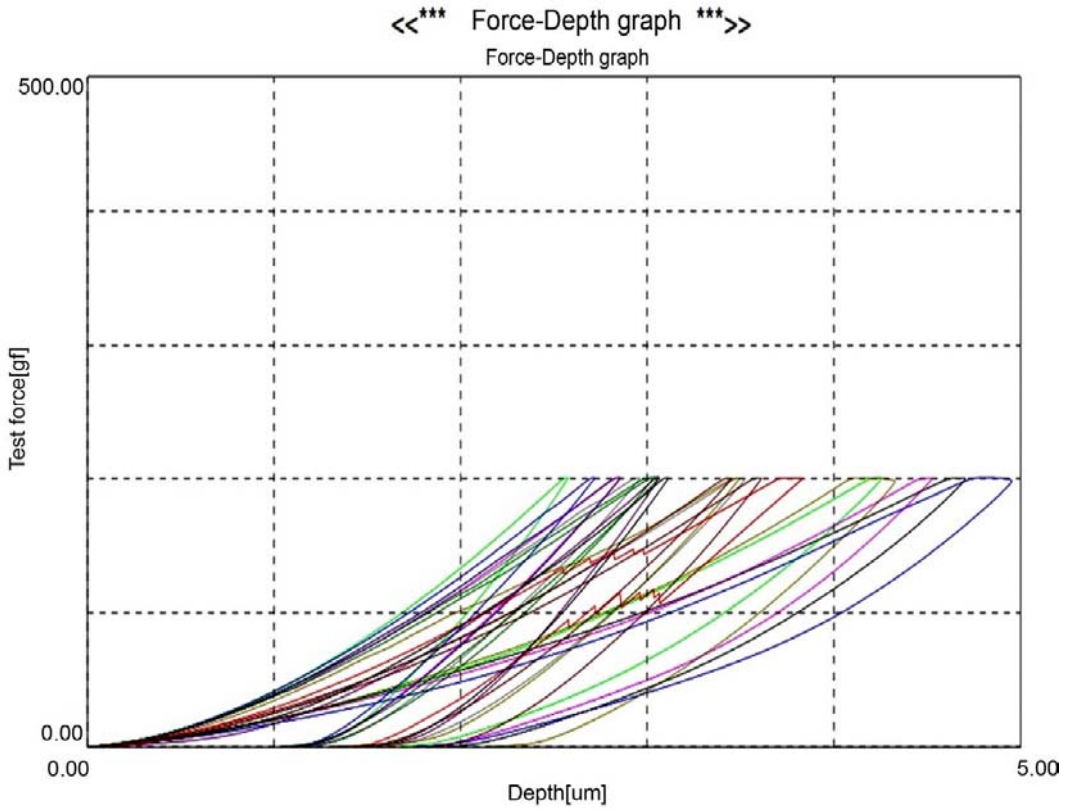

(b)

Figure 6. Micro-mechanical properties of Si-Al-O-N composite at 2 N loading: (a) indenter depth-time dependence; (b) indenter force-depth graph.

From load-unload dependence graph (Figure 6) we determined elasticity module value by determination of rigidity $S = \left(dF / dh\right) h - h_{\max}$. It is a tangent of load-unload graph at the initial point of unloading. A device determines elasticity module of tested material, and its average value in case of our sample equals: E=145 GPa (Table 1). Patterns of indents conform well to graphical data given in Figure 6. Depths of all imprints differ from each other and they vary from 2.5 to 5 μM. Probably for this material 2 N load is somewhat big than optimal load. Figure 5 confirms it. Silicon grain acquired such high energy from diamond pyramid that the crack managed to transect the whole width of the grain several times, because the crack received high energy and detachment was realized from the crack top by the energy that exceeded critical stress intensity. The same was proved at the application of test force (200 g approximately equals to 2 N) at taking indent depth (Figure 6(b)). In this case too indent depths for 18 tests are different and they vary from 2.5 to 5 μM.

Thermo-structural stresses in the process of changes of temperature fields can be induced: by

thermal expansion anisotropy of even only one phase, by anisotropy of dilatation of non-cubic crystalline lattice of materials, by difference in thermal linear expansion of adjacent phases in heterogeneous system, phase transformations, which are accompanied by specific volumetric changes of phases. Methods of quantitative evaluation of resistance to thermal shocks provide mainly determination of resistances to the first order thermo-elastic stresses, which are formed in elastic bodies and in which there are no plastic deformations and phase transformations [20]. If stresses are lower than material hardness, a body will be stable to thermo-shocks [12] and the resistance of such bodies to thermal shocks can be evaluated by the ratio of hardness limit to maximum thermal stress:

$$R = \delta a / a' E \qquad (4)$$

where R - is the factor of resistance to thermal shocks, δ - is mechanical strength of the material at bending, a - is thermal coefficient of linear expansion, E - Young's module, a′ – λyC—material's temperature conductivity, λsd—heat conductivity, y - density, C - specific heat capacity.

The formula doesn't consider sample form, size and dependence of resistance to thermal shock. For real evaluation it is necessary to consider impact of body dimensions.

$$R = \delta \Big/ \left(Ea\beta \left(Tk - To \right) \right) \qquad (5)$$

where *Tk* and *To* - are final and starting temperatures of a body, $\beta = r_m h / \lambda$ and $\beta = \delta h / 2\lambda$ - the sphere and infinite plate, *h*—heat transmission coefficient between the body surface and environment. According to Kingery's opinion, physical properties of material don't suffer changes at alteration of temperature in Δ*Tdestr*. Interval and he recommends the following definition for thermal-shock factor:

$$R' = 2\delta_{destr} \cdot \left(1 - \mu\right) \Big/ Ea = \Delta T_{destr} / B \qquad (6)$$

where B factor depends on body geometry, δ_{destr} - depends on mechanical strength of the material at stretching and μ—Poisson coefficient.

Kingery, Buessem and others [21] [22] [23] recommend that at various conditions of thermal loading, at the evaluation of material resistance to thermal shocks it is necessary to use various criteria. They offer the below given criterion for the study of heat transition conditions, in the process of cooling by water:

$$R = \delta_{bend} \cdot \left(1 - \mu\right) \Big/ 3Ea \qquad (7)$$

when relaxation periods significantly exceed possible service period of work-pieces, no significant thermal stresses occur and selection of materials is based on their elasticity properties, that is on the criteria

$$R' = \delta \left(1 - \mu\right) \Big/ EaR'' = R'\lambda R''' = E/\delta^2 \left(1 - \mu\right)$$

Where R' —is the criterion, which defines material resistance to the formation of cracks in the process of thermal shocks, R'' - is the criterion, which evaluates ability of the material to resist thermal loads, at small values of heat-exchange coefficient; R''' - is the criterion, which defines material resistance to propagation of already formed cracks.

The offered data enable us to conclude that high mechanical strength and heat conduction together with low elasticity properties and thermal expansion provide high resistance of materials to crack formation and such ceramics

can work at high temperature gradients and at high temperatures.

For electro-technical products synthesized by us we used Harcourt's method [2] of cycle loading. Cyclic heating was started at 140˚C, at 20 min hold-time at the end temperature; then it was kept on water bath at 17˚C for 10 minute. The cycle was repeated every 20 min. Plate sizes were $50 \times 50 \times 8$ mm. Results are given in Table 2.

Analysis of the table shows that barium-containing electroceramic synthesized on the base of barite and geopolymers enables us to conclude that celsianceramic B1, with 93% celsian phase, sintered at various temperatures, in definite regimes, with zero open porosity, is resistant and stable than B3. B1 is characterized by high value of thermal resistance - 480˚C. Apparently it is associated with the low coefficient of dilate, which conditions high resistance of work-pieces to thermal shock and correspondingly resistance to stress distribution. In this material concentration of barium and aluminum silicates is low and it amounts to only some percents and their negative impact on resistance to thermal shocks is insignificant. Apparently lower rate of resistance to thermal shocks that is shown by B3 ceramic is conditioned by its multiphase composition: celsian $BaO{\cdot}Al_2O_3{\cdot}2SiO_2$, mulite - $3Al_2O_3{\cdot}2SiO_2$, corundum - Al_2O_3 and vitreous phase, which is more in B1.

Various expansion coefficients of the above referred phases factually exert negative impact on thermal resistance of the material (Table 2). Material structure, its anisotropy and homogeneity determine mostly the rate of thermal resistance. Significant criterion of the resistance to thermal shock of the materials is the presence or absence of closed pores at zero open porosity in consolidated work-piece. They are apt to create thermal flaws in the material on the heated surface. Closed porosity at 1400˚C, is somewhat higher at 1450˚C and 1500˚C (Table 2), which is reflected on the criterion R'. Lower thermal resistance of B3 compared to that of B1, proves indirectly crack formation at the borders of different phases [20]. In the ceramic B1, which is mainly mono-phase one, from 1400˚C, up to 1500˚C and when open porosity is zero, elasticity module and Poisson coefficient suffer insignificant changes (Table 2). Mechanics at plasticity and thermal conductivity of the material sintered at 1500˚C suffer definite decrease which is reflected in R' criterion, which is determining for material evaluation, at the conditions of its exploitation when we pursue to avoid crack formation. It appears that growth of sizes of the closed pores makes impact on these processes. Relatively higher stability of the given properties of the material B1 enables us to think that B1 can be used in the conditions when creation of the cracks which don't affect negatively the integrity of the piece, don't hinder its using [12]. For evaluation of quality of this material we offer the criterion, the value of which at various temperatures is stable than that of B3 (Table 2). The reason of this, according to our opinion is poly phase state of the latter, B1. Generally, high values of the criterion for both materials refer to the fact that at thermal loading they accumulate less energy, which determines lower rate of their decomposition. It should be stated that analysis of ceramic properties is very difficult, because rupture occurs not only thanks to one mechanism, but because of

some absolutely different phenomena at various conditions. The situation is complicated by the fact that one and the same material suffers decomposition differently, depending on stress value, load velocity, prehistory of specimens, environment conditions and temperature. Disregard of any factor will lead us to the significant error. Figure 7 offers curves of material decomposition at various loads.

Table 2

Resistance to thermal shocks of barium containing ceramics

Index of materials, and burn temperature, T °C	Open porosity, %	True porosity, %	Compactness ρ g/sm^3	σ, MPa.	A, 10^{-6} °C^{-1} 20 -900	E, GPa.	μ	R' τ	R'' BT/μ	R''' 10^{-4}M ^{2}/kg
B1 1410	0	14.2	2.99	66.4	4.1	71.32	0.283	163	210.3	225.6
B1 1450	0	7.8	3.03	78.7	4.1	74.59	0.212	161	164.3	220.0
B1 1500	0.1	9.8	2.96	59.3	4.1	72.20	0.280	144	185.8	285.2
B3 1410	0.0	-	2.60	78τ.6	4.1	69.35	0.233	220	420.2	172.9
B3 1450	0.0	-	2.52	56.0	4.1	79.22	0.258	128	244.4	340.0

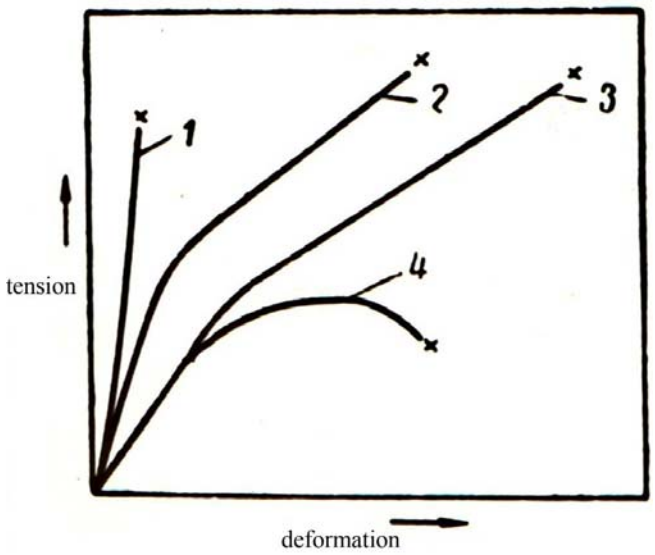

Figure 7. Brittle and plastic decomposition; (1) Brittle decomposition; (2) Plastic decomposition, test at twisting; (3) The same test for stretching; (4) Nominal hardness at rupture

According to the above stated, while discussing the properties of ceramic materials and composites, integration of rupture stress issues is a very hard problem because of coincidence of complex processes in materials. This is why we considered proper to offer the characteristic of rupture stress which will comprise all those conditions and properties which will take place in the process at critical loading of the work-piece and the rupture will be inevitable. It can occur in the cases of external energy charge on the work-piece and as a result, accumulation of energy in the piece, because of thermo-structural changes and external mechanical stress distribution. The formula of decomposition stress energy offered by us is:

$$E_{td} = m * a_{c.p}.$$

Where E_{td} -is energy decomposition tension; m - mass; a - speed of crack propagation.

Decomposition stress energy [1]E_{td} equals to the product of m-mass and crack propagation speed - $a_{c.p}$.

In our case a sample of electro-technical material had a form of a rod, and it had the following sizes:

Length l=110 mm; width b-20 mm; height a=10 mm. Mass of a rod of such sizes that was sintered at 1450˚C - equaled to 45.5 g. The work-piece was fully consolidated by zero open pores. If we admit that in the process of decomposition velocity of crack propagation by its dependence on stress intensity factor (from critical state) on the v-k curve is in the third section (Figure 4), where its propagation takes place by detachment from the top and velocity equals to approximately 2000 m/sec, according to our formula decomposition stress energy will be:

$$E_{td} = 45.5 \times 2000 = 91kj$$

Thus, if we define universal connection between total energy of the work-piece and its mass, we'll receive formula of rupture stress energy offered by us.

3. CONCLUSION

The formula [24] offered by us describes transformations of impact of energies developed as a result of external mechanical stresses and thermal and air-thermal shocks on the work-piece into internal energies in the work-piece. These affect the defects existing in the material and it, in the first place, makes impact on crack propagation. On the crack top, while developing critical Intensities, there occurs pluck from the crack top.

Correlative relation of transformation of external stresses of energies into inner energies of the material was determined which determines propagation of defects existing in the work-piece at high energies exceeding the critical, when stress intensity factor overcomes crack resistance and rupture stress energy develops. Thus, universal relation between total energy developed in the work-piece and work-piece mass is established with respect to external energy of rupture stress.

---

[1]Energy (from Greek energies–action) of the common measure unit for various forms of material movements, which is considered in physics. Various types of energies are used for quantitative characterization of qualitatively different forms of motion and for relevant interactions, such as: mechanical, internal, gravitational, electromagnetic, and nuclear and others. In international system of units—SI energy is expressed in Joules.

ACKNOWLEDGEMENTS

I am grateful to Ilia Vekua Institute of Applied Mathematics of IvaneJavakhishvili Tbilisi State University for assistance in the research of Structural and Micro Mechanical Characteristics.

CONFLICTS OF INTEREST

The author declares no conflicts of interest regarding the publication of this paper.

REFERENCES

[1] Lawn, B. (1999) Fracture of Brittle Solids. Cambridge University Press, Cambridge.

[2] Kovziridze, Z., Hennicke, H.W. and Kharitonov, F. (1998) Thermomechanics of Ceramics. Fachhochschule Karlsruhe Hochschule fuer Technik, Karlsruhe.

[3] Kovziridze, Z., Aneli, J., Nijaradze, N. and Tabatadze, G. (2017) Ceramic and Polymer Composites. LAP LAMBERT Academic Publishing. International BookMarket Service Ltd.

[4] Kovziridze, Z., Nijaradze, N., Tabatadze, G. and Aneli, J. (2016) Ceramic and Polymer Composites. Monograph, Georgian Technical University, Tbilisi.

[5] Budworth, D.W. (1970) Theory of Pore Closure during Sintering. Transactions of the British Ceramic Society, 69, 29-31.

[6] Grifith, A.A. (1920) The Phenomena of Rupture and Flow in Solids. Philosophical Transactions of the Royal Society A, 221, 163-198.

[7] Shvedkov, E.L., Kovensky, I.I., Denisenko, E.T. and Zyrin, A.V. (1991) Dictionary Reference Book for New Ceramic. Academy of Sciences of Ukraine. Institute of Problems of Material Sciences, Kiev, "NaukovaDumka", 115-116.

[8] Richerson, D.W. (1992) Modern Ceramic Engineering. Marcel Dekker Inc., New York.

[9] Grathwohl, G. and Kuntz, M. (2004) Mechanische Eigenschaften im Buch Technische Keramik. Herausgeber W. Kollenberg, VULKAN_VERLAG ESSEN, Germany, 45-55.

[10] Munz, D. and Fett, T. (1999) Ceramics: Mechanical Properties, Failure Behavior, Materials Selection. Springer-Verlag Berlin Heidelberg, New York, 61. https://doi.org/10.1007/978-3-642-58407-7

[11] Grathwohl, G. (1993) Mechanische Eigenschaften keramischer Konstruktions werkstoffe DGM Informations gesellschaftmbh.

[12] Natsenko, A.I. (1971) Thermal Stability of Brittle materials. Journal of Metallurgy, 15, 189-208.

[13] Kingery, W.D. (1963) Measurements at High Temperatures. "Metallurgizdat", Moscow, 466.

[14] Sobolev, I.D. and Egorov, V.I. (1962) Thermal Fatigue and Thermal Shock. In: Stability and Deformation in Uneven Temperature Fields, "Gosatomizdat", Moscow, 194.

[15] Troshchenko, V.T. (1971) Fatigue and Inelasticity of Metals. "Naukova Dumka", Kiev, 268.

[16] Pisarenko, G.S., Troshchenko, V.T., Timoshchenko, V.G., et al. (1962) Stability of Metal-Ceramic Materials and Alloys at Normal and High Temperatures. Kiev. Published by Academy of Sciences of Ukraine, SSR, 275.

[17] Geitwud, B.E. (1959) Temperature Stresses. Moscow Edition, “Foreign Literature”, 349.

[18] Kovziridze, Z., Nijaradze, N., Tabatadze, G., Cheishvili, T., Mestvitishvili, Z., Mshvildadze, M. and Darakhvelidze, N. (2017) Obtaining of Composites by Metal-Thermal and Nitriding Processes in Si-Sic-Al-Geopolymer System. Ceramic and Advanced Technologies, 19, 33-52. http://www.ceramics.gtu.gehttps://doi.org/10.4236/jectc.2017.74009

[19] Kovziridze, Z., Nijaradze, N., Tabatadze, G., Cheishvili, T., Mshvildadze, M., Mestvirishvili, Z., Kinkladze, V. and Daraxvelidze, N. (2007) Obtaining of SiAlON Composite via Metal-Thermal and Nitrogen Processes in the SiC-Si-Al-Geopolymer System. Journal of Electronics Cooling and Thermal Control, 7, 103-122. http://www.scirp.org/journal/jectc

[20] Maslennikova, G.N. and Kharitonov, F.Ya. (1977) Electro-Ceramic, Stable to Thermal Shocks. Moscow. Energy, 9-10.11-18, 163-175.

[21] Kingery, W.D. (1955) Factors Affecting Thermal Shock Resistance of Ceramic Materials. Journal of the American Ceramic Society, 38, 3-15. https://doi.org/10.1111/j.1151-2916.1955.tb14545.x

[22] Buessem, W. (1955) Thermal Shock Testing. Journal of the American Ceramic Society, 38, 15-17. https://doi.org/10.1111/j.1151-2916.1955.tb14546.x

[23] Davidge, R. and Tappin, G. (1967) Thermal Shock and Fracture in Ceramics. Transactions of the British Ceramic Society, 66, 405-422.

[24] Failure Stress Energy Formula. Georgian National Intellectual Property Center “Georgia Patent” (Sakpatenti). Certificate of Deposition 7289.2018.03.27.

UDC 666.946.6

SERPENTINITE-PHOSPHATE COMPOSITIONS FOR BIOLOGICAL PROTECTION OF NUCLEAR POWER PLANTS

Z. Kovziridze, N. Nizharadze, G. Tabatadze, N. Kutsiava, M. Balakhashvili, N. Darakhvelidze, M. Kapanadze, R. Gaprindashvili.

Institute of Bionanoceramics and Nanocomposites Technology, Department of Chemical and Biological Technologies, Georgian Technical University, Georgia, 0175, Tbilisi, Kostava str. 69

E-mail: kowsiri@gtu.ge

Resume: ***Purpose***: The aim of the work is to develop the technology of making serpentinite-phosphate compositions and concretes based on them for the biological protection of nuclear power plants.

Method for protection: Serpentinite-phosphate cement is obtained by combining 65% phosphoric acid and pure serpentinite (serpentinite grinding purity 10% residue on 008 sieve.) the physical and technical properties of samples are studied. The research was conducted using modern chemical, thermal, X-ray structural and petrographic analysis methods.

Results: It is established that the serpentinite-phosphate binder clampproperties depend on the concentration of phosphoric acid.

Conclusion: Both serpentinite-phosphate cement and concretes based on it with various fillers, cast iron powder, steel flakes and serpentinite retain the amount of chemically bound water at high temperatures, which is important for biological protection of nuclear power plants.

The use of serpentinite as a filler has better results.

Keywords: serpentinite-phosphate cement; protective concretes; nuclear reactors; biological protection.

1. INTRODUCTION

The operation of high power nuclear reactors requires a serious approach to biological protection. Its purpose is to reduce the flow of radiation in the reactor core, structures and heat carriers to a level that would be safe from a biological point of view.

The main issue of atomic energy is the more rational use of the properties of uranium and plutonium in nuclear fuel. This problem can be solved by using nuclear fuel in reactors that work on fast neutrons.According to theoretical and practical data, the construction of nuclear power stations based on fast neutrons is considered one of the directions of further development of nuclear energy [1-2].

The main requirement for the material suitable for biological protection is the composition of the material. Weakening of the flow of neutrons takes place during their interaction with the nucleus or atoms of the shielding material atom. As a result of attenuation of fast neutrons or absorption of attenuated neutrons, the flow of neutrons slows

down. The most effective way to weaken (slow down) neutrons [3-4].

Hydrogen is considered to be a substance because the energy reduction of neutrons from a single collision is inversely proportional to the collisionmass of particles. Due to the equality of neutron and hydrogen atom nucleus-proton masses, half of the neutron energy is lost in one act when a neutron is scattered in hydrogen, therefore, to increase the protective properties of concrete against the flow of neutrons, it is desirable to use such concretes, which during hardeningare associated with an increased amount of water [3-4]. Particular attention is paid to the use of concrete at high temperatures. Due to the fact that the constituent components of concrete completely lose chemically bound water during operation, the protective properties of concrete deteriorate sharply. The permissible temperature for concrete depends on the type of mortar and filler [5-6].

Thus, cement, on the basis of which concretes for protective constructions are made, must be chemically bound to a large amount of water and must be able to retain it at high temperatures. They should have enough strength and satisfactory thermophysical technological indicators. Concrete protector under the properties is meant the ability of concreteto the required amount of attenuation of the nuclear device [7-8].

It is practically impossible to prepare concrete that would meet all requirements. According to various researchers, during the construction of protective structures, special concrete is prepared, for which barite, magnetite, and limonite are used as fillers, due to their high water content. But bound water is easily lost at 150°C [9-11].

Link to water belongs to:

1. Chemically bound water, which is formed as a result of the interaction of cement with water.

2. Adsorbed water in the form of a thin layer.

3. Mechanically bound water present in capillaries Magnesia cement is known to be a good material for protection because it contains a large amount of hydrogen than other cements, but atmospheric actions cause damage to concrete made on this cement [12-13].

In order to meet the special, different requirements of modern equipment, there was a need to create materials with grip properties that would be different from those already used. Such rigid materials are considered promising, the basis of which is solidification is completely different chemical and physico-chemical processes. Such materials include compositions that solidify as a result of the reaction of one or another component with phosphoric acid. Such compositions are called phosphate hardening binders, and the effect itself is called phosphate hardening effect. These compositions are divided into two groups. Compositions that solidify 1) at room temperature and 2) when heated.

2. MAIN PART

Phosphate is cement oxide-phosphoric acid. Among the materials of this class, phosphoric acid exhibits special properties due to the electronic structure of phosphorus included in its composition and its ability to form inorganic polymer structures.

In the literature, there are data on the use of chromite ores, talc, asbestos, coals, kaolin, apatites and phosphorites to obtain phosphate compositions [14-17].

Natural raw material serpentinitewas selected for our phosphate cement production.Serpentinite - a mountain rock, in the composition of which there is a large amount of chemically bonded water(12-15 mass %). It loses it above 500°C, more so is important. Due to this serpentinite concrete can be used as an effective material for biological protection of nuclear power plants without special heating devices. phosphoric acid - to receive serpentinite composition it is necessary only one operation of technological process - grinding. Serpentinites deposit is in Georgia. Tsnelisi and Sachkhereserpentinite deposits have been studied and their comparative research has been carried out through chemical, thermal and X-ray structural analysis. The results of chemical analysis are presented in Table 1, thermograms and radiographs in Fig. 1 and 2, respectively.

Table 1

Chemical composition of serpentinites

Name of deposit	Content of oxides, wt.%								
	Fe_2O_3	Al_2O_3	MgO	SiO_2	CaO	SO_3	R_2O	humidity	H.D.
Tsenlisi	8,20	1,70	39,36	37,22	0,56	0,3	0,13	0,32	12,20
Sachkhere	6,45	2,57	33,69	39,92	1,47	-	-	-	15,90

From the chemical analysis of both serpentinite deposits (Table 1), it can be seen that the main components are SiO_2 and MgO, the values of which are 37,22 and 39,36 wt.% (Tsnelisi deposit) and 39.92 and 33.69 wt.%, (Sachkhere deposit), respectively. On the differential heating curve of both serpentinites (Fig. 1), there are three endothermic effects, with maxima: 90°C, 650°C and 790°C, and one exothermic effect, with a maximum of 810°C, which is characteristic of serpentinites. The first endopeak at 90°C is related to the loss of hygroscopic water, the second at 650°C is caused by the dehydration of the mineral serpentine, during which its crystalline paling is broken. After complete loss of crystallization water at 650^0C, dehydrated X-ray amorphous serpentine 3MgO.2SiO2 remains, which is calledmetaserpentine. The third endothermic effect - at 790°-C (Sachkhere deposit) indicates the presence of a small amount of magnesite, $MgCO_3$, in serpentinite, which decomposes at this temperature.The exothermic effect at 810°C is caused by the transformation of crystalline messier into stable anhydrous silicates – forsteriteandmagnesiummetasilicate.

Diffractograms of serpentinites are presented in fig. 2, on which the main component mineral serpentine $Mg_3Si_2O_5(OH)_4$ is highlighted. Its diffraction maxima are: d_{hkl}– 7,30; 4,55; 3,65; 2,646; 2,495; 2.145 Å.

From the results of the comparative study of serpentinite from both deposits, it can be seen that the rocks mainly consist of the mineral serpentine, which is up to 80% of the total mass in the serpentinite deposit, although they differ slightly in chemical composition. This is also confirmed by X-ray structural analysis.

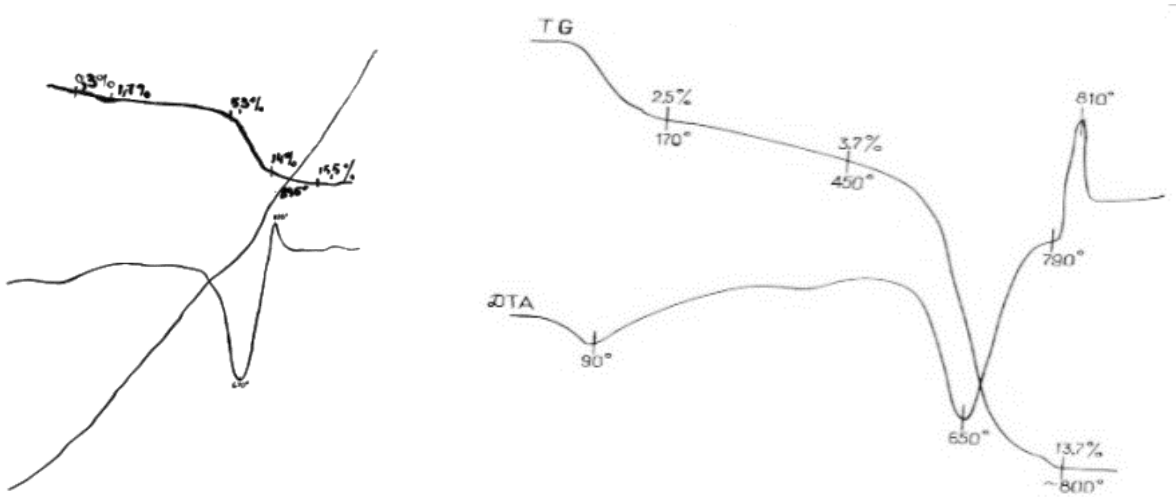

a *b*

Fig. 1. Thermograms of serpentinites: a) Tsnelisi; b) Sachkhere.

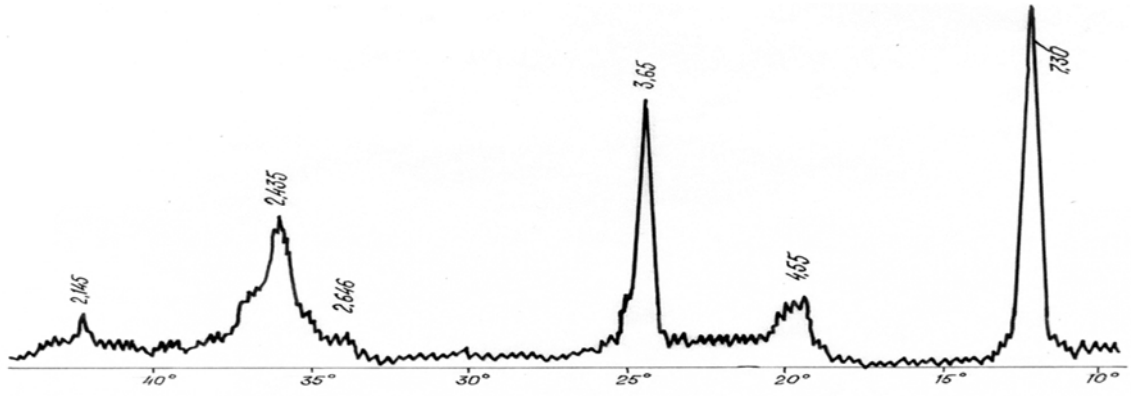

a

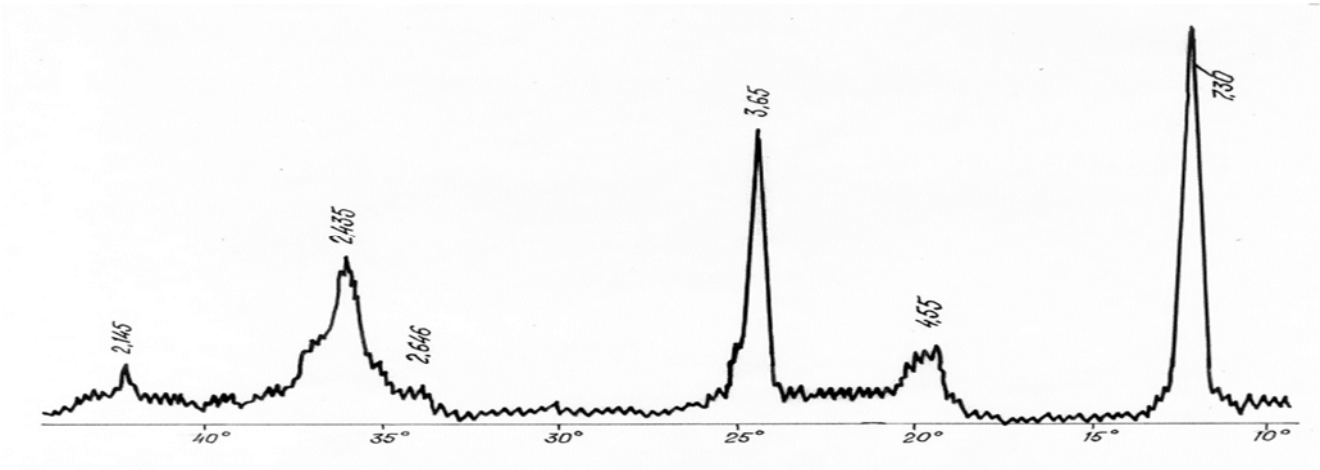

b

Fig. 2. Serpentinite X ray: a) Tsnelisi; b) Sachkhere

orthophosphoric acid interact with substances: metal oxides, clays, slags and others. It forms salts of orthophosphoric acid and they are characterized by astringent properties.

Phosphoric acid it is particularly characteristic that the association of its molecules occurs at the expense of a stable hydrogen bond.

Phosphates have a common structure with silicates, which is related to the main identity of the elements.

The tetrahedra of silicates and phosphates (SiO_4^{4-} and PO_4^{3}) are characterized by the closeness of the sizes and the similarity of the nature of the bonds P-O-P ҷэ Si-O-Si, which is caused by the closeness of the sizes of the radii of the ions of the main elements (Si^{4+} - 0,39A^0,P^{5+}-0,34A^0).

The difference between the chemical nature and the charges of the central atom leads to differences in the structures of silicates and phosphates, which are particularly difficult tobere-vealedin higher molecular structures. To obtain serpentinite-phosphate cement, we took a composition with different concentrations of orthophosphoric acid and serpentinite of different grinding purity. The best results were obtained with 65% H_3PO_4 and pure fine serpentinite (ground fineness 10% residue on 008 sieve).

Serpentinite powder was introduced into the mass at room temperature. Table 2 shows the results of testing H/B/L -20/20/20 mm size samples prepared with this dough the tensile strength limit is determined.

At the same time, we studied the influence of the relative humidity of the environment on the physical and technical properties of the material.

The limit of strength of SPC during compression depending on the relative humidity of the environmentis given in table 3.

The obtained results show that the absolute strength of the serpentinite-phosphate binder increases, but with increasing acid concentration up to 65%, with increasing environmental humidity up to 80%, it drops sharply. Such a dependence is explained by the high hygroscopicity of the formed magnesium phosphates during the use of highly concentrated phosphoric acid, which in this case produces crystal hydrates with low stability by reducing water molecules.

Table 2

Strength limit of serpentinite-phosphate cement in compression (hardening in air with 70% humidity)

designation	solid liquid	Strength limit in compression, MPa		
		3	7	28
Serpentinite phosphate cement	3:1	110	134	280

table 3

The limit of strength of SPC during compression

acid concentration, %.	acid density,g/cm³	environment humidity, %,	solidification time, day and night		
			3	7	28
			Strength limit in compression, MPa		
26	1.16	70 100	42 50	85 79	162 154

Such compositions, in which acid phosphates are obtained, are distinguished by their astringent properties.

Astringency is a property of mainly acid phosphates. Acid phosphates are obtained in serpentinite-phosphate cement. Acid phosphates are obtained in serpentinite-phosphate cement.

The main phases of serpentinite-phosphate cement are $Mg(H_2PO_4)2H_2O$, $Mg(HPO_4)3H_2O$ and unreacted serpentinite.

Below is a thermogram of serpentinite-phosphate cement. The thermogram shows three endo-effects at 125, 180 and 665°C and oneexo-effect at 820°C. At 125°C, the endothermic effect is due to the loss of chemically unrelated water from the sample. Second, with the loss of crystallization water at 180°C, $Mg(H_2PO_4)\cdot 2H_2O$ and $MgHPO_4\cdot 3H_2O$, at 165°C, two molecules of water are lost from $Mg(H_2PO_4)\cdot 2H_2O$, $MgHPO_4\cdot 3H_2O$, 3 molecules of water fromat140-260°C.

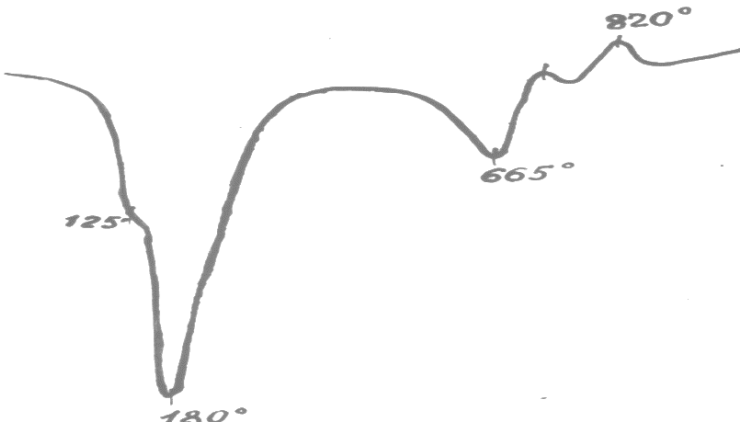

Fig. 3. Serpentinite-phosphate cement thermogram

These losses occur in the range of 140-260°C from crystal hydrate and these two effectssuperimposed by the formation of a single maximum at 180°C. At 665°C is related to the loss of chemically bound water from the serpentinite.

The exoeffect at 820°C is the total effect of the crystal Messer transformation of serpentinite and the polycondensation reactions of magnesium acid phosphates at 680°C.

We have conducted complex physico-chemical studies of serpentinite-phosphate cement stone samples (1) and concrete with serpentinite-phosphate cement serpentinite filler (sample 2,3,4). X-ray structural analysis of samples 1 and 2 showed that they contain significant amounts of the disubstituted magnesium phosphate $MgHPO_4 \cdot 3H_2O$- mineral neuberite. Contains trisubstituted phosphoric acid magnesium - $Mg_3(PO_4)_2$.Only on the radiographs of the same samples, very intense lines of separation between the planes are observed 7,16; 3,60-3,61; 2,51; 2,49 A° and others, which testifies to the fact that in the samples there are sufficient amounts of non-reactive minerals (antigorite, aphrodite, nepuite) containing the original serpentinite. At this time, by comparing the intense lines in these samples, it can be concluded that the content of serpentinite phosphoric acid interaction products, in particular, newberite ($MgHPO_4 \cdot 3H_2O$) is greater in sample 1 than in the second, and the content of the unreactable part of the above-mentioned minerals of the initial serpentinite is on the contrary the second in the sample than in the first, which can be explained by the presence of serpentinite filler in the second sample.

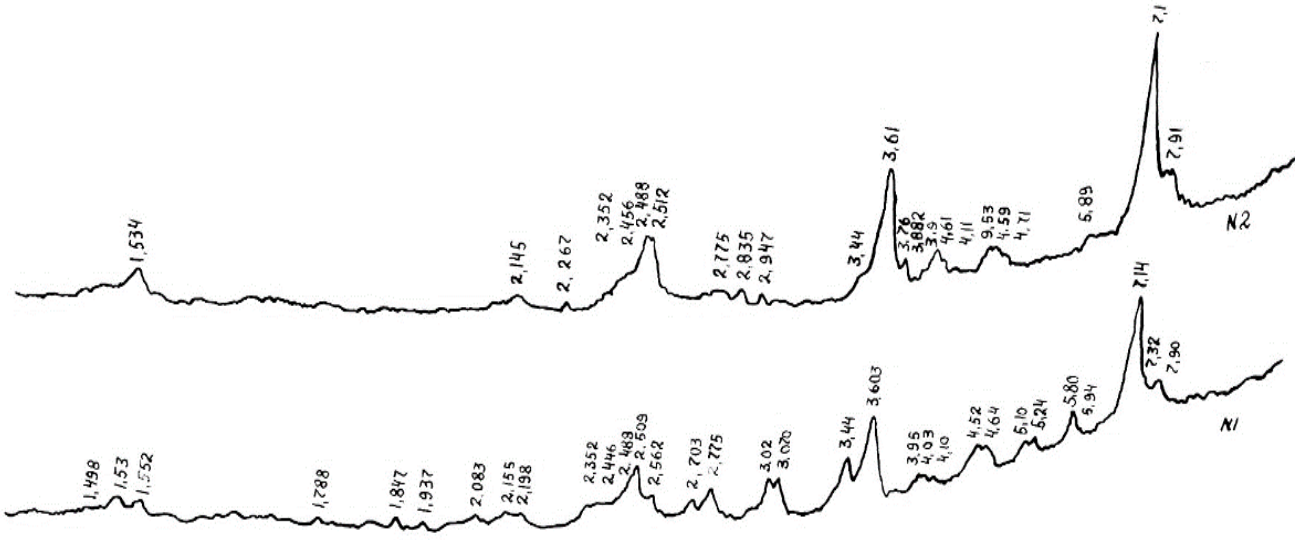

Fig. 4 SFC (№1) and SFC + serpentinite filler (№2)

Differential-thermal analysis of the above-mentioned samples (1,2) and additional samples 3 and 4 confirm the results of X-ray structural analysis. In particular, on the differential heating curve of all samples 1, 2, 3, 4, a broad endothermic effect with a maximum at 700-710°C is caused by the loss of chemically bound water, and an exothermic effect with a maximum at 820-830°C by the transformation of the crystal meser of minerals, which proves that in the samples There

is a considerable amount of the unreacted part of the minerals contained in the initial serpentinite. First, the double endo effect with maximsat120-170°C is related to the loss of weakly bound water from the interaction products of serpentinite and phosphoric acid.

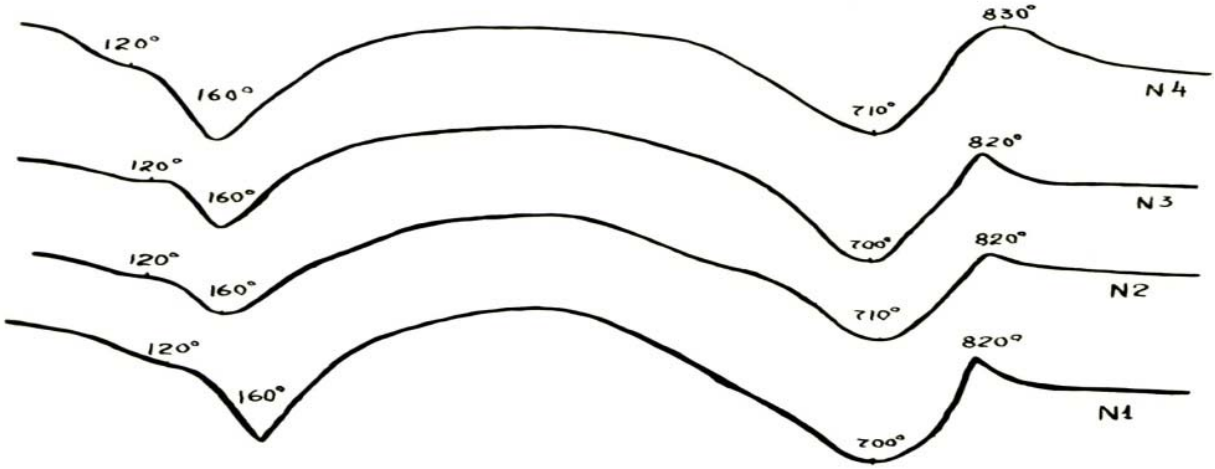

Fig. 5 Differential heating curves of sample 1, 2, 3, 4

We prepared mixtures of SFC and cast ironf-rom powder and the third SPC and steel flakes. We used a 3mm blade. In all cases the SFC-filler ratio was 1:15 by mass. To prepare the solution, we took 10-14% of the dry weight of the acid. Samples were hardened for 28 days.

In order to improve the protective properties of the received phosphate mortar, we added different amounts of cast iron powder and steel flakes as a reinforcement to obtain radiation-proof concrete. The addition of iron was due to the fact that it has a high density, which is necessary for the absorption of radiation.

To prepare the solution, we took 10-14% of the dry weight of the acid. Samples were hardened for 28 days.

As a result of the conducted metallographic studies, it was determined that the particles of the burnt powder are covered with a thin layer of iron oxide, as a result of which the activity of the interaction of iron with water vapor is significantly reduced and the release of hydrogen during the heating of the ferro-cement mixture is reduced by more than half. cement cast iron powder (serpentinite: cast iron)

The ratio by mass was as follows:

mixture #1 1:1; mixture #2 1:2; Mixture #3 1:3

Table 4

Increase in strength with time in cement-cast iron composition

Material	normal thickness of dough,%	Strength limit, MPa. Day-Night					
		in compression			Whilebending		
		3	7	28	3	7	28
mixture1	20	170	195	230	31.4	41.7	50.5
mixture2	16	100	120	150	23.7	25.0	33.2
mixture3	13	25	32	40	13.4	7.4	13.2

Concrete strength indicators are given in Table 4. Due to the fact that concrete will heat up in the process of exploitation for biological protection, as a result of absorption of radioactive radiation energy or exposure to high temperatures, some properties of concretes at high temperatures have been studied. It was found that the strength of such concrete decreases with increasing temperature, but to a lesser extent than that of Portland cement.

In the process of heating the cement-cast iron mixture, gases are released as a result of the interaction reaction of water vapor with a part of finely dispersed cast iron powder. Therefore, we assumed that by replacing cast iron powder with steel flakes, the gas separation process will be significantly reduced from cement. A steel blade with a diameter of 3 mm was used.

The ratio of SFC-steel sheet was as follows: #1 – 1:1; # 2 – 1: 1.5; #3 – 1:2.

Table 5

Mechanical strength of SFC-steel powder composition

Material	normal thickness of dough,%	Strength limit, MPa. Day-Night					
		in compression			While bending		
		3	7	28	3	7	28
№ 1	12	11.5	15.0	45.0	25.1	28.0	42.0
№ 2	10.5	13.0	16.0	52.0	31.5	33.0	46.0
№ 3	7.3	7.0	10.0	27.0	18.5	22.5	31.5

The hardening of concrete and the increase in strength occur intensively, both in the first days and in the following days, which is caused by the good adhesion properties of phosphate cement to

steel flakes. These mixtures: high construction properties, preparation with simple technology, and high bending strength indicators are very important for biological protection bending constructions. The steel plate here plays the role of a reinforcing component. The values of settlement, water absorption and bulk masses were determined.

By determining the limit of the bending strength of concrete samples in the interval of 20-500 ^{0}C, it is shown that the strength increases up to 3000C, and then the strength does not actually decrease with the increase in temperature. Also, up to 400^{0}C, there is a slight settling, then the picture is reversed, which proves that partial oxidation of iron is taking place.

Table 6

Strength limit of serpentinite-phosphate cement-steel flake composition depending on compression temperature

Material	Strength limitwhile compression, MPa, temperature^{0}C						Volumetricmass	
	20	100	200	300	400	500	20	500
#1	450	520	550	550	500	480	2550	2375
#2	520	580	600	570	550	500	2675	2430
#3	270	340	350	300	280	260	2810	2650

Thus, at a temperature of 400-500 0C, all mixtures, both on cast iron powder and with steel flakes, practically do not decrease in volume, which is very important for protective materials that work at this temperature.

Due to the need to ensure normal conditions for the operation of protective structures, the issue of slowing down neutrons is of great importance. This is related to the water content of the materials.

As it is known, the amount of water in concrete is a function of temperature. Of great importance is the time course of the moisture diffusion process from the concrete and how much water remains in the concrete after a long time of concrete work at high temperatures.

To determine the ability to hold water, we prepared samples with a size of 50×50×50 mm. After hardening for 28 days, we heated the samples up to 900°C, with an interval of 100°C. The mass loss is calculated by the formula:

$$(q^1-q^2/100)\times 100$$

where: q^1 is the initial mass of the sample

q^2 mass of the sample after heating.

To determine the amount of water at 500^{0}C after a long time, we measured chemically bound water after 500, 1500, 3000 and 5000 hour delays using the above method.

We took 500^{0}C as the working temperature because, as will be shown below, the samples lose the main mass of water at 400^{0}C, the rest at 600^{0}C, in the temperature interval of 400-500^{0}C, an

insignificant amount of water is lost.The results are presented in Table 7.

As can be seen from Table 7, both pure serpentinite-phosphate cement and its mixtures at 500^{0}C contain 7,2 to 1,6% link water, during long-term heating up to 500°C, chemically bound water does not decrease at all.

Table 7

Change of chemically bound water in concrete depending on heating temperature

Material	normal thickness of dough, %.	Watercontent, %, temperature,^{0}C						
		20	100	200	300	400	500	600
spc	38	27.3	21.0	12.2	12.0	7.5	6.0	3.1
spc+serp. fill.1:1	22	17.8	15.9	15.1	11.5	8.6	5.1	5.0
spc +serp. fill.1:2	21	17.2	15.0	14.3	11.5	7.2	7.2	5.0
spc +serp. fill.1:3	19	16.4	14.4	14.1	10.4	7.0	6.4	5.3
spc+castironburb. 1:1	20	9.8	7.4	6.7	4.2	4.0	4.0	4.0
spc+castironburb. 1:2	16	9.4	7.0	6.3	3.6	3.3	3.0	3.0
spc+castironburb.1:3	13	8.6	5.1	4.8	3.0	2.8	3.6	3.6
spc+SFC+steelsheet1:1	12	6.7	5.4	5.2	3.5	2.3	2.3	2.3

3. CONCLUSION

Thus, as serpentinite-phosphate cement, as well as concretes based on it with various fillers, cast iron powder, steel flakes and serpentinite retain the amount of chemically bound water at high temperatures. But using serpentinite as a filler has better results.

REFERENCES

1. A.E. Desov, Heavy and hydrated concrete. Moscow. Gosstroyizdat. 1977 year, page 351.
2. Radiation protection from nuclear power plants. Moscow. "Atomizdat". 1990 year, page 352.
3. https://cen.acs.org/energy/nuclear-power/Combating-corrosion-worlds-aging-nuclear/98/i36
4. https://www.frontiersin.org/articles/10.3389/fenrg.2021.751654/full
5. https://www.epa.gov/radtown/nuclear-power-plants
6. P.V. Matyukhin, B.N. Pavlenko, P.N. Iastrbinski, B.A. Doroganov, N.I. Churkashina, Heat-resistant radiation-protective materials used at

high temperatures. "Refractories and technical ceramics". 2014. No. 7-8. pages 23-25

7. A.V.Yastrebinskaya, P.V. Matyukhin, Z.V. Pavlenko, A.V. Karaulov, N.I. Churkashina, The use of hydride-retaining composites for the protection of nuclear reactors from electron radiation. "International Journal of Applied and Fundamental Research". 2015. 12-16. pages 987-990.
8. P.V. Matyukhin, A.V. Yastrbinskaya, Z.V. Pavlenko, The use of modified iron ore to obtain structural materials for the biological protection of nuclear reactors. "Achievements of modern natural science". 2015. 9-3. pages 507-510
9. https://cen.acs.org/energy/nuclear-power/Combating-corrosion-worlds-aging-nuclear/98/i36
10. https://www.frontiersin.org/articles/10.3389/fenrg.2021.751654/full
11. https://www.epa.gov/radtown/nuclear-power-plants
12. https://www.epa.gov/radtown/nuclear-power-plants
13. https://world-nuclear.org/information-library/safety-and-security/safety-of-plants/safety-of-nuclear-power-reactors.aspx .
14. E.N.Zedginidze, N.S.Nizharadze, M.S.Ter-Grigoryan. Serpentinite-phosphate clinker material. Copyright certificate N 689987.
15. E.N. Zedginidze, N.S. Nizharadze, M.S.Ter-GrigorianiM.M. Sichiovi.Preparation and study of serpentinite-phosphate cement. All-Union Conference "Physical and chemical studies of phosphates" Leningrad, 1981. p. 228-235.
16. E.N. Zedginidze, N.S. Nizharadze, Z. Marka-zeni, M. Livshitsi and others. Clinker material based on serpentinite, copyright certificate, N 1258824, Bulletin of Inventions, N 35, 09/23/86.
17. E.N. Zedginidze, N.S. Nizharadze, Z.V. Sikha-rulidze. Serpentinite-phosphate clinker mate-rial for solving the problem of adhesion of the material with silicate bricks. Collection of works of the Tbilisi Research Institute of Building Materials. Edition X11, 1988. p. 119-123.

UDC 666.762.93

OBTAINING AND STUDY SMART COMPOSITES IN THE B_4C-SIC-SI-AL-AL_2O_3–CARBON FIBER SYSTEM

Z. Kovziridze, N. Nijaradze, G. Tabatadze, T. Cheishvili, M. Mshvildadze, N. Kuciava, M. Balakhashvili, N. Darakhvelidze

Technical University of Georgia, Institute of Bionanoceramics and Nanocomposite Technology, Georgia, 0175, Tbilisi, Kostava Str. 69

E-mail: kowsiri@gtu.ge

Resume: *Goal-* to obtain SIALON containing composites by reactive sintering method in **SiC-B_4C-Si-Al-Al_2O_3** system. Using this method of synthesis, it became possible to obtain composites with different percentages of SIALON. Our task was also to study the phase composition in the SiC-B_4C-Si-Al-Al_2O_3 system.

Method. The obtained mass was grounded in an attritor and the consolidated composite was obtained by hot pressing at 1800^{0}C., 40 minutes, delaying at final temperature for 8 min. under 30 MPa pressure.

To study the phase composition of the composites, we conducted an X-ray structural analysis on the DRON-3 device, and to study the microstructure, we conducted research on an optical microscope and a raster electron microscope “Nanolab 7” of the company "OPTON”. The values of the electrical parameters of the study composites were calculated on the basis of the obtained "lgp- t" dependence.

Result. In **SiC-B_4C-Si-Al-Al_2O_3** system we obtained composites with a matrix composed of: β-SIALON, silicon carbide, corundum and nanoparticles of boron nitride.

Conclusion. The phase composition of the obtained composite provides high physical-technical and performance properties of these composites. Compression strength-2187 MPA, Bending strength-285 MPa, Thermal expansion coefficient a_{20-700}=3.8 10^{-6} ^{0}C.

Key words: composite; electron microscope; phase composition; β-SIALON.

1. Introduction

SIALON is a general name for a large family of silicon nitride-based ceramic alloys, it was first adopted in the beginning of 1970.β-Sialon is the most well-known phase. Its chemical formula $Si_{6-Z}Al_ZO_ZN_{8-Z}$ (z=0–4.2) and its hexagonal crystal structure are similar to the structure of β-Si_3N_4.

SIALON is distinguished by: high hardness, strength, wear resistance. It retains these properties under high temperature conditions.

Composites working at high temperatures should be characterized by high density, hardness, thermal resistance and should retain these properties when working at high temperatures. Composites obtained from highly refractory oxide ceramics retain their

hardness at high temperatures but are characterized by a high coefficient of thermal expansion and therefore low thermal resistance. Carbide-based ceramics have a relatively high coefficient of thermal expansion, but they are oxidized easily when working at high temperatures. Because of this, science has turned its attention to obtain super high-strength composites - SIALONs [1-7]. The results of our work [8-10] show that the composites obtained with the SIALON matrix are highly refractory materials with high performance properties and retain these properties when working at high temperatures. For the study we used electron microscopic, optical and X-ray phase analysis methods.

The paper describes the preparation of a superceramic composite with high macro and micromechanical properties of SIALON carbide at relatively low temperatures using an innovative, simple technology. As is known, SIALONS are obtained at temperatures of 1800-2000 ^{0}C. With the help of vitrified (96 mas. % glass phase) perlite-2-3 mas.% dopant, we obtained similar material at 1450 ^{0}C and in the composition with boron carbide, silicon carbide and aluminum oxide, we were able to obtain eutectic precipitation at relatively low temperature - 1620 ^{0}C by hot pressing. The material is so hard, that it damaged the diamond beads when trying to treat it, and a 3000 atmosphere water jet failed to cut the specimen.

X-ray is performed on DRON-3. Electron microscopic research was performed on a raster electron microscope “Nanolab 7” of the company "OPTON”. No special form of samples is required for this study, only a sample fracture is required. It should be noted that the fracture is better to be new, because after some time the surface of the fracture might be covered with dust particles or oxides, which reduces the contrast and makes it difficult to distinguish phases In addition, the ions continue to move on the surface of the new fracture for some time, which makes the study very interesting.

2. Main part

To obtain the composites, we prepared mixtures, the composition of which is given in Table 1. To C-10 composite we have added carbon fiber, which is characterized by high elasticity modulus (200-935GPa), high- tensile strength (1-3GPa), with these properties it is the desired component, since it strengthens the composite material [11].

The samples were made in a cylindrical shape by the semi-dry method, the molding pressure was 20 MPa. After drying the samples were burned out in a silite oven at a temperature of 1450^{0}C. Mode 5^{0}C /min. At the final temperature the samples were kept for 40 minutes.

The physical-technical characteristics and electrical properties of the finished samples, compression strength and bending strength, impact viscosity, density, thermal resistance and thermal expansion coeficients were studied.

The bending strength was measured on a German-made disrupting machine R-100, which has a device determining the strength limit of the specimens on a three-point bend. The loading speed was 5 mm/hr.

Table 1

Material composition of CN-9 and CN-10 composites

	Composition of the initial component, mass%									
Composite index	Prosyanaya kaolin (Ukraine)	Al	Al_2O_3	SiC	Si	Perlite Aragats (Armenia)	Y_2O_3	MgO	B_4C	Carbon fiber
C-9	6,5	18.0	22.0	18.0	22.0	2.0	1.5	1.0	9.0	_
C-10	_	20.0	19.0	20.0	22.0	_	1.5	1.0	13.5	3

When determining the bending strength limit, the maximum stress is calculated by the following formula:

$$\sigma_{bend.} = 3/2.\ Pl_0/bh^2,$$

where: P- is the force at which the sample was disrupted, kg; l_0 - distance between supports at 3-point load = 25 mm; b - sample cross-section width, mm; h- the height on which the stress is applied to the specimen, mm. The test results of C-9 and C-10 composites are given in Table 2.

Table 2

The physical-technical characteristics of C-9 and C-10 composites

Compo-site name	Density g/cm³	compres-sion strength $\sigma_{press.}$MPa	Bending strength $\sigma_{bend.}$MPa	Impact viscosity a, kj/m²	Thermal resistivity constant, $\Delta a_t(K^-)$	Thermal expan-sion coefficient α, 10^{-6}(20-700°C)
C-9	3,06	1840,6	261	17,14	$-5{,}7\cdot10^{-3}$	3,88
C-10	2,97	2187,5	265	17,50	$-2{,}6\cdot10^{-2}$	3,80

Impact viscosity was determined by the pendulum impact testing machine. When the sample is crushed, the scale marks the swing angle of the pendulum β. Impact-bending strength is calculated by the following formula:

$$A_{imp.} = A/S$$

where: A - work spent to crush sample, kilo joules (kJ); S - the cross-sectional area of the samples, m². For the C-9 composite samples: the cross-sectional dimensions were 1 cm x 0.35 cm; $a = \frac{6,0}{1\times0,35}$=17,14 kJ /m² ;for the C-10 composite samples: the cro1ss-sectional dimensions were 1 cm x 0.2 cm; $a = \frac{6,0}{1\times0,2}$= 17.50 kJ / m².

As can be seen from Table 2, the bending strength and the impact viscosity of both composites (C-9, C-10) are almost the same and amount to 261; 265 MPa and 17.14; 17.50 kj/m² respective-

ly. Ceramic composites experience thermal load sand gas-thermal impacts when working at high temperatures. In all ceramic materials there are invisible micro-cracks [12] and when the strength of the product is less than the loads, these loads are converted into the decomposition stress energy. At critical loads, high energies develop, causing decomposition of the product.

To determine these energies, Z. Kovziridze proposed a formula for calculating the failure stress energy [13-14], which establishes a universal interdependence between the failure stress energy of a product, the mass of the product, and the rate of crack development under critical stress conditions. The formula for calculating the failure stress energy is as follows:

$$E_{td}=ma_{c.p.},$$

Where E_{td} is the failure stress energy, kilo joules; m-sample mass, g; $a_{c.p.}$- the crack development rate – 2000 m/sc.

In our case the sample dimensions were 5,2x5,2x45mm, the sample mass was 3.86g. According to Z. Kovziridze's formula the failure stress energy is:

$$E_{td}=ma_{c.p.}=3,86x2000=7,72 \text{ kJ}.$$

The thermal expansion coefficient of the composites (C-9, C-10) was determined with the help of a quartz vertical dilatometer -DKV for measuring the temperature coefficient of linear thermal expansion in the temperature range (20-700^{0}C). Table 2 and Figure 1 show that this indicator is the same for both composites and is a = 3.88 and $3.80 \cdot 10^{-6}$, respectively.

It is known from the literature [13] that the coefficient of thermal expansion of corundum ceramics is high and is $\alpha_{20\text{-}300C}= 6,2 \cdot 10^{-6}$. While the low-oxygen content of refractory compounds, namely silicon carbide, is a = $5,18 \cdot 10^{-6}$ and is characterized by high thermal resistance [15] It should be noted that the composites we obtained (C-9, C-10j) are characterized even by a lower coefficient of thermal expansion, respectively a = 3,88 and $3.80 \cdot 10^{-6}$ and a correspondingly higher thermal resistance, which is very important for composites that have to work for a long time at high temperatures and in an aggressive medium (Fig. 1).

Electrical characteristics have been established for the composite of both compositions (on the device created by T. Cheishvili - CH-24) which were obtained as a result of the "resistance-temperature" dependence experiment. The volumetric electrical resistance of the composites was determined in the section allowing measurements at high-temperatures in the range of 20-300^{0}C, by using an electron ohm meter as the measuring instrument. Graphite electrodes were placed on the surface of the prismatic samples (the upper measuring electrode had a diameter of 14 mm and the lower measuring electrode had a diameter of 16 mm).The dependence of the test specimens on the "specific resistance-temperature" is linear, revealing the peculiarities that an increase in temperature causes a decrease in electrical resistance. Besides the C-9 specimen is characterized by lower values of electric resistance than the specimen C-10. The difference between the electrical resistances is particularly noticeable at room temperature (the difference is approximately by three degree), but it is less evident at high temperatures (the difference decreases to one degree), which is clear from the material reflecting the results of the experiment (Fig. 2).

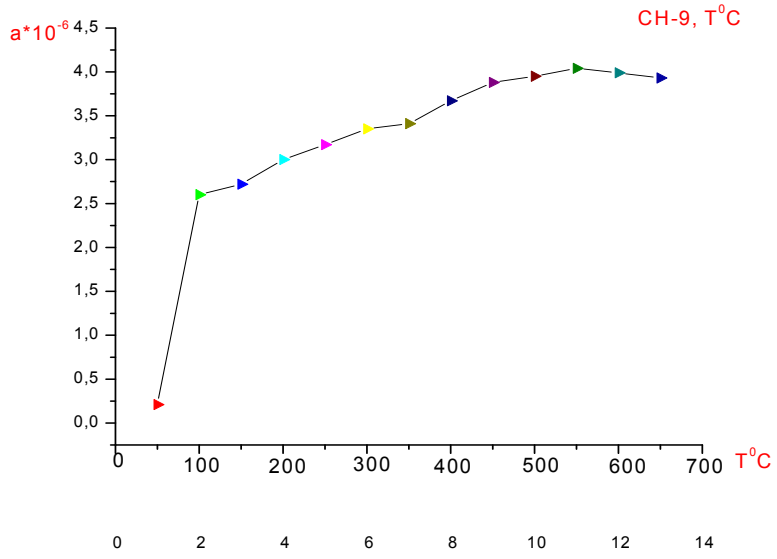

a

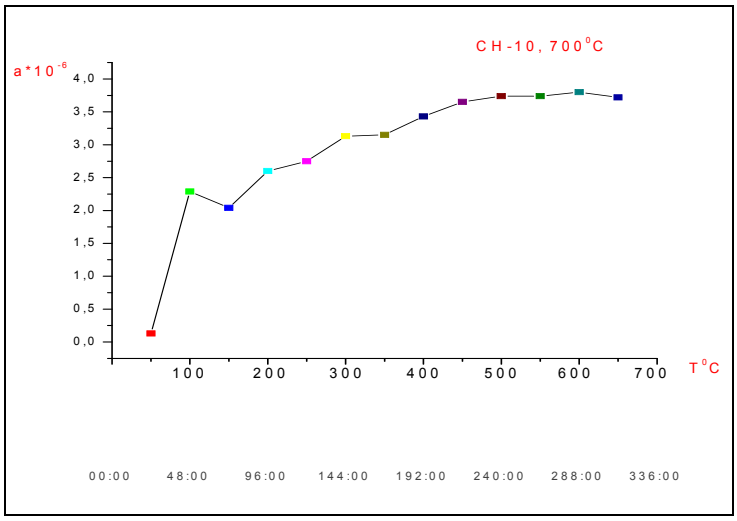

b

Fig. 1. Thermal expansion coefficient and temperature interdependence

The values of the electrical parametersof the study composites were calculated on the basis of the obtained "lgp- t" dependence. Three electrical characteristics were determined for both composites: the temperature coefficients of electrical sensitivity (B) and electrical resistivity (α_T) the activation energy of electrical conductivity (Ea), the value of which are presented in Table 3. The difference between the electrical characteristics was found to be significant (C-10 composite data are approximately 5 times higher than those obtained for C-9 composite).

It should be noted that both composites have a negative α_T (resistance decreases with increasing temperature) and low value of Ea- (realization of electronic type of electrical conductivity is expected for both materials).

The results obtained should be related to the basic phases represented in C-9 and C-10 composites obtained by the synthesis at 1450^0C, under the same conditions.

According to the results of X-ray phase analysis, the leading phase in the composite of both compositions is SIALON. They also contain five other crystalline compounds of different nature. Due to their electrical properties they can be divided into two groups: Dielectrics (a- Al_2O_3, BN, AlN) and semiconductors (SiC, Si). Considering the identical conditions for obtaining the C-9 and C-10 composites, the factor determining their low resistance and activation energy values could have been the number of SiC and Si solid phases with semiconductor properties existed in the study materials.

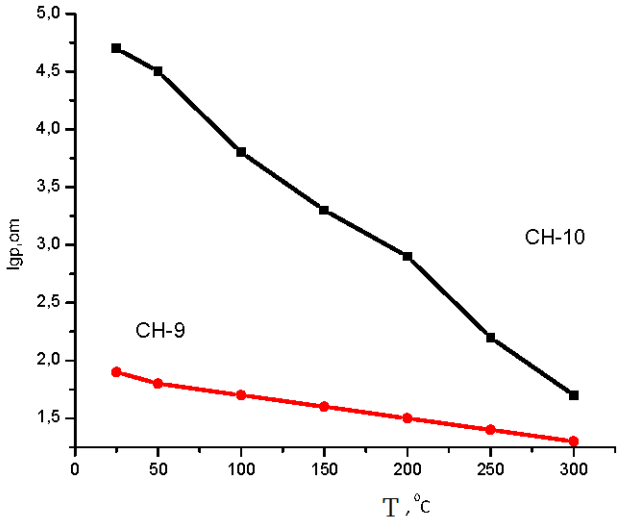

Fig. 2. Specific electrical resistance and temperature dependence

Based on the comparison of the electrical characteristics of both composites, it can be assumed that the concentrations of SiC and Si in the C-9 composite must be higher than in the C-10 composite. This could be detected by two approaches: by determining the amount of SiC and Si or by the density of the materials. Both approaches proved to be unusable for C-9 and C-10 composites, since quantitative calculations based on the available X-ray were impossible (due to the abundance of crystal phases and the coincidence of their characteristic intensity peaks) and also the negligible differences between mass densities. (d = 3.02 for C-9; d = 2.98 g /cm^3 for C-10). In any case, the number of SiC in C-9 could not have been higher than in C-10, judging by the material composition of the test composites.

At the same time, X-ray phase analysis revealed the presence of Si in both composites, which could affect the electrical conductivity of the composite. But the Si content in the initial mixture (according to the material compositions) is identical and amounts to wt. 22%. At the same time, the C-9 composite body contains two natural rocks (kaolin and perlite) that contain silicon dioxide. Kaolin (6.5 wt.%) and perlite (2.0 wt.%) provide approximately 5.2 wt.% and 3.0 wt.% Si in the C-9 composition, respectively. The reason for this is the structural breakdown of the mineral kaolinite in the geopolymer (kaolin) caused by the temperature and the possibility of conducting the parallel alumothermic process:

$$4\ Al + 3\ SiO_2 = 2Al_2O_3 + 3Si.$$

This process will result in an additional 2.4% by weight of Si in the C-9 composite, and it is practically expected that the amount of Si in C-9 will be

24.4% by weight. A contributing factor to the uptake of Si from SIO_2 may be the formation of a liquid phase caused by the low-temperature melting of perlite-1240^{0}C. Aluminum nitride is formed by the reaction of a portion of the aluminum powder in the initial mixture with nitrogen by the following reaction:

$$2\ Al + N_2 = 2\ AlN.$$

Table 3

Electrical characteristics values of the composites

Sample №	Coefficient of electrical sensitivity, B(K)	Activation energy of electrical conductivity, ΔE(ev)	Temperature coefficient of electrical resistance, $\Delta a_t(K^-)$
C-10	-7170	1,24	$-2{,}6\cdot10^{-2}$
C-9	-1560	0,27	$-5{,}7\cdot10^{-3}$

As a result of decomposition of kaolinite at high temperatures part of the aluminum powder restores silicon from SIO_2 according to the reaction above. This process could lead to a change in the ratio between an increase of the amount of semiconductor Si and AlN carrying the insulating properties in favor of Si, this would lead to the increase in electrical conductivity in the C-9 composite.

Structural study

The test specimens were prepared using the same technology as described in previous papers [16-21], i.e. the SIALON was synthesized in the nitrogen medium at 1400–1450^0 C, and then the obtained mass was grounded in an attritor and the consolidated composite was obtained by hot pressing at 1800^{0}C., 40 minutes, delaying at final temperature for 8 min. under 30 MPa pressure.

70 μM of study samples of the composite obtained in this mode were cut from 70 mm diameter and 8 mm thick discs. The cut was made on a 395-M profile grinding machine with a 100 mm-diameter metal binding diamond cutting disc, diamond grain size 50/40 μm, cutter rotation speed 4000 rpm, cutting speed 0.7 mm / min.

The surface of the cut specimens was ground on a 3G71 flat-bottomed grinding machine with a 200 mm- diameter diamond abrasive disc on a Bakelite binder, diamond grainsize-50/40μm.

Phase analysis of hot-pressed samples was performed on an X-ray machine DRON-3 using CuKα rays.

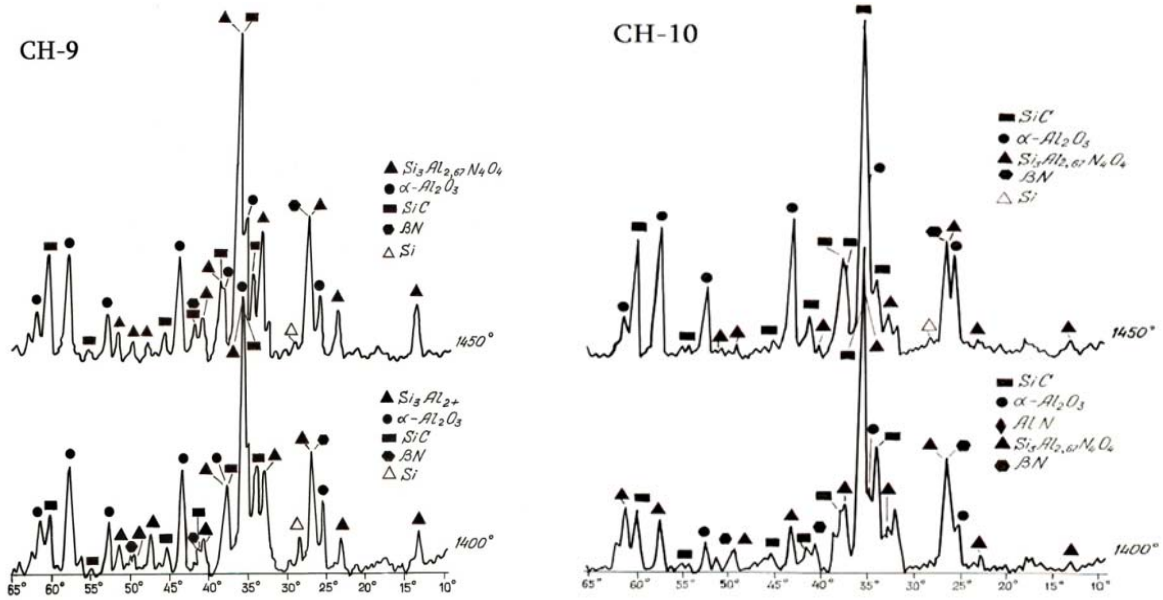

FIg. 3. C-9 and C-10 composites X-ray (1400-1450^{0}C)

Examination of the X-Ray patterns of the samples burned out at 1400-1450^{0}C (Fig. 3) shows that at 1400^{0}C the characteristic reflexes of the SIALON are already observed in both composites, and at 1450^{0}C their intensity is relatively increased. Judging by the intensity of the characteristic peaks of the SIALON, the number of SIALONs formed in the C-9 composite is relatively larger than in the C-10 composite, which can be explained by the presence of kaolin in the C-9 composition. In our opinion, this is due to the nitrogenation of the thermodynamically active kaolinite core $Al_2O_32SiO_2$, which was formed as a result of the decomposition of the mineral kaolinite. The following phases have been observed in both composites: Si-AL-O-N, SiC, α-Al_2O_3, BN, and Si (small amount unreacted.).

Boron carbide in the composites was converted to boron nitride upon burning out in nitrogen medium at 1400^{0}C by the following reaction: $B_4C+2N_2=4BN+C$, which in the case of both composites is in small quantities. Newly formed, fine-grained boron nitride improves the microstructure, which is a prerequisite for high mechanical properties, such as: high thermal conductivity, low thermal expansion, good resistance to thermal shocks, easy workability, chemical inertness and low wettability with molten metals. It is used in radiators, boron-alloyed silicon semiconductors, welding trays, crucibles, microwave tubes, sputtering targets, high-precision welding, foundry production, etc.

Analysis performed using an optical microscope showed that the composites in both cases were silicon carbide and corundum grains located in the matrix (Fig. 2). At the same time the microstructure of C-10 composite is more fine-grained. It can be assumed that during the sintering process of C-9 composite, due to the composition of these composites, more liquid phase is generated than during the sintering process of C-10, contributing to the sintering intensity, which is evidenced by the relatively low porosity of C-9 composite. At the same

time, the liquid phase promotes the appearance of small grains and their subsequent recrystallization into large grains.

Electron microscopy shows the surface of a well-sintered specimen, on which crystals of the basic phases contained in C-9 composites are clearly seen, namely silicon carbide and corundum grains distributed in the SIALON matrix, even the finest grains of boron nitride are also observed, which are better seen when magnified at close-up (Fig. 4).

When identifying grains of silicon carbide and corundum, along with SEM images, we relied on the results of X-ray diffraction analysis and X-ray spectral microanalysis.

Figure 5 shows the micro-X-ray spectral analysis image s of the C-9 and C-10 composites, the spectrum of the 3 sections and the scheme of the constituent elements, their percentage content, which shows that the main constituent (matrix) of the composite is SiAlON-BN.

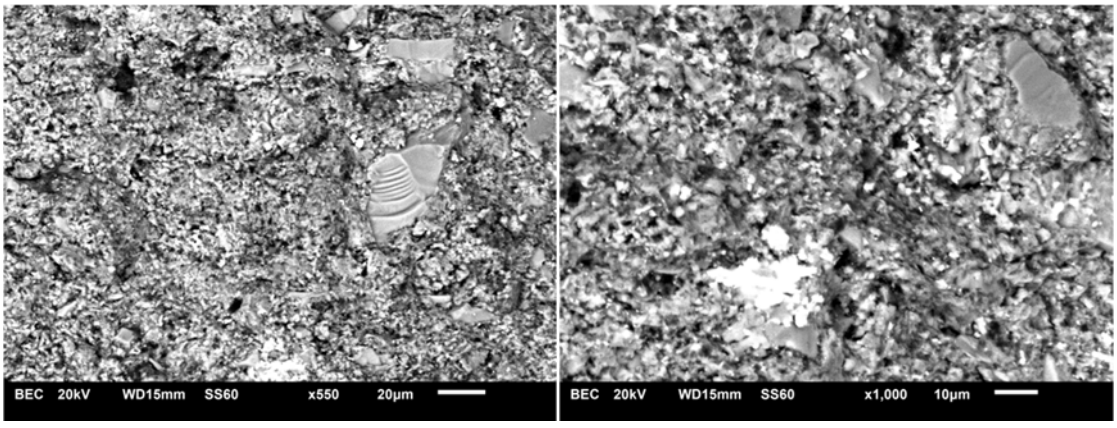

a) b)

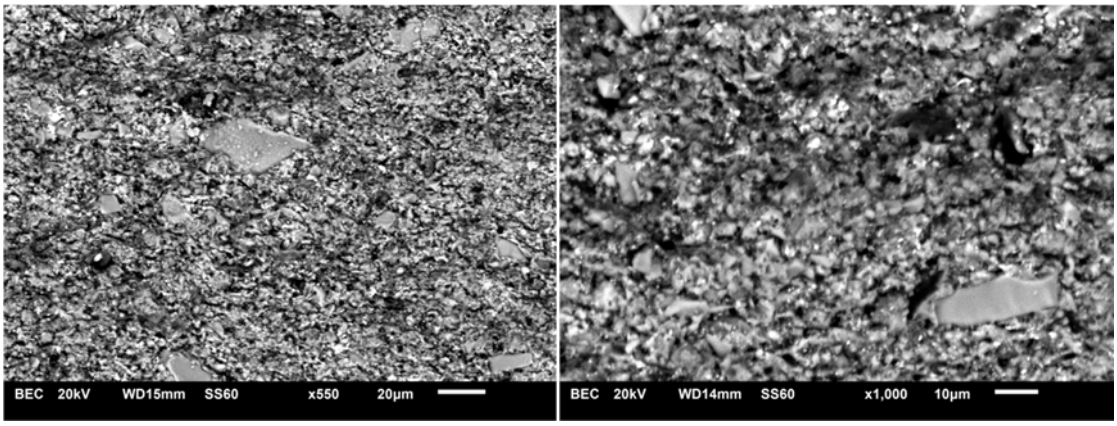

c) d)

Fig.4. C -9 (a, b) and C -10 (c, d) composites Electronic-microscopic images at different magnifications. X - 550; X-1000

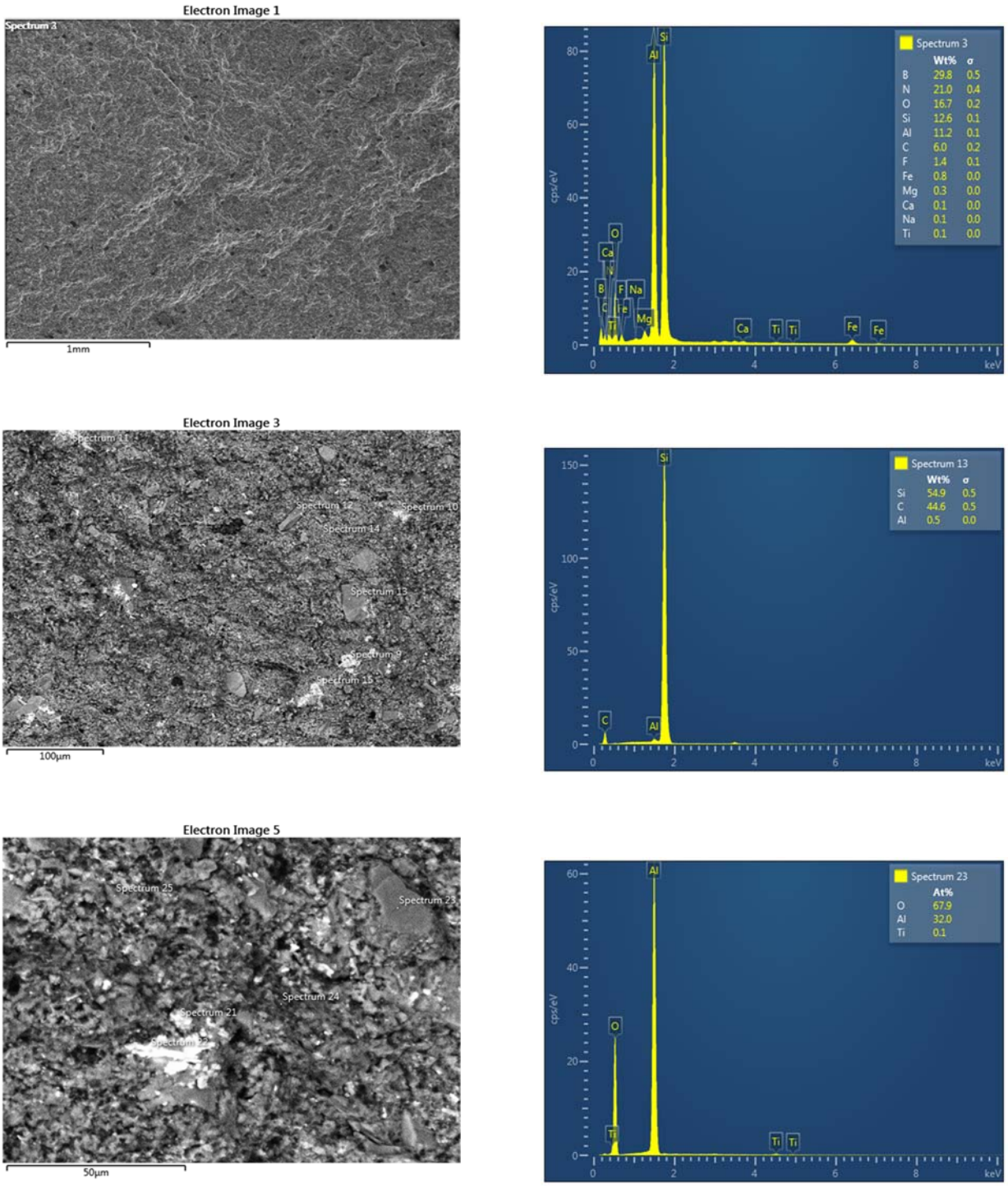

Fig. 5. Electronic-microscopic and
micro -X-ray spectral images of C -9 composite

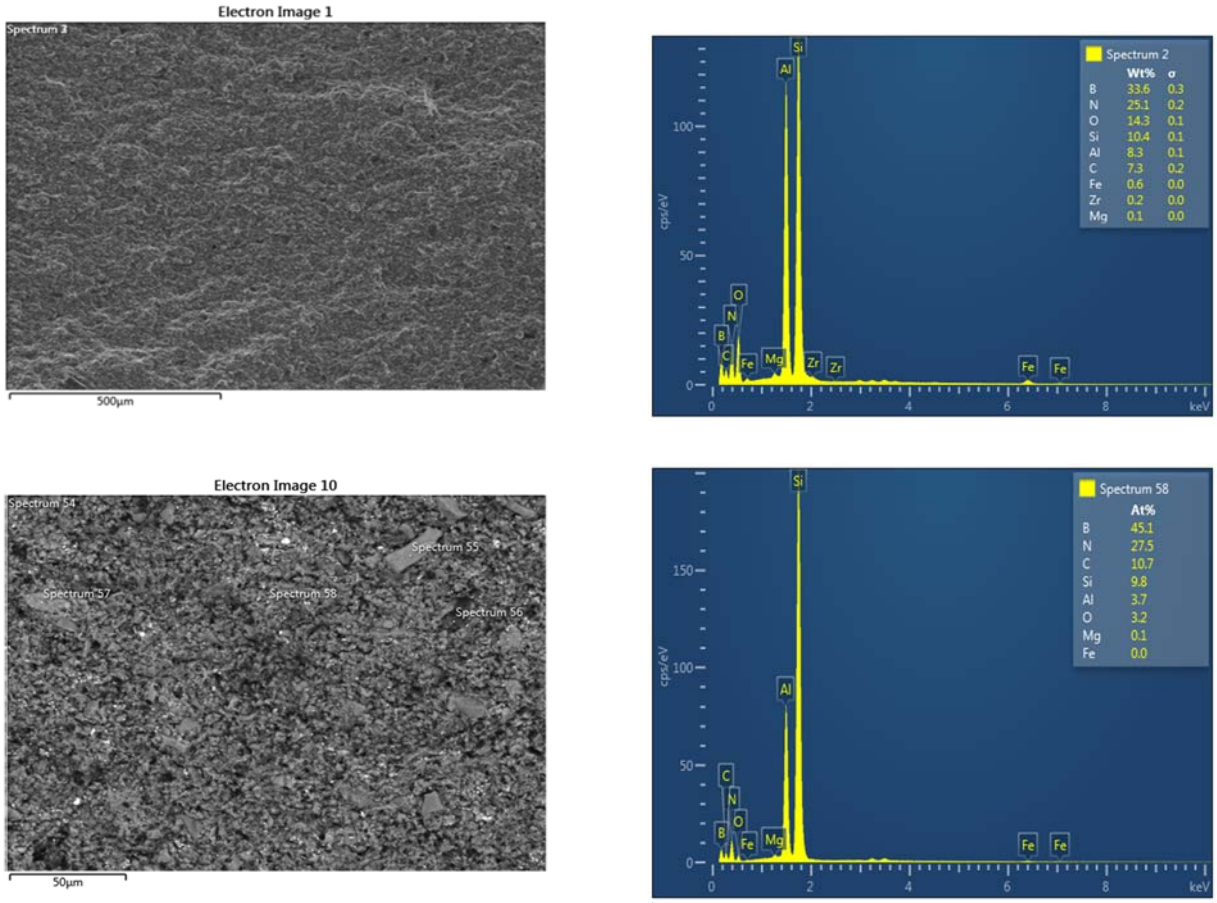

Fig. 6. Electronic-microscopic and microrentgeno -X-ray spectral images of C -10 composite

The results of micro-X-ray spectroscopy and electron microscopy of the given composites are consistent with X-ray structural analysis. In the matrix of both composites there are represented: β-SiALON-Al_2O_3-SiC, BN crystals are distributed in the matrix.

To determine the porosity, we selected the field of vision and determined its area. In the field of vision, we calculated the number of pores according to the size of their diameter; determined the volumetric content and the middle diameter of pores for each composite. The total pore content in C-9 composite is approximately Pvol = 3,7%, for C-10 -Pvol = 4,8%, the middle size of the pores makes up Pm ≈ 3,75 and 4.5 µM accordingly.

The maximum and minimum size of SiC grains in C-9 composite is 9-3 µM, middle size = 6 µM; in C -10 composite - 8-4 µM, middle size = 6 µM.

The maximum and minimum size of aluminum oxide grains is 1 / 1µM for C-9 composite and 1/ 0,8 µM for C-10 composite. The average size of aluminum oxide grains in each composite is 1 and 0.8µM, respectively. As for boron nitride, its dimensions are minimal and approximately equal to an average of 200 nM.

The average grain size in total Km = 6.5 and 6.6 μM, respectively. Glassy phase volume fraction Gvol = 3 and 1% respectively;

Crystal shape factor

F_{kfC-9}=Dmax/Dmin=10.56/5.54=1.91;

F_{kfC-10}=Dmax/Dmin=10.56/6.25=1.69.

Crystal distribution factor in the matrix by our visual estimation, F_{kd} = 0.9.

The unreacted residue of silicon is about 2 wt. %. In other cases, the Si mass in the than initial composition should be taken to be no more 18-19 percent. The carbon fiber dopant increased the mechanical properties by 3 wt.% in C-10 (Table 2). The crystalline phase is: in C-9, 100-(V porous +V glassy)=100-(3.7+3) =93.3, while in C-10: 100-(V porous++V glassy) = 100-(4.8 + 1) = 94.2.

Table 4

Data on phase components in C-9 and C-10 composites

Composite	Phase name	Field of vision S, μM²	Number of counted grains (pores), n	Grains (pores) Dmid. μM	Max. size of grain (pore) Dmax. μM (average)	Min. size of grain (pore) Dmin. μM (average)	F_{kf}-shape factor Dmax/Dmin
C-9	SiC	2070	12	11	9	3	
	Al2O3		250	1	1	1	
	SiALON		55	14	32	18	
	BN		45	0.2	0.25	0.16	
	Average		90.5	6.5	10.56	5.54	1.91
	Pores		10	3.75	4	3,5	1,15
C-10	SiC	2070	15	10	8	4	
	Al2O3		280	0.8	1	0.8	
	SiALON		50	9	33	20	
	BN		45	0.22	0.27	0.18	
	Average		97.5	6,6	10.56	6.25	1.69
	Pores		12	4.5	5	4	1.25

The dependence of the micro- and macro- mechanical characteristics of the materials on the crystalline phase content in the composite was calculated according to Z.Kovziridze's [22] formula:

$$\sigma_d = \frac{\text{P.Fkd}}{\text{Km Kv Fkf}},$$

Where: P-load; Km- middle size of crystals; K v- volume fraction of crystals in the matrix; F_{kd}- crystals distribution factor in the matrix, which is determined by the researcher; in case of equal distribution it equals to 1, in case of unequal distribution = 0.9; Fkf-crystal shape factor, is taken as the

ratio of the largest characteristic size of a crystal to the smallest, which allows us to characterize the shape of a given set of crystals, according to which we are able to define correlation of mechanical characteristic in the matrix from the crystal phase characteristics in our proposed formula. By inserting the data of Table 4 into the formula we get:

$$\sigma_d = \frac{2187.5 \text{ x } 0.9}{6.5 \text{ x } 94.2 \text{ x } 1.69} =$$

$$= \frac{1968.75}{1035} = 1.9.$$

The dependence of the macro-mechanical characteristics of the materials on the porous phase content in the composite was also determined according to Kovziridze [23] formula.

$$\sigma_{m/p} = \frac{P}{F_p \cdot P_d \cdot P_{vol} \cdot P_m} =$$

$$= \frac{2187.5}{0.9 \text{ x } 1.25 \text{ x } 4.5 \text{ x } 4.8} = \frac{2187.5}{24.3} =$$

$$= 90 \text{ MPa}/\mu M^2$$

Where: P-is load, MPa; F_p- shape factor of the pore; Pd- pores distribution factor in the matrix. Determination of this value and the evaluation of its significance depends on the researcher, based on the morphological picture depending on how the pores are distributed in the material and what size they are. The value of the factor can vary from 1 to 0.8. If the pores are evenly distributed in the matrix and are about the same size, the factor is determined to be equal to 1; if the pores are unevenly distributed, the factor equals to 0.9 and if the coalescence process of pores is initiated, factor is 0.8; Pvol.-volumetric fraction of the porous phase in the matrix; Pm- the average size of the pores.

3. Conclusion

The obtained composites have been studied and determined the phase composition of the composites; in the case of both composites the main phase, i.e. the matrix is SiAlON-SiC-Al2O3, in which the BN grains are distributed, originated in the nitrogenation process as a result of the decomposition of boron carbide by nitrogen and the replacement of carbon with nitrogen. The composites are well sintered and the crystals are bonded together with a layer of SiAlON. Material of high physical-technical characteristics is obtained. Composite with low resistance (specific resistance approximately about 10^2 ohm.M), activation energy (E = 0.27 eV) and the temperature coefficient of electrical resistance ($\Delta\alpha$ T = 0.057 k^{-1}) with β-SiAlON matrix.

Acknowledgement:

We express our gratitude to Shota Rustaveli Georgian National Science Foundation.The work is done with the grant of the Foundation Ys-18-077 Young Scientists Grant 2018.

References

1. Osman Sahin, Orhan Uzun, Malgorzata Sopicka-Lizer, Hasan Gocmez, Ugur Kolemen. Dynamic hardness and elastic modulus calculation of porous SiAlON ceramics using depth-sensing indentation technique. Journal of the European Ceramic Society 28 (2008) p.1235–1242.

2. Z. Hou, F. Ye, L. Liu, - Effects of pore shape and porosity on the dielectric constant of porous β-SiAlON ceramics, J. Eur. Ceram. Soc. 35 (2015) 4115–4120.
3. G.J. Zhang, J.F. Yang, T. Ohji, - Fabrication of porous ceramics with unidirectionally aligned continuous pores, J. Am. Ceram. Soc. 84 (6) (2001) 1395–1397.
4. B. Li, K. Liu, C.R. Zhang, S.Q. Wang, - Fabrication and properties of borazine derived boron nitride bonded porous silicon aluminum oxynitride wave-transparent composite, J. Eur. Ceram. Soc. 34 (15) (2014) 3591–3595.
5. J.F. Yang, Y. Beppu, G.J. Zhang, T. Ohji, S. Kanzaki, - Synthesis and properties of porous single-phase β-SiAlON ceramics, J. Am. Ceram. Soc. 85 (7) (2002), 1879–1881.
6. C. Zhang, R. Janssen, N. Claussen, - Pressureless sintering of β-SiAlON with improved green strength by using metallic Al powder, Mater. Lett. 57 (2003)3352–3356.
7. S.-L. Hwang, I.-W. Chen, - Reaction hot pressing of α- and β-SiAlON ceramics, J. Am.Ceram. Soc. 77 (1994) 165–171.
8. F. Çalıskan, Improvement in sinterability of β-SiAlON produced from kaolin, J. Alloy. Compd. 602 (2014) 14–149.
9. Z. Kovziridze, N. Nijharadze, G. Tabatadze, T. Cheishvili, Z. Mestvirishvili, E. Nikoeleishvili, M. Mshvildadze, N. Darakhvelidze. Obtaining of Nanocomposites in SiC-SiAlON and Al_2O_3-SiAlON System by Alumothermal Processes. //Journal of Electronics Cooling and Thermal Control, 2014, 4, 105-115.
http://dx.doi.org/10.4236/jectc.2014.44012
10. Bradley A. Newcomb, Han G.Chae, - Handbook of Properties of Textile and Technical Fibres (Second Edition) 2018, Pages 841-871.
11. Z. Kovziridze, N. Nijharadze, G. Tabatadze, N. Darakhvelidze, Z. Mestvirishvili, -Smart Materials in the System SiAlON-SiC-Al2O3-TiB2-ZrB2, Bit's 2nd Annual World Congress of Smart materials 2016. p. 558. Singapore
12. Griffith A.A-phil, Trans. Roy. Soc. London A. 221.1920.1963.
13. Kovzirize Z. The Decomposition Stress Energy Formula. Georgian Ceramics Association, Journal "Ceramics and Advanced Technologies"#1 (39), 2018. pg. 11-23.
14. Z.Kovziridze. Failure Stress Energy Formula. Journal of Electronics Cooling and Thermal Conrtol. 2018.8. pp. 31-47.
Http: // www.scirp.org/journal/jectc.
15. SamsonovG.V., Physico-chemical Properties of Oxides, M., Metallurgy, 1978.
16. SamsonovG.V., Properties of High-melting-point Compounds, Short Reference Book. M., Metallurgy. 1978.
17. Kovziridze Z., NiJaradze N., Tabatadze G., Cheisvili T., Daraxvelidze N., Mestvirisvili Z., Msvildadze M., Nikoleisvili E. – Obtaining Si-AlON,s by Nitroalumthermal Processes, Georgian Ceramics Association, Journal "Ceramics and Advanced Technologies", # 2 (32), 2014, pg. 23-31.
18. Z.Kovziridze, N.Nijharadze, G.Tabatadze, T.Cheishvili, Z. Mestvirishvili, E.NikoeleiShvili, M.Mshvildadze, N.Darakhvelidze. - Obtaining of Nanocomposites in SiC-SiAlON and Al_2O_3-SiAlON System by Alumothermal Processes.

Journal of Electronics Cooling and Thermal Control, 2014, 4, pg. 105-115.
http://dx.doi.org/10.4236/jectc.2014.44012

19. Enquan He, Jianshe Yue, Lei Fan, Chao Wang and Hongjie Wang, - Synthesis of single phaseb-SiAlON ceramics by reaction-bonded sintering using Si and Al_2O_3 as raw materials.
doi:10.1016/j. scriptamat. 2011.03.040.
20. Peng Jiang, Xiao fang Wu,Wendong Xue, Jun-hongChen,Wei Wang,Yong Li; - In-situ synthe-sis and reaction mechanism of β-SiAlON in the Al-Si_3N_4-Al_2O_3 compositematerial /http://dx.doi.org/10.1016/ j.ceramint. 2016.10.088.
21. Xing Deng, Xiangcheng Li, Boquan Zhu, Pin-gan Chen; - In-situ synthesis mechanism ofplate-shaped β-Sialon an ditseffect on Al_2O_3–Crefractory properties
http://dx.doi.org/10.1016/j.ceramint.2015.07.071
22. Z. Kovziridze. - The Formula of Dependence of Mechanical Characteristics of Materials on Crystalline Phase Composition in the Matrix. Advances in Materials Physics and Chemistry Vol.10 No.8, August 2020. ISSN: 2331-1959.
DOI: 10.4236/ampc.2020.108013.
23. Z. Kovziridze. - Macro-Mechanical Properties Porous Phase Dependence Formula. Journal of the Georgian Ceramists Associstion. Ceramics and Advanced Technologies.Vol. 20 1(39). 2018. Pp. 28-34.

UDC 543.4:546.72

OF IRON (III) WITH AZO PRODUCTS OF ACETYL ACETONE COMPLEX FORMATION

M. Tsintsadze, I. Ugrekhelidze. M. Kochiashvili

Georgian Technical University, Department of Chemistry, Georgia, 0175, Tbilisi, Kostava str. 69

E-mail: i.ugrexelidze@gtu.ge

Resume: ***Purpose.*** For the photometric determination of iron, a new class of reagents is used - ethyl acetate azone products, which generate different functional groups at the expense of the tautomeric weight shift, and as a result, complexation reactions proceed selectively. Dissociation and stability constants for analytical evaluation of organic reagents of this class are also determined.

The aim of this work is to study the complex formation of iron (III) with azone products of acetyl-acetone, which contain different functional groups.

Method: The mentioned ligands were obtained by azo-conjugation reactions in a weak alkaline environment. The purity of the reagents was controlled spectrophotometric ally by the absorption spectra of the solutions and by the method of thin layer chromatography. Their composition and structure are established by different physic-chemical methods of analysis.

Result: At the expense of shifting the tautomeric equilibrium, the following compounds were obtained: - 3-(2-hydroxy-3-sulfo-5-nitrophenylazo) pentane-2,4-dione (L^1), 3-(2-hydroxy-3,5-disulfophenylazo) pentane-2,4-dione (L^2), 3-(2-hydroxy-3-sulfo-5-chlorophenylazo) pentane-2,4-dione (L^3), 3-(2-hydroxy-4-nitro-phenylazo) Pentane-2,4-dione (L^4), 3-(2-hydroxyphenylazo) pentane-2,4-dione (L^5). The result is also the possibility of their use for the photometric determination of iron in zinc alloys.

Conclusion: The effect of free ions, masking substances and functional groups on binary and multi-ligand complexes of iron(III) has been studied by photometric method. Optimum conditions and a new class of reagent have been found, the effect of which significantly increases its selectivity.

Key words: functional groups; influence of tautomeric equilibrium shifts.

1. INTRODUCTION

Photometric methods of analysis are currently widely used for the determination of metals.

Azone compounds are one of the best for the determination of iron (III).

Complex formation of iron (III) with azo derivatives of acetyl acetone - 3-(2-hydroxy-3-sulfo-5-nitrophenylazo) pentane-2,4-dione (L^1), 3-(2-hydroxy-3,5-disulfophenylazo) has been studied) pentane-2,4-dione $\left(L^2\right)$, 3-(2-hydroxy-3-sulfo-5-chlorophenylazo) pentane-2,4-dione $\left(L^3\right)$, 3-(2-hydroxy-4-nitrophenylazo) pentan-2,4-dione $\left(L^4\right)$, 3-(2-hydroxy¬xyphenylazo) pentane-2,4-dione $\left(L^5\right)$.

2. MAIN PART

experimental part. solutions and reagents.

The reagent is synthesized according to the method [2], its composition and structure are determined by analysis by various physico-chemical methods and are given in picture (1).

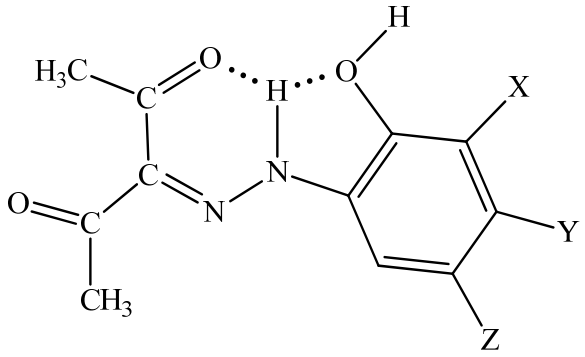

L¹ X = SO_3H; Y = H; Z = NO_2
L² X = Z = SO_3H; Y = H
L³ X = SO_3H; Y = H; Z = Cl
L⁴ X = Z = H; Y = NO_2
L⁵ X = Y = Z = H

Picture (1). of reagents 3-2-hydroxy-3-sulfo-5-nitrophenylazo¬ Structure of pentanedione

We prepared M solutions of azone compounds ((L^1, L^2, L^3, L^4, L^5) $1 \cdot 10^{-3}$ by dissolving them in ethanol, and dissolving the reagent in acetone. Fixanol HCl (pH 1-2) and ammonia-acetate solutions (pH 3-11) were used to create the required acidity. We controlled the pH of the solutions using a glass electrode ionometer H-130.

The synthesis was carried out in aqueous and mixed ethanolic solutions. The dissociation constant of the reagents was determined according to the Schwarzenbach equation. The following values of the dissociation constants of the reagents were calculated L^{1-5}:

$pK_1 = 5{,}71 \pm 0{,}01$ $pK_2 = 8{,}84 \pm 0{,}01$ (L^1)
$pK_1 = 6{,}03 \pm 0{,}03$ $pK_2 = 9{,}78 \pm 0{,}06$ (L^2)
$pK_1 = 6{,}28 \pm 0{,}01$ $pK_2 = 10{,}14 \pm 0{,}01$ (L^3)
$pK_1 = 6{,}35 \pm 0{,}04$ $pK_2 = 10{,}22 \pm 0{,}04$ (L^4)
$pK_1 = 6{,}50 \pm 0{,}01$ $pK_2 = 10{,}41 \pm 0{,}01$ (L^5)

Tools. We measured the optical density of the solution on a spectrophotometer "Lambada-40" (PerkinElmer company) with computer support and on a photoelectric colorimeter КФК-2 1 cm. layer thickness in the cuvette. We controlled the pH of the solutions with a pH-121 glass electrode pH meter.

Results and their judgment

The study of the proteolytic properties of the reagents showed that when the negative inductive effect of the functional groups introduced into the aromatic part of the molecule increases, their acidic properties increase. Based on the quantum-chemical data, it can be assumed that pK1 characterizes the deprotonation of the –OH group, which is in the ortho state in the aromatic part of the molecule, and pK2 - the deprotonation of the hydrazone form (=N–NH–).

Bieru's method is used to determine stability step constants:

$$[\mathrm{L}] = \frac{(2-m)\cdot c_{\mathrm{L}} - [\mathrm{H}^+] + [\mathrm{OH}^-]}{[\mathrm{H}^+]\cdot K_1 + 2[\mathrm{H}^+]^2 \cdot K_1 K_2},$$

$$\alpha_{\mathrm{L(H)}} = 1 + [\mathrm{H}^+]\cdot K_1 + [\mathrm{H}^+]^2 \cdot K_1 K_2,\ \bar{n} = \frac{c_{\mathrm{L}} - [\mathrm{L}]\cdot \alpha_{\mathrm{L(H)}}}{c_{\mathrm{Fe}}}$$

Where $c_{\mathrm{L}} = 2\times 10^{-3}$ mole/l, $c_{\mathrm{Fe}} = 1\times 10^{-3}$ mole/l, Fe : L = 1 : 2, K1 and K2 are reagent protonation constants; m-point of neutralization.

Table 1 shows the logarithms of stability constants of L1-5 complexes.

table 1

Logarithms of stability constants of L1-5 complexes

L	L[1] [11]	L[2]	L[3] [11]	L[4]	L[5] [12]	acetylacetone
lgK_1	10.43±0.02	11.53±0.03	11.68±0.02	11.93±0.05	12.24±0.03	9.8
lgβ_2	20.54±0.04	22.11±0.04	22.63±0.03	22.85±0.04	23.14±0.07	18.8
lgβ_3	–	–	–	–	–	26.4

The results of potentiometric titration showed that the stability constants of FeIII complexes with L1-5 change in the following order: L5 > L4 > L3 > L2 > L1. The comparison of the stability constants showed that the functional groups introduced into the aromatic part of the molecule affect the change in the order of stability of the complexes, and L5 complexes are characterized by the highest stability. This is related to the less negative value of the induction effect –H.

The calculation of complex formation functions ($\bar{n}$) showed that they change in the limits of 0 < 2, which in Fe(III) acetylacetonates change as follows: 0 < 3. This shows that when introducing functional groups into the acetylacetone molecule Reaction centers change. It seems that the ratio of components in the complexes during transition from Fe(III) acetylacetonates to acetyl-a-cetonate azo product complexes is related to steric factors and reactivity of tautomeric forms of reagents. Comparison of stability constants shows that complexes with L1-5 are characterized by higher stability. Thus, the high analytical capability of L1-5 ligands can be predicted.

Azone products of acetylacetone react with iron(III) ions in a weak acidic environment to form yellow soluble compounds. The maximum color of the solutions will be revealed under the following conditions pH 2.0 (λ_{max} = 443 nm) L^1, pH 3.5 (λ_{max} = 414 nm) L^2, pH 4.5 ($\lambda_{max.}$ = 432 nm) L^3, pH 4.5 ($\lambda_{max.}$ = 413 nm) L^4, pH 5.5 ($\lambda_{max.}$ = 395 nm) L^5

The result of the experiment shows that upon introduction of electron-accepting groups into the aromatic part of the molecule, the speed of the complex formation reaction increases, i.e. complexes

L^1, L^2, L^3, L^4 and L^5 and are formed within 5, 15, 25, 40 and 55 minutes, respectively, and are stable for a long time. The ratio of reactive components in the complexes is determined by the approximate yield method of Starik-Barbanel, by the methods of equilibrium shift and iso-molar series. The molar absorption coefficients of the complexes were calculated by the saturation method.

The degree of polymerization of the complexes was also calculated according to the following equation [24]

$$\gamma = (\lg A_i / A_k) / [(q+1)\lg\{(c_i \varepsilon l - A_i)/(c_k \varepsilon l - A_k)\}]$$

where A_i, A_R are the optical densities of the complex solutions in tests I and k; ε - complex absorption molar coefficient; l - the thickness of the solution layer in the cuvette, cm; c_i, c_k - copper concentration I and k; q - the number of reagent molecules in the complex.

The polymerization coefficients of the complexes were calculated. It is established that these compounds do not polymerize, they are in monomeric form.

table 2

Main photometric characteristics of the reaction of iron(III) with azo products of acetylacetone

reagents	pH	λ_{max}, nm	Δλ, nm	$\varepsilon_{max.}\cdot10^{-4}$	Bar interval under Berry's law, μg/ml
1,10-phenanthroline	2-9	512		1.11	
2,2'-dipyridyl	3.5-8.5	522		8.60	
L_1	1.0-4.0	443	50	1.45±0.01	0.11-2.24
L_2	2.5-5.5	414	31	1.34±0.01	0.22-2.24
L_3	2.0-6.0	432	39	1.38±0.01	0.18-2.24
L_4	3.5-6.0	413	67	1.01±0.01	0.22-1.79
L_5	3.5-7.0	395	35	0.83±0.01	0.45-4.03

It can be seen from the table that when a functional group is introduced into the aromatic part of the molecule, the stoichiometry of the components in the complexes does not change, but the molar absorption coefficients increase and significant bathochromic effects were observed during complex formation in the following order: $L^2 < L^5 < L^3 < L^1 < L^4$. It can be seen that there is a correlation between the stability of the complexes and the molar absorption coefficient. The relative sensitivity of the reaction of iron(III) with L1-5, 1,10-phenan-throline and 2,2-dipyridyl shows that it is the most sensitive using the equation and based on the calculated mole fractions of L1-5 and for ionic forms, construct distribution diagrams of reactants in solutions. under conditions of complex formation [; pHopt.=2.5-6] The most reactive form of reagents is H2L, whose content at pHopt. is 100%.

The complex formation scheme can be written as follows:

$$Fe^{3+} + 2H_2L \xrightarrow{pH\ 2.0} FeH(L)_2 + 3H^+ \qquad L^1$$

$$Fe(OH)_2^+ + 2H_2L \xrightarrow{pH\ 3.5} FeH(L)_2 + H_2O + H_3O^+ \qquad L^2$$

$$Fe(OH)_2^+ + 2H_2L \xrightarrow{pH\ 4.5} FeH(L)_2 + H_2O + H_3O^+ \qquad L^3$$

$$Fe(OH)_2^+ + 2H_2L \xrightarrow{pH\ 4.5} FeH(L)_2 + H_2O + H_3O^+ \qquad L^4$$

$$Fe(OH)_3 + 2H_2L \xrightarrow{pH\ 5.5} FeH(L)_2 + 3H_2O \qquad L^5$$

3. CONCLUSION

The influence of free ions and masking substances on the complex formation process has been studied.In terms of selectivity, L1 is superior to 1,10-phenanthroline and 2,2-dipyridyl.

REFERENCES

1. M. Tsintsadze, M. Kochiashvili, I. Ugrekhelidze. Emission spectrum analysis (theoretical foundations and laboratory practice). Stu, ch. 2018.
2. Alieva R.A., Aslanov E.O., Nagiyev Kh.J., Espandi F.E., Chiragov F.M. Spectrophotometric determination of iron (III) by 1-phenyl-2,3-dimethylpyrazolone-5-azopyrogallolol and 8-hydroxyquinoline // Chemical Journal of Azerbaijan, No. 3, 2011, p. 35-39.
3. Alieva R.A., Chiragov F.M., Mamedova F.M., Valiev V.N. Determination of dissociation constants and stability constants of complexes of Schiff bases based on acetylacetone // Reports of ANAS, 2004, P. 60, No. 5-6. p.120.
4. Alieva R.A., Mamedova F.M., Chiragov F.M. Spectrophotometric study of a colored compound of iron (III) with bis-[2,34-trihydroxyphenylazo]benzidine in the presence of 1,10-phenanthroline // Chemistry of complex compounds, III scientific conference of the republic, Baku: Baku University, 2006, p.72-741.
5. Alieva R.A., Mamedova F.M., Chiragov F.M. Spectrophotometric study of iron (III) with 2-oxopropyl-N-[2-hydroxy- 3,5-disulfonyl] azomethine in the presence of diphenyl guani-

dine // News of Baku University, 2004, No. 3. p. 26-30.

6. Alieva R.A., Mamedova F.M., Chiragov F.M. Azerbaijan Chemical Journal, 2005, No. 4. pp.16-18.
7. Alieva R.A., Mamedova F.M., Chiragov F.M. Spectrophotometric study of the complexation of iron (III) with 2-oxopropyl-N-[2-hydroxy-3-sulfo-5-nitrophen-yl]azomethine in the presence of cetylpyridine bromide//Proceedings of the IX Scientific Conference "Inorganic Materials Science and Physico-Chemical". Baku: Baku University, 2004, p.242-246.
8. Mamedova F.M. Spectrophotometric study of iron (III) with bis-[2,34-trihydroxyphenylazo]benzidine in the presence of cetylpyridine ammonium bromide // II Scientific Conference of the Republic "Young Chemist". Baku: Baku University, 2006, p.95-96.
9. Mamedova, F.M. No. 1. pp.151-152.
10. Surova T.V., Ikashina T.V., Kuznetsova T.N. Test method for the determination of iron (III) using benzohydroxamic acid in dairy products. Analysis of environmental objects. Tez. report 4th All-Russian Conf. Ecoanalytics-2000 with int. Participation, Krasnodar, 2000, p.139.
11. Abdullaev R.A. Study of the analytical capabilities of new acetyl-acetone derivatives for the extraction-photometric determination of inorganic ions: Candidate of Chemical Sciences. Baku, 1990, 140 s.
12. Mamedova F.M. Spectrophotometric study of the complex formation of iron (III) by azomethine derivatives of acetylacetone in the presence of third components // XI scientific conference of doctoral students and young researchers. Baku: Baku University, 2006, p. 27.
13. Aksenova A.G., Gavrilenko N.A., Mokrousov G.M. Determination of iron(2+, 3+) by reagents immobilized in a polymethacrylate matrix // Abstracts of the VII conference "Analytics of Siberia and the Far East". Novosibirsk: Institute of Catalysis SB RAS, 2004, vol. 1. p. 175.
14. Alekseevsky V.A., Nosirova R.N. Separation and concentration in analytical chemistry // Proceedings of the international symposium dedicated to the anniversary of Academician Yu. A. Zolotov, Krasnodar, 2002. Krasnodar 2002. p. 137-138.

Alieva R.A., Mamedov M.F., Chiragov F.M. +) // Vesti. Baku. university Natural Ser. n. N 4. 2005. art. 25-28.

UDC 678

EMI ABSORBER MATERIALS BASED ON GRAPHENE/POLYMER COMPOSITES

N. Jalagonia, T. Kuchukhidze, N. Darakhvelidze, L. Kalatozishvili, E. Sanaia, G. Bokuchava, B. Khvitia

Ilia Vekua Sukhumi Institute of Physics and Technologies, 0186 Tbilisi, Georgia. Str. Mindeli 7

(Presented by Academy Member Shota Samsoniya)

E-mail: natia.jalagonia@yahoo.com

Resume: A growing demand for electronic and communication devices in various spheres of industry has given rise to a new challenge, known as electromagnetic pollution. The electromagnetic (EM) radiation caused pollution is so serious that the WHO has included this problem in a number of the most harmful problems for human health. Correspondingly, the development and manufacture of novel electromagnetic interference (EMI) radiation shielding materials has become rather urgent. An ideal EMI shielding material should be light, thin and characterized by a high EMI absorption degree, a broad absorption band and multi-functionality.

Polymers offer several advantages over traditional metals and ceramics used for EMI shielding. They can be easily shaped into a wide variety of morphologies and are substantially lighter. For purpose, Graphene structures containing polymer (Acrylnitrilbutadienstyrol and Polydimethylsiloxane) nanocomposites is developed for application as EMI shielding material. The reflection coefficients of the produced absorbing materials were measured in the frequency range from 10 KHz to 6 GHz. The reflection measurements were performed by ASTM D4935 (Standard test methods for measuring the electromagnetic shielding effectiveness of planar materials) method. The structure and composition of the obtained materials were studied by UV, XRD, Raman and SEM. Obtained polymer nanocomposites have potential to use as EMI shielding material.

Keywords: Graphene; Polymer; Nanocomposite; Electromagnetic; Shielding.

1. INTRODUCTION

Recently electromagnetic radiation has been considered a dangerto electronics, biological systems, high quality information and safety technologies, etc., for when the electromagnetic waves interfere with a signal coming from an electronic device, a noise known as the electromagnetic interference pollution (EMI) occurs. In general, EMI pollution may be considered as an unwanted action in modern engineering that can lead to a serious human health disorder, such, for example, as a headache, sleeping disorders, trepidation etc.The EMI affects the life and performance of electronic devices used in communication facilities (cell phones, computers, etc.), electronic appliances (microwave ovens, etc.,) and in the automobile industry (integrated electronic systems, etc.). Thus, such kind of pollution has become a global challenge and its reduction is achievable only by making the electric

radiation shielding materials. The EMI shielding/ protective shell is determined by its radiation absorptive/reflective capacity, which serves as a barrier to radiation leakage into a material. Generally, conducting materials are used as the EMI shield, such, for example, as metals, although they are characterized of less flexibility, more weight and high prices. Therefore, the active work on the production of such new polymeric composites that could compete with the above-mentioned materials is under way [1-3].

After discovery of the unique properties of graphene, new possibilities for research and development of polymer nanocomposites have been opened up. The sphere of application of the innovative polymer nanocomposites produced by using other graphene and carbon nanostructures is enormous, since such nanocomposites can be characterized by extraordinary multifunctional properties [4-6], which further increases the number of products applied in innovative technologies. Based on the composition and processing complexity, a serious question for mass production of such nanocomposites is how control over the structure, dispersion degree, and morphology will be exercised, so that a material with best properties is produced.

The shielding efficiency in terms of refection/ absorption (SE_T) Shielding efficiency (SET) could be defend as parameter that measures how well a material impedes the EM energy of a certain frequency when passing through it.Fig 1 represents the possible interactions of EM waves with materials.

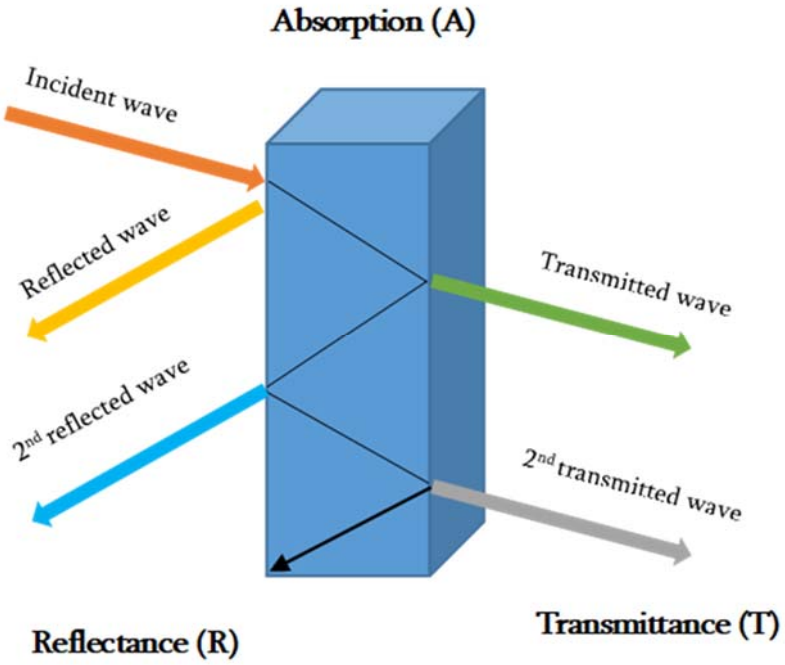

Fig. 1. Schematic diagram of incident, reflected and transmitted power and electro-magnetic field intensities when an EM wave is incident on a 3D material

When the EM waves fall on the front-face of the material then a certain part of the incident power (P_I) is reflected (P_R), while a certain part is absorbed and dissipated in form of energy, and the remaining part is transmitted (P_T) through the shielding material. Therefore, three different processes namely refection, absorption and multiple internal reflections contribute to the whole attenuation, corresponding to shielding effectiveness SE_R, SE_A and SE_M, respectively (Diagram 1).

$$SE_T = 10 \log \frac{PI}{PT} = 20 \log \frac{EI}{ET} = 20 \log \frac{HI}{HT} = SE_R + SE_A + SE_M \quad (1)$$

Here P, E and H are the intensity of force, electric and magnetic fields, the radiation incident (I), reflection (R) and transmittance (T). When it concerns the shielding efficiency from **EMI** of the composite materials, this can be studied as their electroconductivity function, which, in turn, depends on the conductivity, morphology, and dispersive power of a filler, as well as the interaction between thefiller's particles and the matrix molecules:

$$\delta = \frac{1}{\sqrt{\pi f \mu \sigma}} \quad (2)$$

where σ is electroconductivit in c/cm, μ is magnetic conductivity of the material, which equals 1 for nonmagnetic materials and f is radiation frequency within the MHz limits [4,5] (Diagram 2):

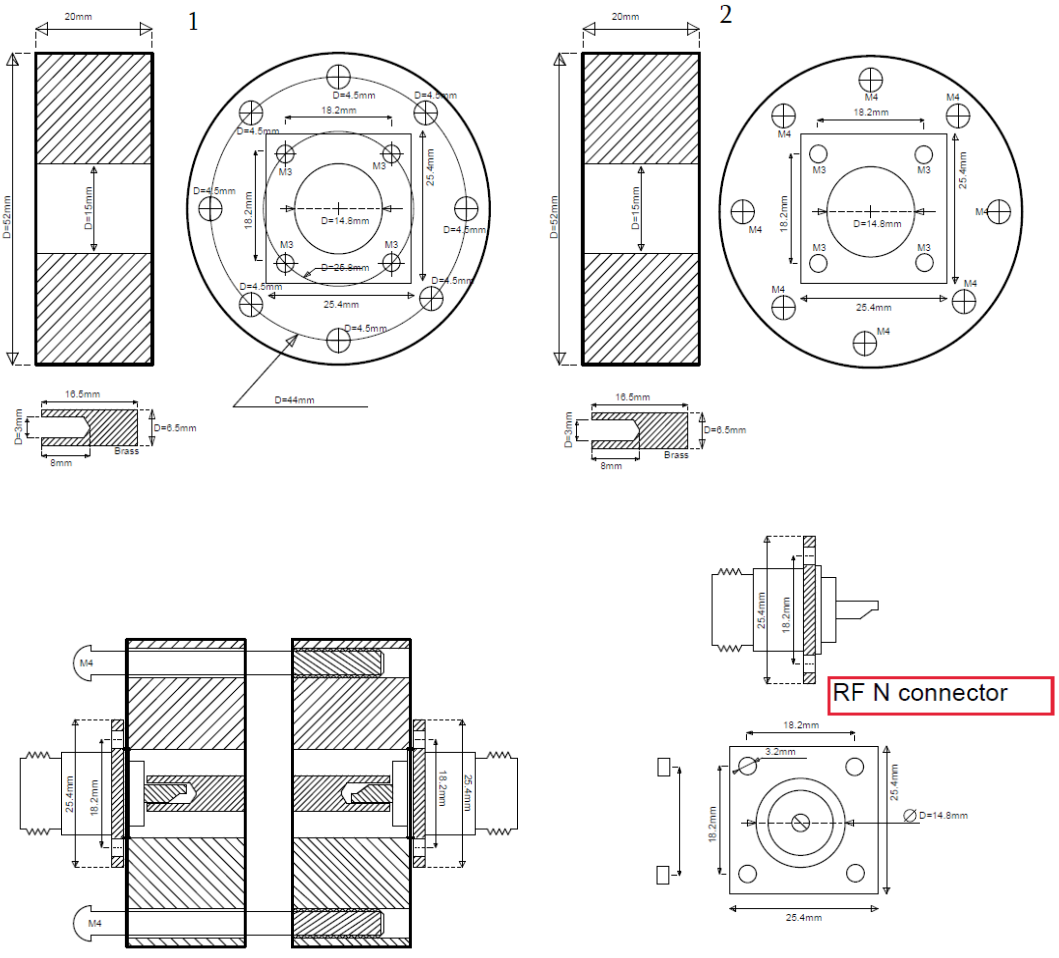

Fig. 2. Measuring device of electromagnetic wave absorption effectiveness

Measuring technology: To fulfill the tasks an electromagnetic radiation protective device has been designed and manufactured. The device consists of two (52 mm diameter and 20 mm thick, with a 15 mm hole) disks, interconnected by 8 M4 screws; it is desirable that initially the whole "completed" duralumin cylinder be drilled with a 15 mm drill in the center, ensuring thus the complete registration of the centers with the hole diameter. Also desirable would be drilling of 8 3.5 mm holes for M4 screws and then 200mm-thick disks would be cut. After cutting, the first disk holes will be widened up to 4mm, while M4 screws will be cut in the second disk. 4 N connectors will be attached on both disks by the M3 screw. The disks 1 and 2 are made of duralumin or brass cyinders, D=55-60 mm.

Polymers. Polymers offer several advantages over traditional metals and ceramics used for EMI shielding. They can be easily shaped into a wide variety of morphologies and are substantially lighter. Conducting polymers are used in different fields: in sensors, to protect metals from corrosion, in energy storage devices, etc. The character of conducting polymers depends on their doping degree, dopant ion sizes, water content, etc. In spite of the fact that conducting polymers possess a whole number of advantages, they still are not sufficiently flexible and processable in the case of mass production [7, 8]. Therefore, there are frequents cases of using non-conducting polymers and of adding dopants into them, because such polymers are cheap and accessiible, less time-consuming and enfironmentally-friendly. In addition, they allow for their mass production. In order to improve the electric and thermal conductivityand mechanial properties, a polymer is added with metals or carbon nanostructures. There are several methods of filler doping in the polymer matrix: solution mixing, melt mixing and the *in situ*polymerization. Upon using the solutions mixing method, the polymer and the filler are solved in the same solvent, then mixed together, removed from the solvent and dried. The *in situ* polymerizationis applied where the polymer is insoluble and thermally unstable.

2. MAIN PART

Synthesis of graphene oxide (RGO). Synthesis of graphene oxide have conducted by intercalation method from graphite. Graphite flakes (2 g) mixed in 50 mL of H_2SO_4(98%) and potassium permanganate (6 g) very slowly during 1 h. The flask kept under at ice bath (27-35°C) with continuous stirring. After 1 h 100 ml waterwas added in the mixture. Then continue stirring again about 1 h and 20 mL $H_2O_2$was added. After washing and filtration, the mixture centrifugation has done. Stable graphene oxide suspensions have obtained which used as reinforcement materials in ceramic composite.

Synthesis of reduced graphene oxide. The obtained GO was mixed with 100 mL of water and sonicated for 1 h using an ultrasound homogenizer. Obtained suspension was carried out in microwave and collected reduced graphene oxide powder.

Preparation of polymer nanocomposites. Polymer nanocomposites were obtained by mixing the calculated amounts of Polydimethylsiloxane (PDMS) and Acrylnitril-butadien-styrol (ABS) dissolved in chloroform (5 wt.%) and reduced gra-

phene oxide. The mixture was evaporated and dried. Then obtained solid composites were pressed.

The structure of the obtained graphene oxide, reduced graphene oxide and polymer nanocomposites were characterized by XRD (Diffractometer DRON-3M), Ultraviolet–visible "DRA-WELL" DU-8600R, Electronic microscope, Raman spectra were registered with a Raman microscope Nanofinder High End (Tokyo Instruments). The reflection measurements were performed by ASTM D4935 (Standard test methods for measuring the electromagnetic shielding effectiveness of planar materials)method.All measurements were conducted at room temperature.

Results and discussion

Graphene is a single atomic layer of sp^2 carbon atoms. Few- and single-layer transferable graphene nanosheets were first obtained by mechanical exfoliation ("Scotch-tape" method) of bulk graphite [9-10]. Graphene has unique physical-chemical properties. Today graphene and it's derivatives (graphene oxide, reduced graphene oxide and etc.) are widely used for preparation of graphene/composites.

Graphene oxide, obtained by oxidation of graphite contains oxygen functional groups (-COOH, -OH, -O-O-, -CHO),after reduction of it, reduced graphene oxide(rGO) is received, in which C:Oratio increases due to partial removal oxygen atoms (deoxygenation). Many methods are used for obtaining of reduced graphene oxide such as, using organic and inorganic compounds as reducers; treatment of graphene oxide suspensions by ultrasound homogenizer and microwave. Interest in GO increased dramatically after graphene, a single layer of graphite, was first isolated [11].

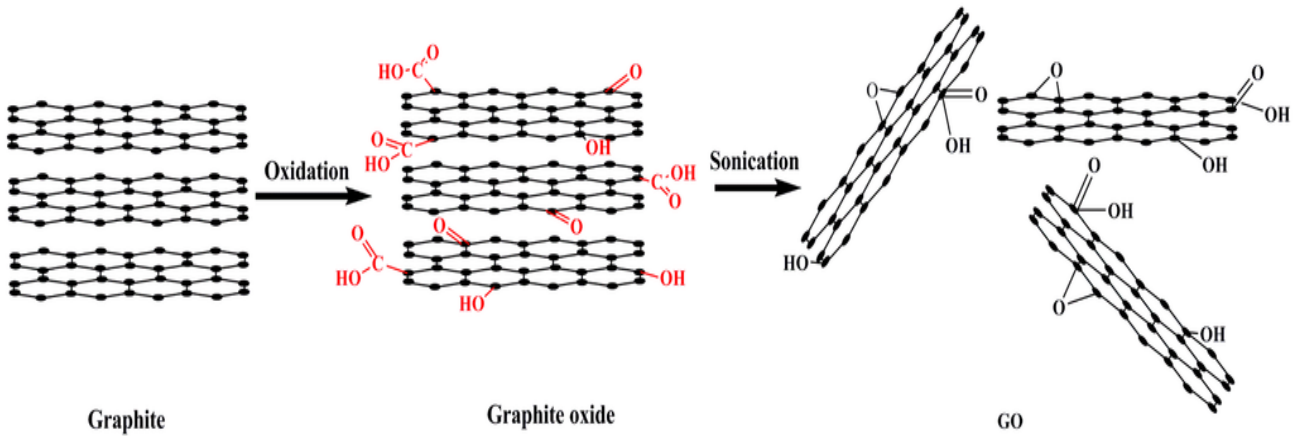

Fig. 3. Scheme of the preparation of GO

The properties of graphene-polymer based composites depend on filler distribution, ratio of filler to polymer, the type of polymer matrix, and filler and matrix bonding. In our research we have synthesized RGO and mixed into matrix.

For purpose, Graphene based polymer (PDMS and ABS) nanocomposites were synthesized. Scanning Electron microscopy was used to study the morphology and structure of materials. SEM images (Fig.4) shows that nanocomposites reveal the porous structures.

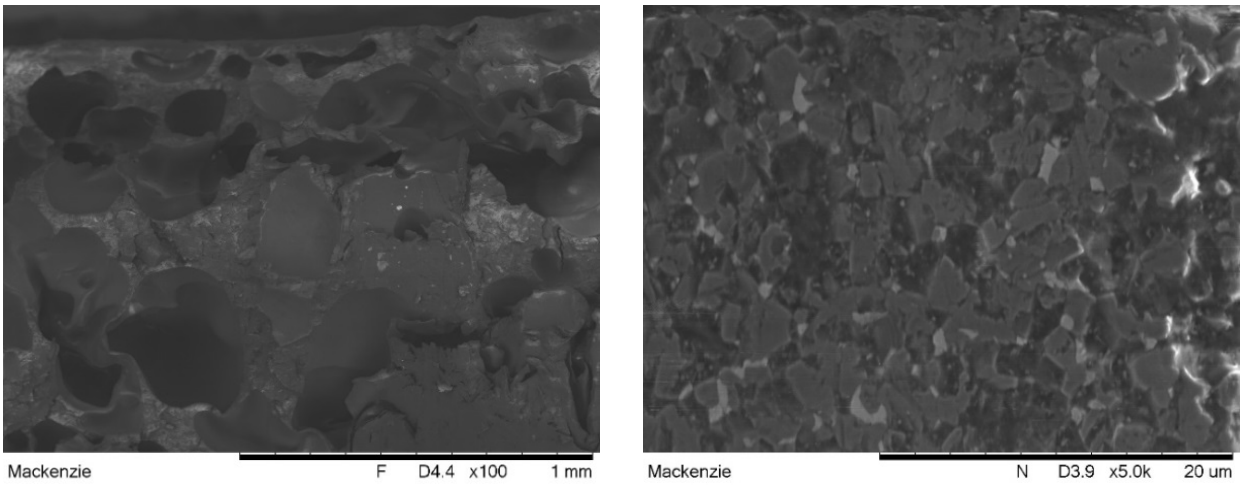

Fig. 4. Micrographs of polymer nanocomposites

RGO structure was investigated by XRD method, this is the most widely used technique for general crystalline material characterization. Characteristic diffraction peak at 10°was observed for grapheneoxide.The Raman spectrum of Graphene oxide observed D mode at ≈1350 cm-1 and G mode at ≈1600 cm-1 corresponding to common-mode lattice vibrations. The intensity of G mode is higher than that of D mode for GO.

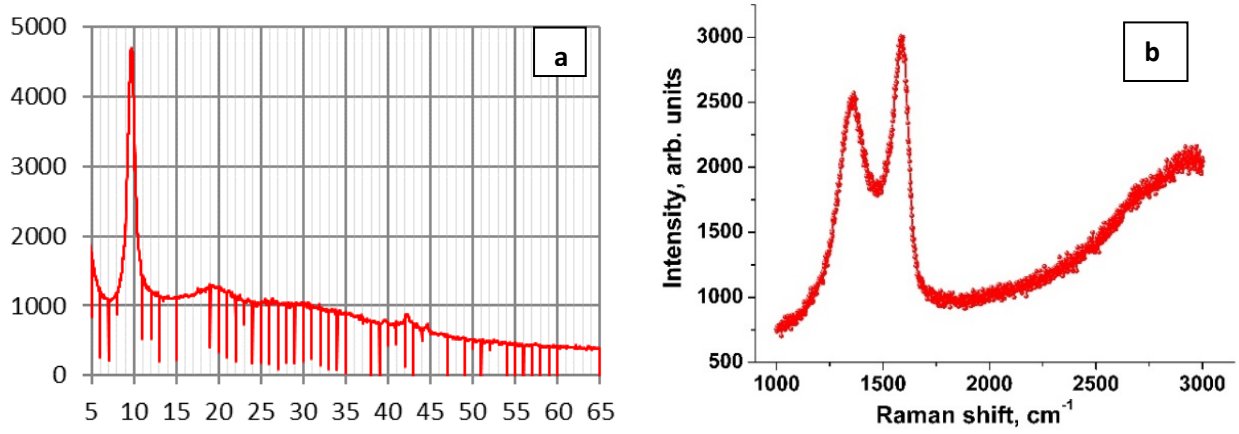

Fig. 5. XRD (a) and raman (b) spectra of GO

In the UV-Vis spectra (Fig. 6), the main peak at 230nm and the shoulder peak at 300nm stand for π-π* transitions of C=C bond from graphitic carbon of GO and n-π* transitions of C=O bond from oxidized carbon of GO respectively.

Ultrasound homogenizer method of reduction has a fundamental role in the synthesis of GO sheets, because it is relatively simple and cost-effective compared to classical methods. The GO can be well dispersed in water by sonication due to the hydrophilic nature of its graphene layers. The obtained suspension was mixed with magnetic stirring and then treated by microwave.

The reflection measurements were performed by ASTM D4935 for graphene based PDMS/ABS nanocomposites.Materials were measured in the frequency range from 10 KHz to 6 GHz.We can note that materials can absorption ability in the ≈ 4.5 – 5 MHz area.

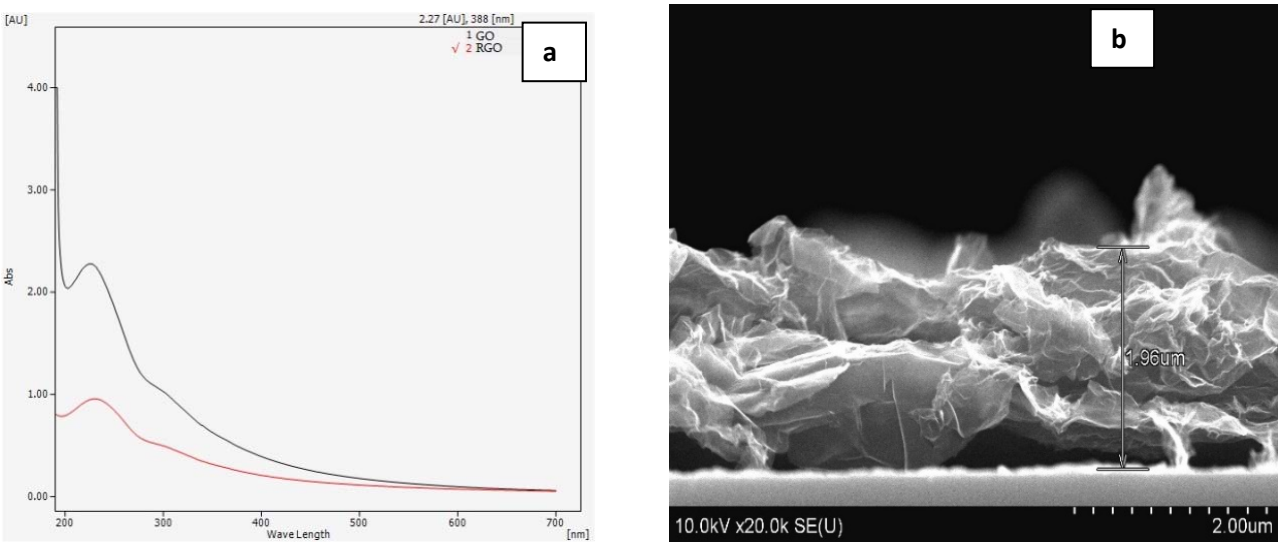

Fig. 6. UV-Vis spectra (a) and micrograph (b) of GO

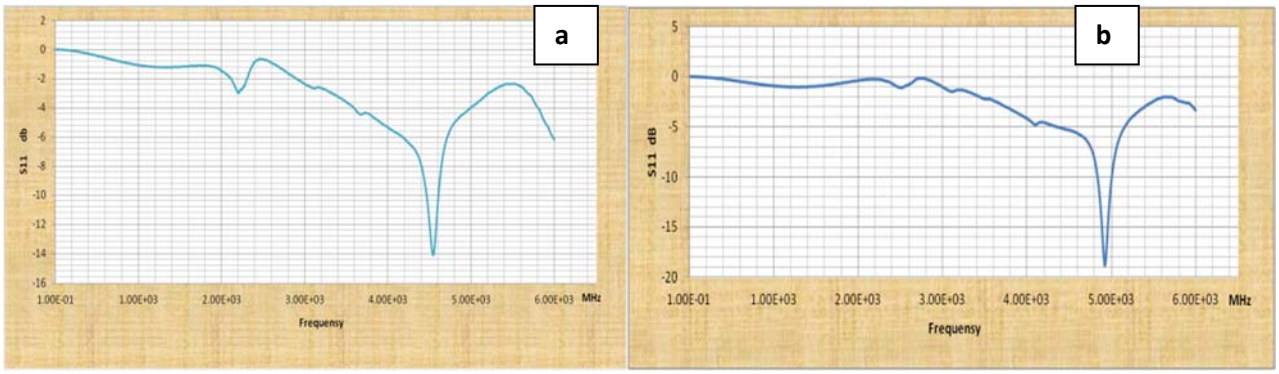

Fig. 7. Graphene oxide based on ABS (a) and PDMS (b) nanocomposites

3. CONCLUSION

This work hasdeveloped a method of reduced graphene oxide production, where the reduction was achieved usingultrasonic waves. The materials identification and structural-morphological characterization were undertaken using XRD, UV, Raman and SEM. The reflection measurements carried out by ASTM D4935method.Thegraphene-based nanocomposites developed in this study have a potential to use as EMI shielding material.

ACKNOWLEDGMENTS

This work was supported by Shota Rustaveli National Science Foundation of Georgia (SRNSFG) (Grant number CARYS_19_315).

REFERENCES

1. Jian, B. Wu, Y. Wei, S. X. Dou, X. Wang, W. He and N. Mahmood (2016) ACS Appl. Mater. Interfaces, 8, 6101–6109;
2. Gupta A. and Jha R. K. (2015)A survey of 5G network: Architecture and emerging technologies, IEEE Access, vol. 3, pp. 1206, 1232;
3. Junge, J. Wolf, N. Mora, F. Rachidi, and P. Pelissou. (2014) Electromagnetic interference control techniques for spacecraft harness, in Proc. Int. Symp. Electromagn. Compat. (EMC/ Tokyo), Tokyo, Japan, May, pp. 840-843;
4. KukhtaA.V, Jalagonia N., Kuchukhidze T., Archuadze T., Sanaia E., Bokuchava G, Mikelashvili V. (2019). Synthesis and Properties of RGO-Fe_3O_4 Based Hybrid Nanomaterial and its ABS Polymer Composite. J. of Nanosci. (World Scientific Publishing Company) v.18, No 3-4, 1940076, 201;
5. Jalagonia N., Hrubiak A., Kuchukhidze T., Kalatozishvili L., Sanaia E., Bokuchava G., Petrova-Doycheva I., Moklyak V. (2019), Obtaining of Nanocomposites Based on Comb-type Siloxane and Reduced Graphene Oxide. J. of 'Nanosistemi, Nanomateriali, Nanotehnologii", National Academy of Sciences of Ukraine. V. 17, No 3, 465–472, 2019;
6. Dhand V., Rhee K.Y., Kim H.J., Jung D.H. (2013), A Comprehensive Review of Graphene Nanocomposites: Research Status and Trends. J of Nanomaterials (763953):14;
7. Shahadat M., Khan M. Z., Rupani P. F.,. Embrandiri A, Sultana S., Ahammad S. Z., Ali S. W. and Sreekrishnan T.(2017), Adv. Colloid Interface Sci., 249, 2–16;
8. Li Y., Zhao Y., Lu X., Zhu Y. and Jiang L.(2016), Self-healing superhydrophobic polyvinylidene fluoride/Fe_3O_4@polypyrrole fiber with core–sheath structures for superior microwave absorption. Nano Res. 9, 2034–2045;
9. Novoselov K. S., Geim A. K., Morozov S. V., Jiang D., Zhang Y., Dubonos S. V., Grigorieva I. V., Firsov A. A. (2004), Electric Field Effect in Atomically Thin Carbon Films. Science,306, 666–669.
10. Geim A K, Novoselov K S, (2007). The rise of grapheme. J. Nature materials, 6(3): 183-191.
11. Natia Jalagonia, Tinatin Kuchukhidze, Nino Darakhvelidze, Leila Kalatozishvili, Ekaterine Sanaia, GuramBokuchava, Badri Khvitia - EMI Absorber Materials Based on Graphene/polymer Composites. BULLETIN OF THE GEORGIAN NATIONAL ACADEMY OF SCIENCES, vol. 15, no. 2, 2021. Pp. 83-89.

THE GEORGIAN CERAMISTS ASSOCIATION JOINED
THE INTERATIONAL CERAMIC FEDERATION SINCE 2008

THE GEORGIAN CERAMISTS ASSOCIATION HAS BEEN A MEMBER
OF THE EUROPEAN CERAMIC SOCIETY SINCE 2002

THE GEORGIAN CERAMIC ASSOCIATION WAS FOUNDED IN 1998
THE MAGAZINE WAS FOUNDED IN 1998

TBILISI, "CERAMICS AND ADVANCED TECHNOLOGIES", Vol. 24. 2(48). 2022

Reference of magazine is obligatory on reprinting

Print circulation 4,5. Contract amount 50. Printed A4 format.

GEORGIAN CERAMISTS ASSOCIATION. Tbilisi. Str. Kostava 69. Phone: +995 599 151957
E-mail: kowsiri@gtu.ge, Zviad Kovziridze

http://www.ceramics.gtu.ge